ISSN 0144 - 1396

AYRS 120-II

AMATEUR YACHT RESEARCH SOCIETY

AYRS

Advisers to the Professionals since 1955

21st Century Multihulls

by

Joseph Norwood Jr

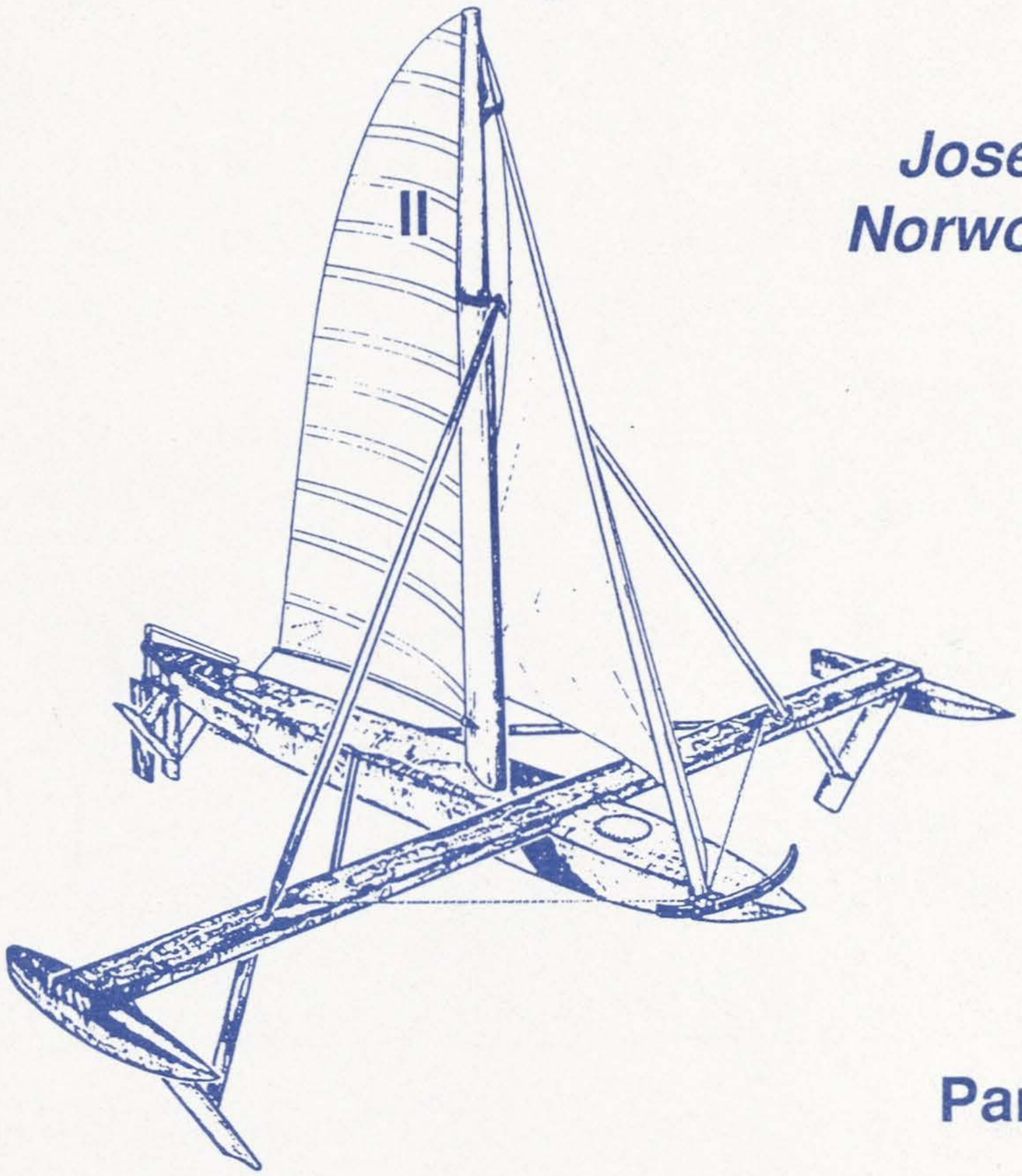

Part II

21st CENTURY SAILING MULTIHULLS

Joseph Norwood, Jr.

Part II

Sections 7 – 12

(including references)

The Amateur Yacht Research Society

Founded in 1955 to encourage Amateur and Individual Yacht Research

President
HIS ROYAL HIGHNESS
THE PRINCE PHILLIP, DUKE OF EDINBURGH
KG KT OM GBE QSO

Vice Presidents
Austin Farrar FRINA
Beecher Moore
Sir Reginald Bennett
Dick Newick (USA)
Founder: the late Dr John Morwood

COMMITTEE 1995/1996

Fred Ball	Surrey	Chairman
Ian Hannay	Hampshire	Vice Chairman
Michael Ellison	Plymouth	Hon Treasurer
Graeme Ward	Surrey	Hon Secretary
Theodor Schmidt	Switzerland	European Rep.
Frank Bailey	USA	North American Rep.
Tony Kitson	Twickenham	Publications
Simon Fishwick	Hertfordshire	Newsletters & Boat Show
Robert Downhill	Sussex	Speed Week
Roger Glencross	Wimbledon	Coordinator
Fiona Sinclair	Maidenhead	Index
Alistair Stewart	London NW2	
David Trotter	Somerset	
John Perry	Hampshire	

The Society (open membership) furthers the theory and practice of nautical science and related subjects. Educational Charity (No 234081) and a company (No 785327) without share capital, limited by guarantee.

Subscription £25.- or $50.- USA
Entrance fee £5.- or $10.- USA
Life Membership donations £1,000. or $2,000.

Amateur Yacht Research Society
BCM AYRS, LONDON WC1N 3XX

7 ROTORS

in which we find that a rotating circular cylinder with fences may provide maximum sailing performance at minimum cost

In this chapter we will discuss the application of the Magnus effect in the form of a vertical rotating cylinder to ship or yacht propulsion, and show that there have been missed opportunities that could have led decades ago to the development of very high performance sailing craft.

Wings, sails, foils, and turbine blades all produce lift by being trimmed at an angle of attack í to the apparent wind. The rotor produces its lift by rotation. This is shown in Fig. 7-1 where we see that the role of angle of attack θ is taken by the velocity ratio $\alpha = v/V_A$ in the case of the rotor. Here, v is the circumferential speed of the rotor

$$v = \omega a = 2\pi a/60 \text{ x RPM} \qquad (7\text{-}1)$$

where a is the radius of the rotor.

There are three ways to understand lift production. In the case of sails, foils, and wings arranged at an angle of attack to the wind, the wind is pushed off course, batted aside if you will, by its encounter with the underside of the wing. By virtue of Newton's third law of motion, the action of deflecting the wind must give rise to a recoil force equal to the rate of production of transverse momentum of the air. This recoil force is the lift. When the wind encounters a wing, the path around the leeward side of the wing is longer than the windward path. Thus the wind speed on the leeward side increases and that on the windward side is retarded in order that the air get back together in the wake with no discrepancies. According to Bernouilli's law

$$p + \tfrac{1}{2} \rho V^2 = \text{const} \qquad (7\text{-}2)$$

an increase in velocity V must be accompanied by a decrease in pressure p and vice versa. Therefore the pressure on the leeward side of the wing is less than that on the windward side. This pressure difference times the area of the wing is the lift force. The most precise way to view lift production, and the most appropriate way for rotors, is in terms of the *Magnus Effect*, whereby the interaction of a vortex ζ bound in the sail or rotor by virtue of the velocity difference on the two sides interacts with the free-stream wind velocity V to produce a force

$$F_L = \tfrac{1}{2} \rho V_A^2 A C_L$$

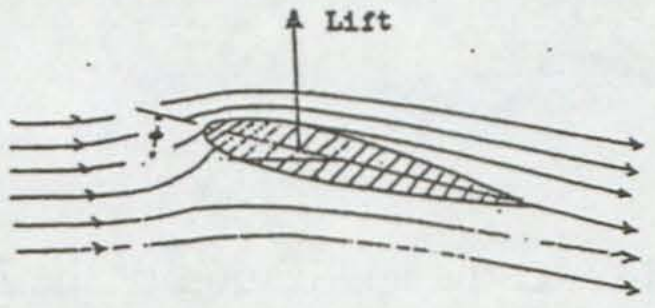

For ideal wing/sail/foil, $C_L = 2\pi\phi$

where ϕ is the angle of attack in radians

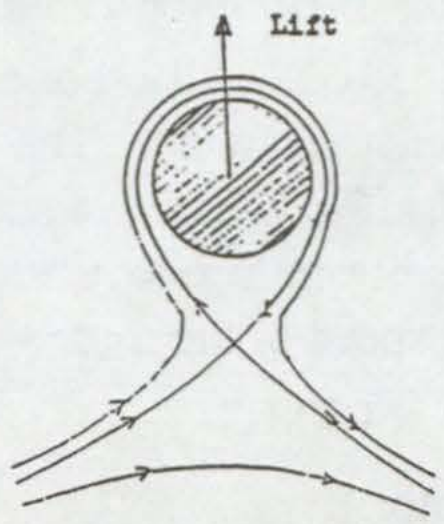

For ideal rotor, $C_L = 2\pi\alpha$

where $\alpha = v/V_A$

Fig. 7-1. Lift production by a wing (or sail or foil) in terms of angle of attack, and by a rotor in terms of velocity ratio.

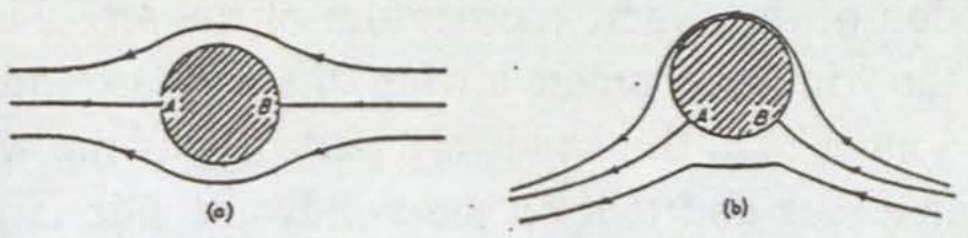

$\alpha = 0$ $\alpha = 1.4$

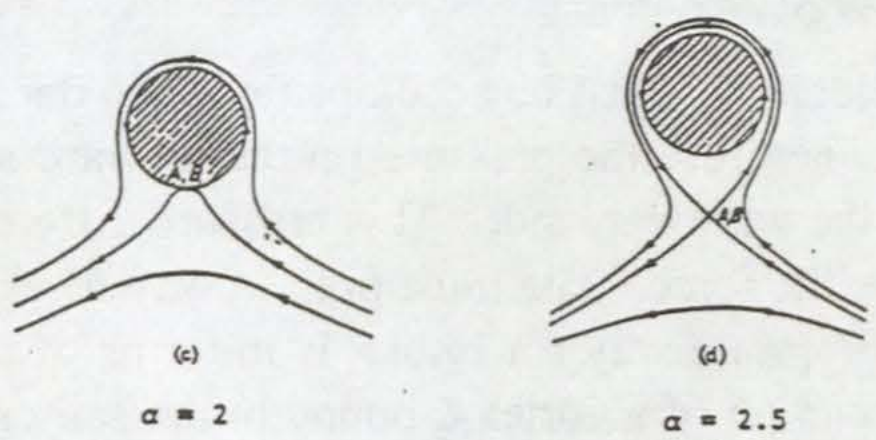

$\alpha = 2$ $\alpha = 2.5$

Fig. 7-2. Streamlines for a cylinder rotating at various circumferential speeds v in a steady uniform flow of velocity V. $\alpha = v/V$.

$$F = \rho V \times \zeta \tag{7-3}$$

perpendicular to both the vorticity and velocity vectors. In order to understand the workings of a rotor, we must first look at the description in terms of ideal flow. The steady uniform wind velocity V is perpendicular to the axis of an infinite circular cylinder of radius *a*, rotating with peripheral speed v. The resultant velocity field in polar coordinates centered on the axis of the cylinder is [7-1]

$$Ur = -V(1 - a^2/r^2)\cos\theta \tag{7-4}$$

$$U_\theta = V(1 + a^2/r^2)\sin\theta + av/r \tag{7-5}$$

This velocity field is depicted in Fig. 7-2 for several values of $\alpha = v/V$. We note that the flow has stagnation points A and B for which $U_r = U_\theta = 0$. We see from Eqs. (7-4) and (7-5) that these stagnation points are given by

$$\begin{aligned} &\text{for } r = a \text{ at all } \theta \\ Ur = 0 \qquad &\text{for } \theta = 90° \text{ and } 270° \text{ at all } r \\ &\text{for } r = a \text{ if } \theta = -\sin^{-1}(\tfrac{1}{2}\alpha) \;;\; \alpha \le 2 \end{aligned} \tag{7-6}$$

$$\begin{aligned} U = 0 \qquad &\text{for } \theta = 270°,\ r/a + a/r = \alpha \;;\; \alpha \ge 2 \end{aligned} \tag{7-7}$$

Thus, for v = 0 there are two stagnation points at r = a, θ = 0° and 180°. As $\alpha = v/V$ approaches 2, these points move along the lower surface of the cylinder and coalesce into a single point at r = a, θ = 270°. For $\alpha > 2$, the stagnation point moves radially away from the cylinder. Its radial location as a function of α is found by solving the second line of Eq. (7-7).

$$r/a = \tfrac{1}{2}[\alpha + (\alpha^2 - 4)^{1/2}] \;;\; \alpha \ge 2 \tag{7-8}$$

The other piece of information that we can glean from ideal flow theory is the lift force on the rotating cylinder. The Magnus force is given by

$$F_L = \rho l V \Gamma \tag{7-9}$$

where ρ is the mass density of the air, *l* is the length of the cylinder, and Γ is the circulation defined by

$$\Gamma = 2\pi av \tag{7-10}$$

The aerodynamic force generated by flow over a wing or sail of projected area A is given by

$$F_L = \tfrac{1}{2}\rho V^2 A C_L \tag{7-11}$$

where C_L is the lift coefficient, which essentially measures the strength of

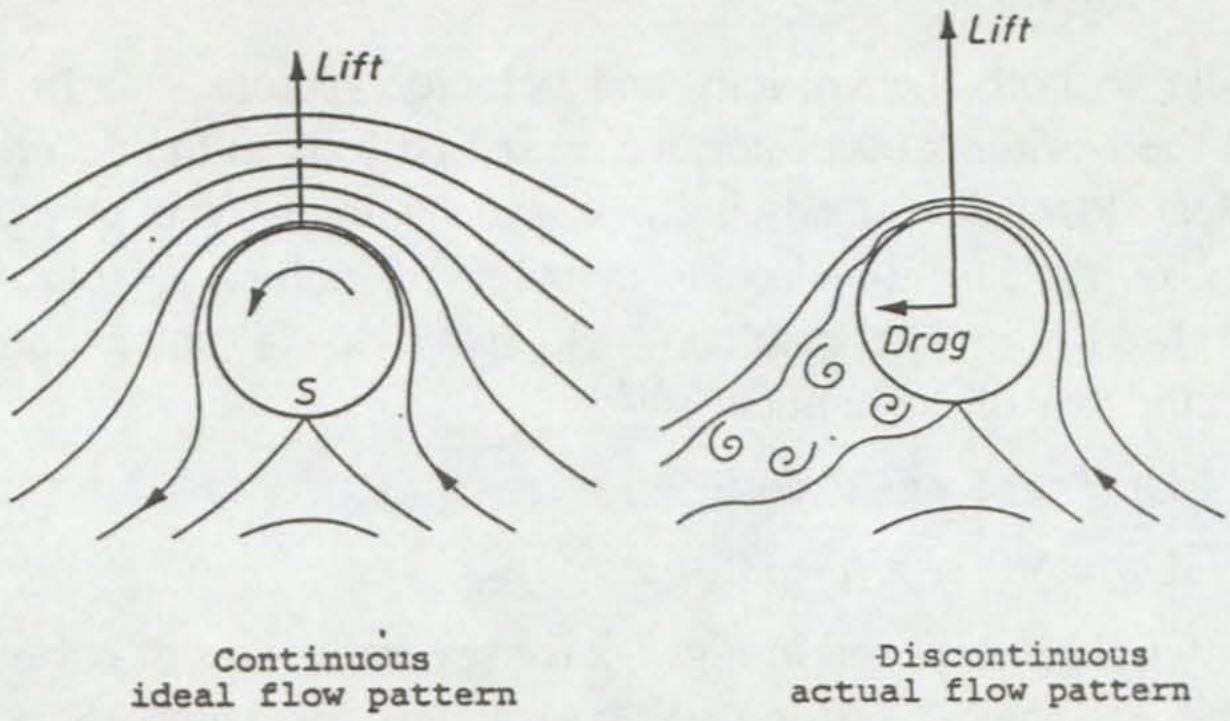

Continuous
ideal flow pattern

Discontinuous
actual flow pattern

Fig. 7-3. Comparison of actual and
ideal flow around a rotating cylinder, $\alpha = 2$.

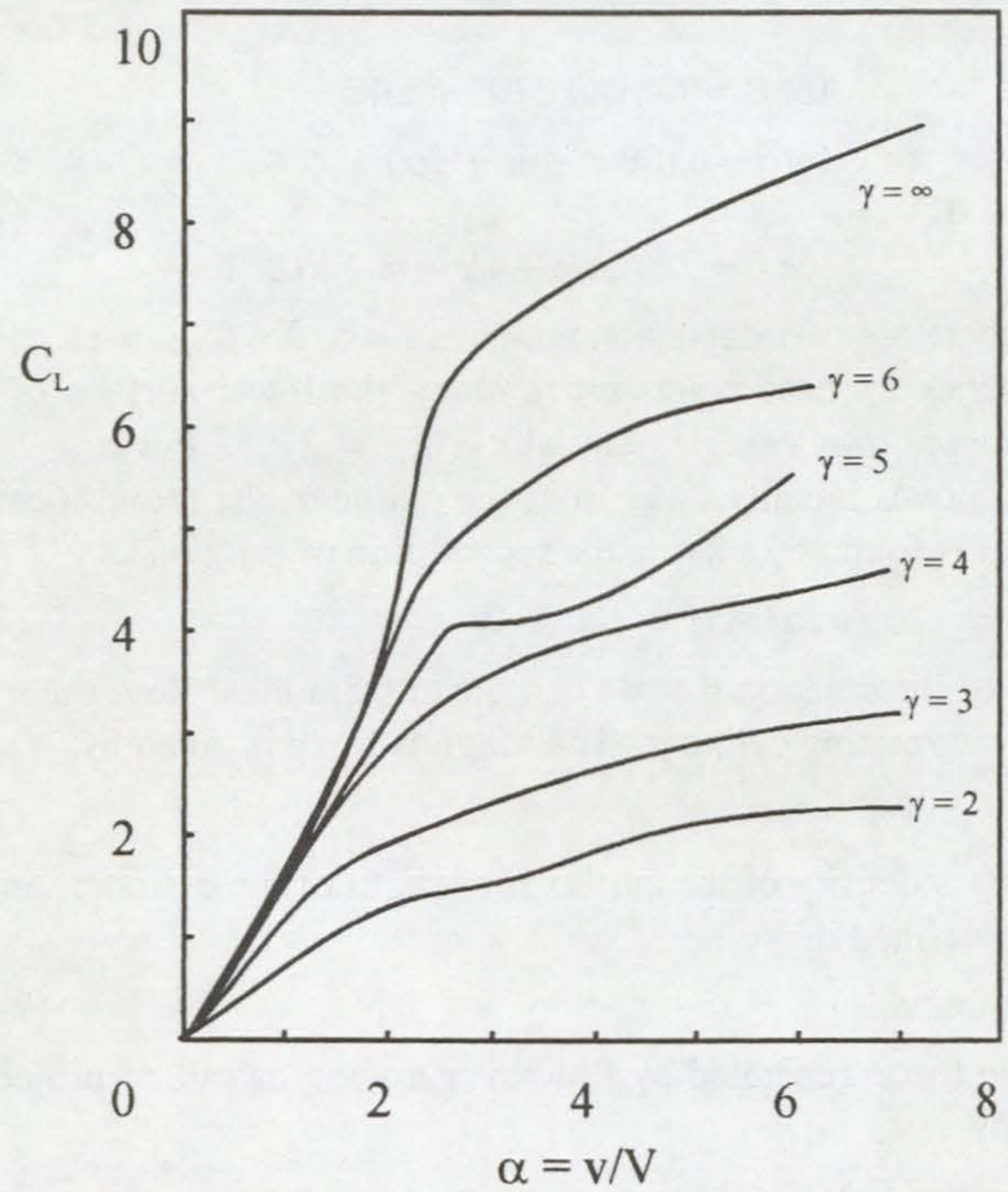

Fig 6 -4 Experimental curves of lift Coefficient C_L as a function of $\alpha = v/V$
for rotating cylinders without fencing, for various aspect ratios $\lambda = ½l/a$

the bound vortex generated by a unit area of the lifting device in question. For the rotating cylinder, A = 2a*l* , and we see by comparing Eqs. (7-9) and (7-11) that the lift coefficient for a rotating cylinder in ideal flow is

$$C_L = 2\pi\alpha \qquad (7\text{-}12)$$

In the real world, the flow is not ideal. Flow separation occurs on the downstream side of the cylinder that reduces the lift coefficient and gives rise to a drag coefficient C_D. This behaviour is depicted in Fig. 7-3[7-2]. The other real-world effect that decreases sail, wing, or rotor performance is axial flow tending to bleed high-pressure air around the end to the low-pressure side and, in effect, to short-circuit the lift production. This is countered by making the lift device as long as possible (high aspect ratio) and/or by retracting dams or fences to inhibit the axial flow.

In Figs. 7-4 and 7-5, we show experimental curves of C_L and C_D as a function of α = v/V for various values of aspect ratio, γ = ½*l*a. In these experiments there were no fences[7-3]. In Figs. 7-6 and 7-7, we show the results of experiments on a cylinder of aspect ratio γ = 12 with fences at both ends having diameter 1 (no fence), 1.5, 2, and 3 times the diameter of the rotor[7-4]. Experiments of this sort established in the 1920's that it would be possible to drive a windship using vertical rotors in place of sails.

In the years 1925-26, the German engineer, Anton Flettener, developed his "rotorship". As a full-scale test following wind tunnel tests at Göttingen, the barquentine *Buckau* had its rig removed and was refitted with two rotors, each about nine feet in diameter and about 60 feet high. Fences of 11 foot diameter were fitted to the upper ends[7-5]. These rotors were driven by DC electric motors at any speed up to 700 RPM in either direction. The weight of the two rotors and their driving plant was 7 tons as compared with a weight of 35 tons for the rig that they replaced. The projected area of the rotors was about one tenth that of the former sailing rig. Since the force on the rotor is a function of α = v/V, the Göttingen experiments predicted that the pressure on the rotors would not increase past a certain limit even if the wind speed were to increase substantially. This prediction was fully borne out in *Buckau's* sea trials. Figure 7-8 shows a) the total force on both rotors when driven at a circumferential speed of 24 m/s and c) when stationary, v = 0. Curve b) shows the force on the bare masts and rigging of the original barquentine rig. Thus we see that Buckau was much less vulnerable in storm conditions with rotors than with the original rig, and with the inherent self-reefing property of the rotors is able to keep sailing under conditions where an ordinary sailing ship would

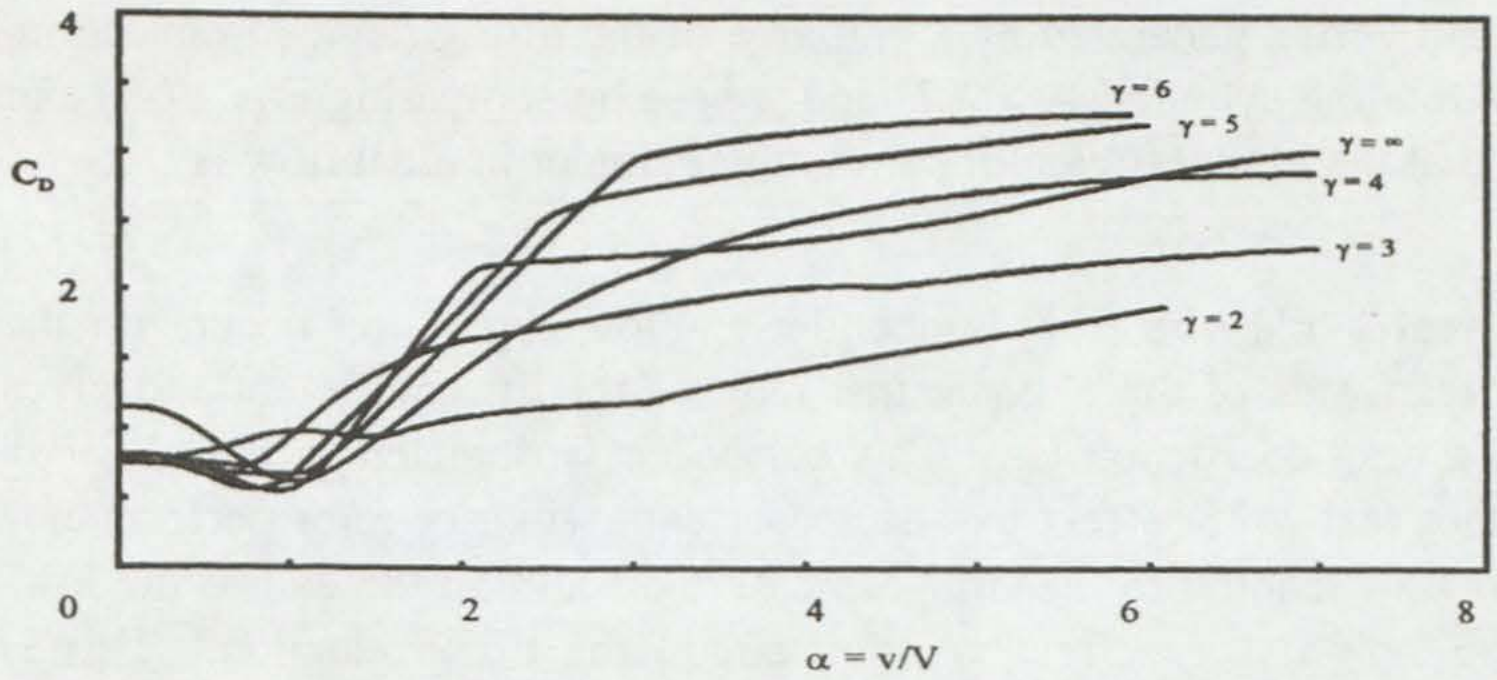

Fig. 7-5. Experimental curves of drag coefficient C_D as a function of α = v/V for rotating cylinders without fencing, for aspect ratios, $\lambda = \frac{1}{2}l/a$

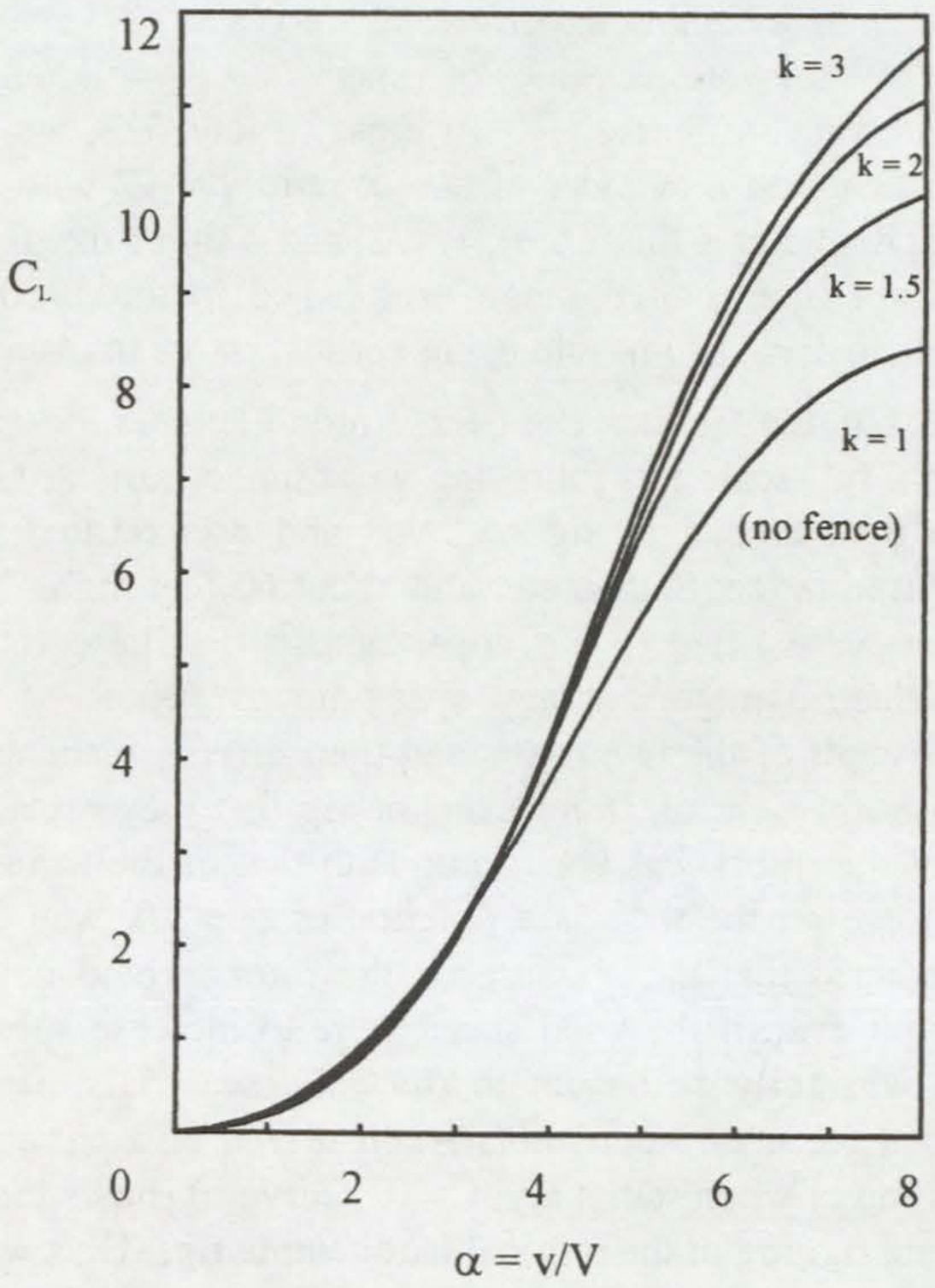

Fig. 7-6. Experimental curves of drag coefficient C_L as a function of α = v/V for rotating cylinders with end fences having radius ratio κ = A/a, where A is the fence radius. Aspect ratio λ = 12 in all cases.

be hove to. Figure 7-9 shows the lift-drag diagram for the rotors and for the original rig. We see that the optimum ratio C_L/C_D is about 3.6 for the rotors and for the original rig. This ratio, as we have seen, measures the ability of the ship to point into the wind. Thus the rotors offered no improvement on the original rig for sailing to windward. That, and the availability of cheap fossil fuel and efficient energy transfer via the screw propeller doomed Flettner's effort to revitalize commercial sail.

This is essentially where the rotor application to marine propulsion rests, unimproved since the 1920's. The idea was reconsidered during the oil shortage of the 1970's, but was dropped along with all other schemes to reintroduce commercial sail in the wake of the subsequent decline in the price of oil[7-3,6,7]. In the experimental work performed on rotors in the 1930's, there lay a missed opportunity, however. Between 1926 and 1934, a Scottish engineer, Alexander Thom, carried out a vast program of investigations on rotating cylinders[7-8]. In his last paper[7-9], he showed that it is possible to devise fencing sufficiently effective to enable lift- to-drag ratios of over 30 to be attained. Instead of using fences only at the ends, Thom built a model rotor with discs of three times rotor diameter spaced every 0.75 rotor diameters. The overall aspect ratio was 12.5. The lift and drag coefficients obtained with this configuration are plotted in Figs. 7-10 and 7-11 together with curves for a rotor of aspect ratio 12 having end fences of three rotor diameters [taken from Figs. (7-6) and (7-7)], and the lift curve for ideal flow from Eq. (7-12). We see that fencing along the entire length of the rotor entirely changes the flow pattern from that experienced in the case of end fencing only. On the lift curve (Fig. 7-10), we see that the slope is much closer to the ideal, and on the drag curve (Fig. 7-11), we see that the minimum of the drag advances from α = 2-3 typical of end fencing only, to α = 5. No amount of fencing affects the phenomenon of flow separation on the downstream side of the cylinder, however the flow separation is less for the higher values of α that are permitted by the Thom fencing configuration. It is certain Thom fencing is much more effective in reducing axial flow than is end fencing only. This implies that the Thom configuration may be relatively insensitive to changes in aspect ratio.

Thom's data predicts a much higher maximum lift-to-drag ratio than is attainable with unfenced rotors or with rotors fenced only on the ends. This is shown in Fig. 7-12 wherein we display the lift-drag curve for a range of rotors having various aspect ratios and fence-to-rotor diameter ratios. For rotors with end fencing only, L/D varies from 1.45 for a short

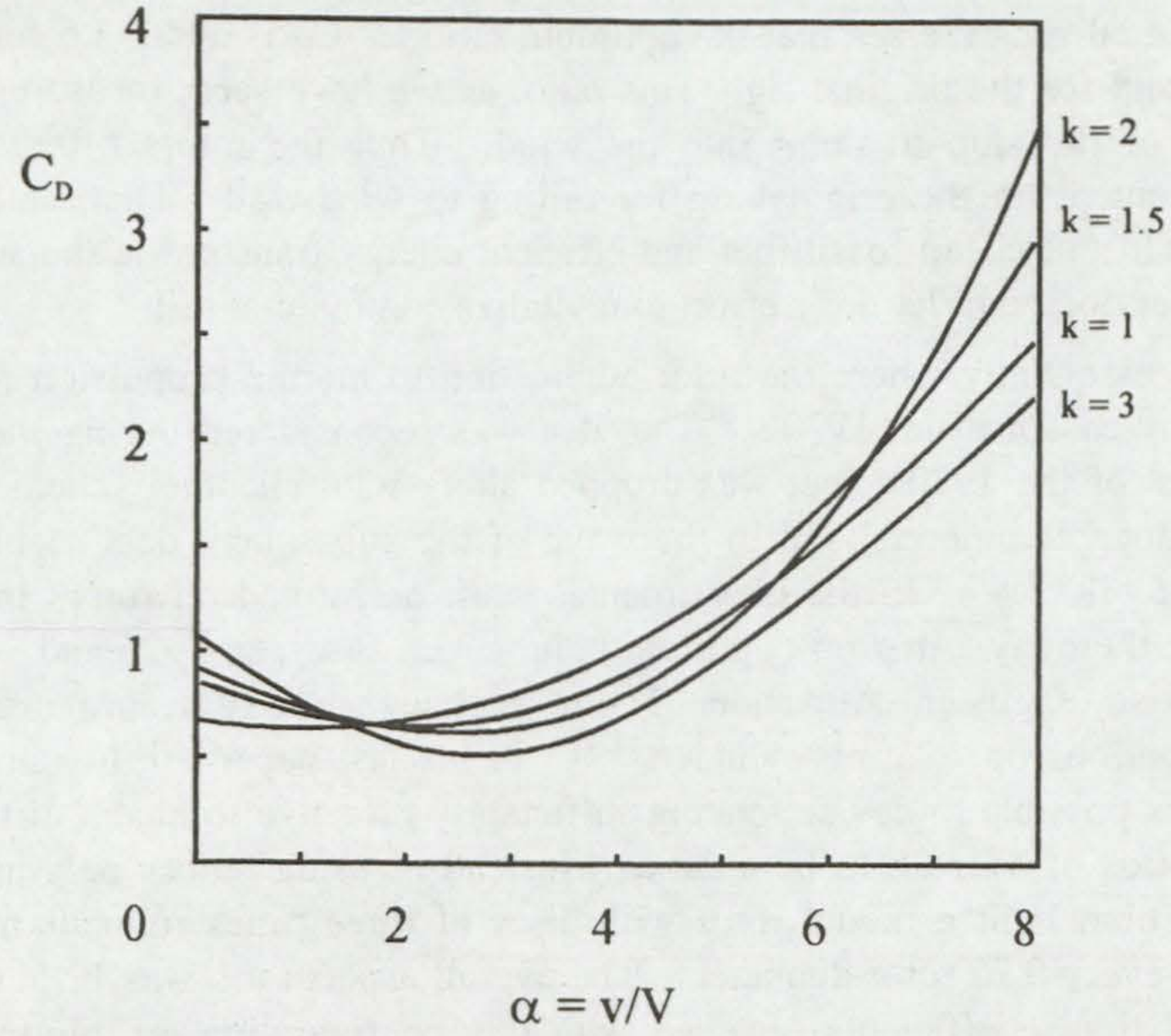

Fig. 7-7. Experimental curves of drag coefficient C_D as a function of α = v/V for rotating cylinders with end fences having radius ratio κ = A/a, where A is the fence radius. Aspect ratio λ = 12 in all cases.

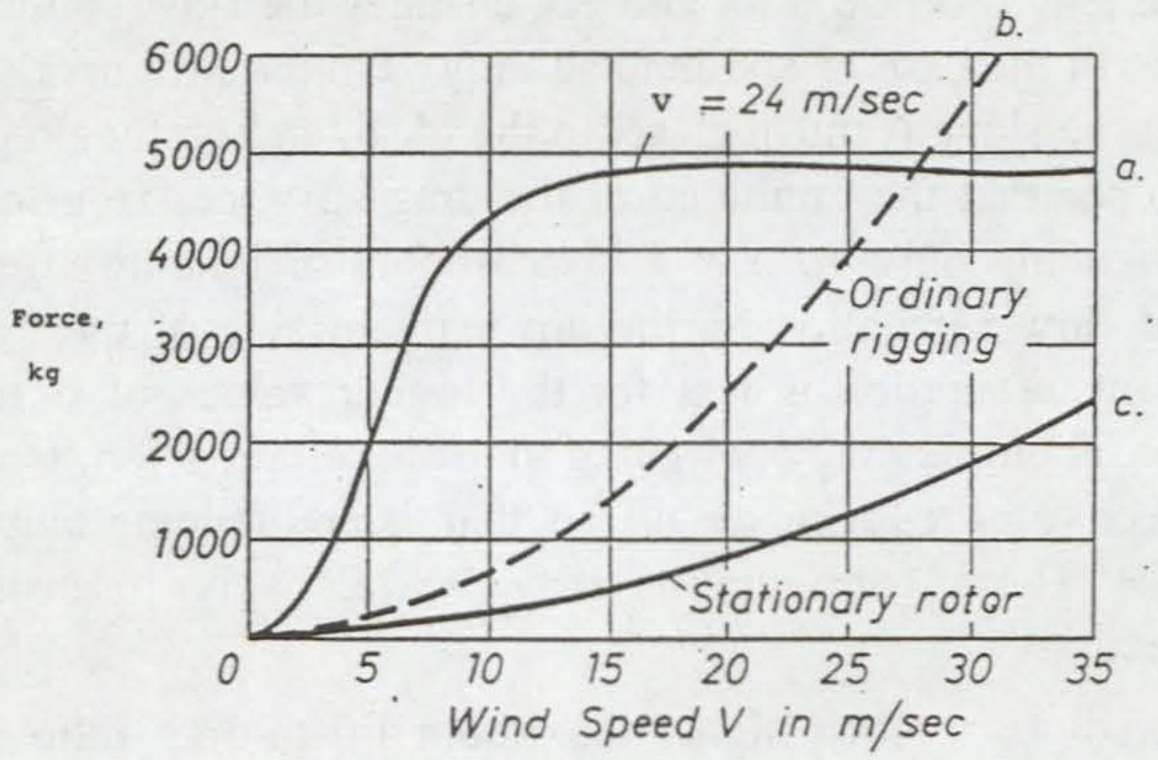

Fig. 7-8. Total force on a) *Buckau's* rotors when driven at circumferential speed 24 m/s and c) when stationary, both plotted as a function of wind speed V. Curve b) shows the drag of the bare spars and rigging of *Buckau's* former barquentine rig [7-2].

($\lambda = 2$) rotor with no fence ($\kappa = 1$) to L/D = 6 for $\lambda = 12$, $\kappa = 3$. The configuration of Thom[7-9], with $\kappa = 3$ fences spaced every 0.75 rotordiameters is fundamentally different in its flow pattern. Whereas drag begins to increase at $C_L \leq 2$ for rotors with end fencing only, the Thom rotor achieves CL > 16 before fencing action breaks down and C_D begins to increase. The optimal L/D increases from 6 to 35 for the same aspect ratio! Apparently end fences alone are not able to prevent axial flow for $C_L > 2$, however the distribution of fences in the Thom rotor is quite effective in circumventing axial flow up to much higher values of C_L. It seems likely that the onset of drag increase coincides with that value of α for which the stagnation line A,B moves past the rim of the fence at r = 3a (see Fig. 7-2). Why then, in view of these measurements, have Thom rotors not been applied to ship or yacht propulsion? The answer has to do with Thom's assessment of the power required to turn the rotor. It is evident upon examination of [7-9] that Thom made a scaling error·that unduly prejudiced his evaluation of the applicability of the results.

Since the power required to turn the rotor at speed υ (revs per sec) is simply related to the torque, N

$$P_R = 2\pi\upsilon N \tag{7-13}$$

the problem of determining P_R is resolved by determining the torque. Using the Newton relation[7-10]

$$N = -\mu \int_0^{2\pi} [\partial U_\theta/\partial r]_{r=a} a^2 \ell d\theta \tag{7-14}$$

where μ is the viscosity of air, Eq.(7-5), and the definition of *Reynolds number*

$$R_e = \frac{2\rho V a}{\mu} \tag{7-15}$$

we find for the torque required to rotate a cylinder of length *l* and radius a at speed υ in a wind of speed V for the case of ideal flo

$$N = \rho\upsilon V l (2a)^3 (\pi^2/R_e) \tag{7-16}$$

where ρ is the mass density of air.

Thom measured the torque required to turn his model rotor in terms of a torque coefficient k_q defined by

$$N = \rho\upsilon V \ell (2a)^3 k_q \tag{7-17}$$

Thom's measured values of k_q are given in Table 7-1. Using these data, we

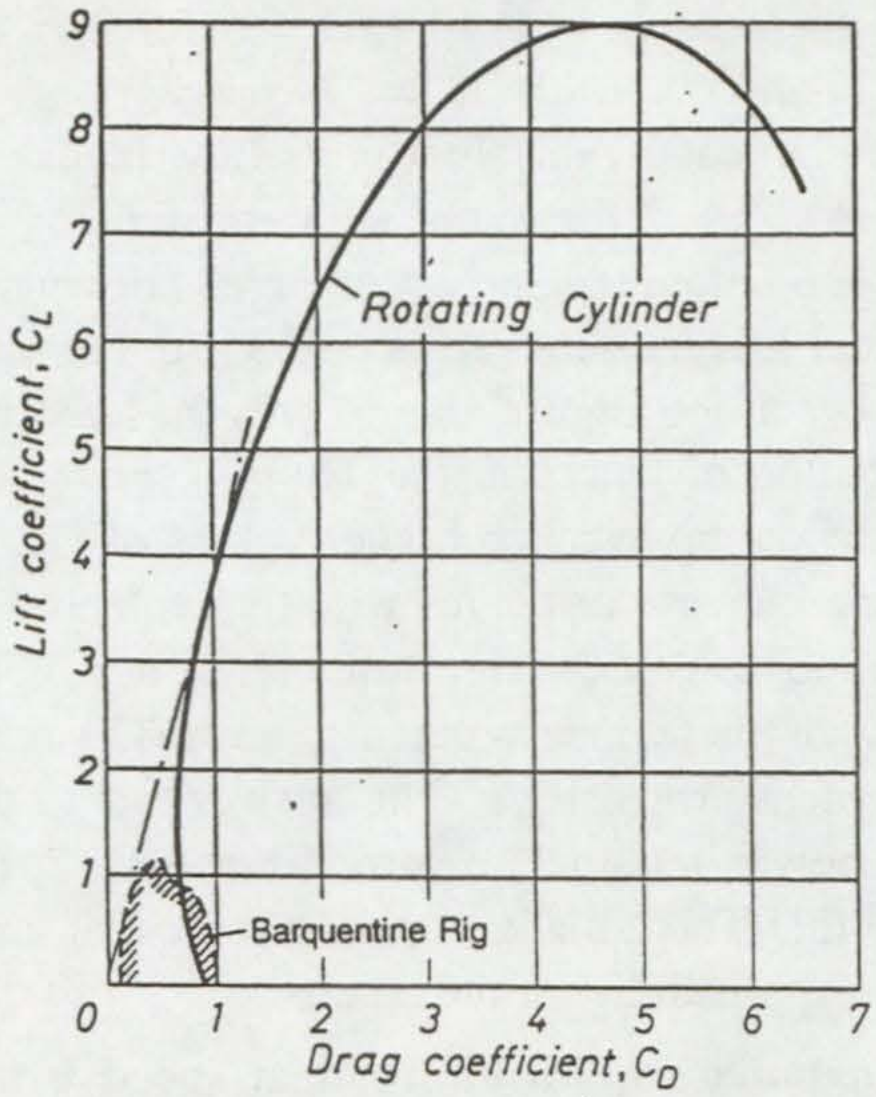

Fig. 7-9. Lift-drag plot for *Buckau's* rotors and for the former barquentine rig [7-2].

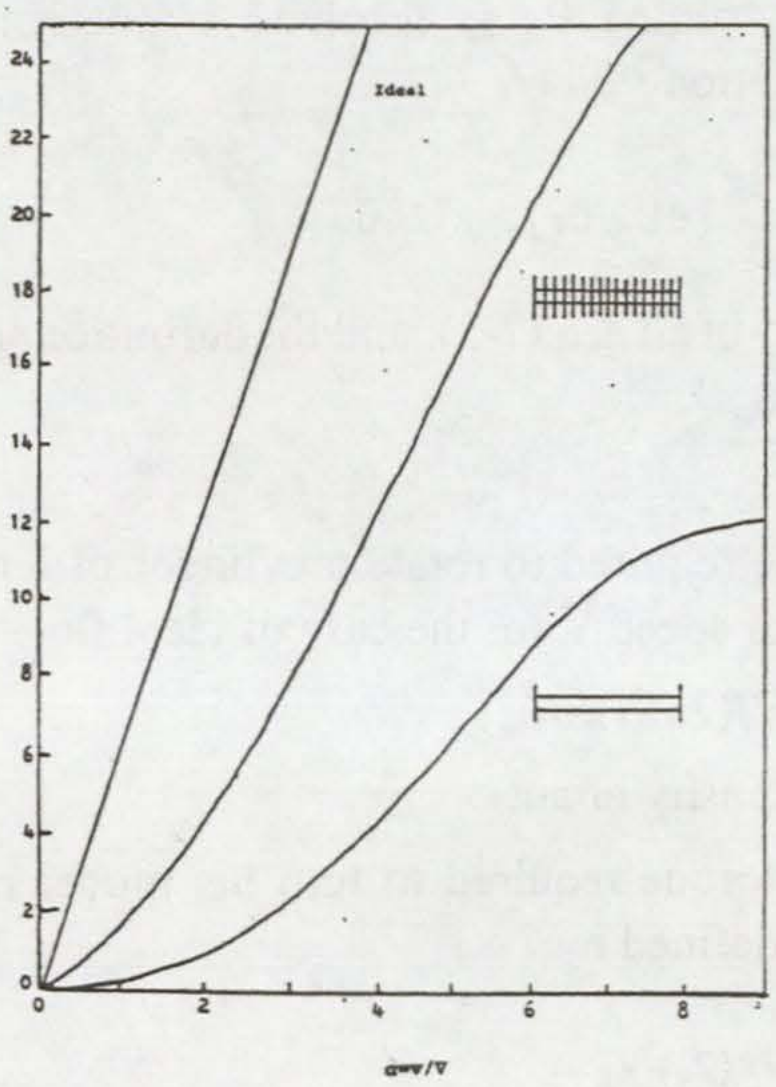

Fig. 7-10. Lift coefficient CL versus $\alpha = v/V$ for ideal flow, the Thom rotor, and for a rotor of $\lambda = 12$, $\kappa = 3$ having only end fences.

can derive an empirical equation for k_q (which Thom did not do) in order to scale the results

$$k_q = 2137 \frac{\upsilon^{0.3561}}{R_e^{0.8873}} \qquad (7\text{-}18)$$

that we may compare with the theoretical result for ideal flow obtained by equating Eqs. (7-16) and (7-17)

$$k_{q,ideal} = \pi^2/R_e \qquad (7\text{-}19)$$

In order to show that Eq. (7-18) is consistent with Thom's measurements, we plot it in Fig. 7-13 and display the data points from Table 7-1.

Using Eqs. (7-13), (7-15), and (7-18) and expressing the length of the rotor in terms of the aspect ratio $\lambda = \frac{1}{2}l/a$, we produce an expression for the power (in horsepower, 550 ft-lb/s) required to turn a rotor of projected area $A_R = 2al$, aspect ratio λ, at speed ratio $\alpha = v/V$ in a wind of speed V_A

$$P_R = 6.14 \times 10^{-6}\, V_A^{2.47}\, A_R^{0.379}\, \lambda^{0.621}\, \alpha^{2.36} \text{ (hp)} \qquad (7\text{-}20)$$

where we have used $\rho = 2.38 \times 10^{-3}$ slugs/ft^3 and $\mu = 1.22 \times 10^{-5}$lb/(ft/s) [7-11]; V_A is in knots and A_R is in ft^2.

Thank you for sustaining your interest through this tedious discussion of power requirements. It was necessary in order to establish with certainty my conviction that Thom failed to exploit his discovery owing to scaling error. In his paper he calculates the example of a rotor one foot in diameter, 12 feet long, fitted with 3 foot diameter discs every 9 inches. He further assumes $\alpha = v/V = 6$, with $v = 600$ ft/s and $V = 100$ ft/s, $\upsilon = 191$ revs/s for which he assumes $k_q = 4.1$. If we look at Table 7-1, we see that he took the value of k_q appropriate to $\alpha = 6$, neglecting the fact that this is only true for his model rotor with $\upsilon = 72.3$ revs/s and Re = 6300. Thom then calculates using Eq.(7-17) that the power required is **4830 horsepower** and for this reason drops the whole scheme. This error amounts to a total neglect of the scaling laws. The appropriate value of Reynolds number for his example is 6.25×10^5 for which we calculate using Eq. (7-18), $k_q = 0.099$ and a power requirement of about 118 hp, which is intuitively much more reasonable.

In order to clinch the argument, I built a Thom rotor 6 inches in diameter, 38 inches long, and turned it at 3600 RPM ($\upsilon = 60$ revs/s) using a 1/3 hp electric motor. The power requirement predicted by Eq. (7-20) is about 0.3 hp; Thom would have predicted about 25 hp.

We now want to find the criteria for rotor design with the aim to make the

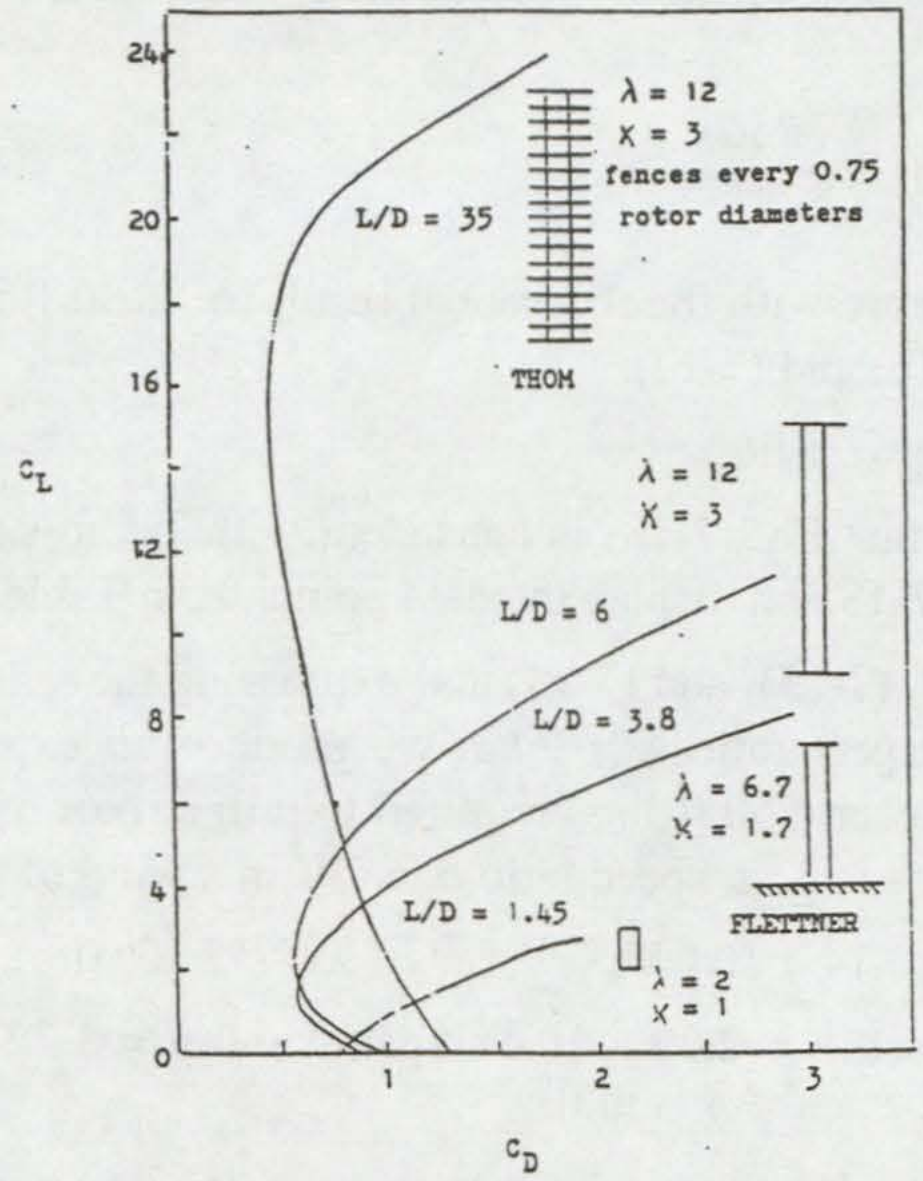

Fig. 7-11. Drag coefficient C_D versus $\alpha = v/V$ for the Thom rotor and for a rotor of $\lambda = 12$, $\kappa = 3$ having only end fences. Ideal flow produces no drag.

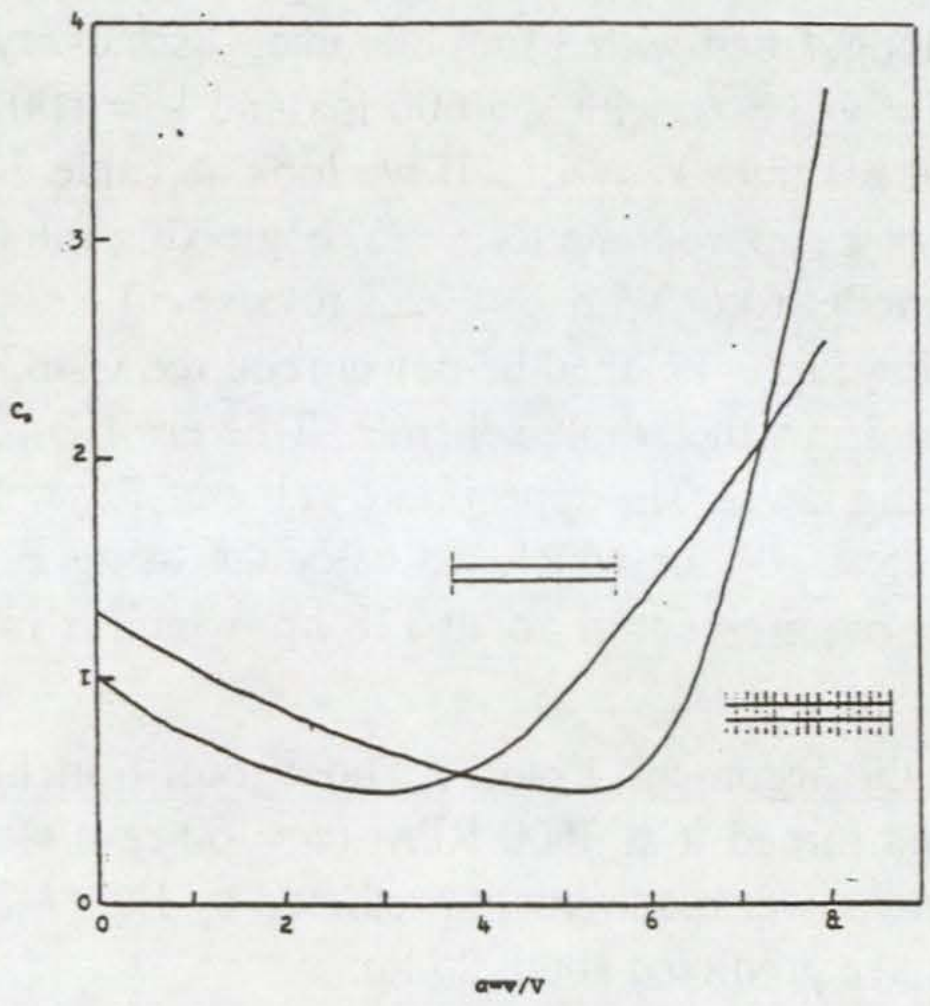

Fig. 7-12. Lift-drag plot for rotors.

power output to power input ratio P_p/P_R as large as possible consistent with other design requirements, and second, to see if trans-ocean voyaging ispractical from the point of view of the input power requirement. Going back to Eq. (7-20) for the rotor power, we will for simplicity evaluate for a course angle $= 90°$ for which

$$V_A = (V_B^2 + V_T^2)^{1/2} = V_B(1 + X^{-2})^{1/2} \tag{7-21}$$

From chapter 2, we take Eq. (2-21) for X with $\gamma = 90°$ in the form

$$\frac{A_R L}{W} = \frac{8.4X^2}{[C_L - XC_D][X^2 + 1]^{1/2}} \tag{7-22}$$

Equations (7-21) and (7-22) can be used to eliminate V_A and A_R from Eq. (7-20), and with a little algebra we find

$$\frac{V_B}{P_R^{0.405}} = \frac{93.5[L/W]^{0.153}}{\lambda^{0.251}} [(C_L - XC_D)^{0.153}X^{0.694}] / [\alpha^{0.955}(X^2 + 1)^{0.424}]$$

$$= \frac{93.5[L/W]^{0.153}}{\lambda^{0.251}} f(\alpha,X) \tag{7-23}$$

which we would like to maximize for any application where input power is limited. Note that $A_R L/W$ as given by Eq. (7-22) is a function of α (which entirely determines C_L and C_D) and X. The function f defined in Eq. (7-23) is also a function only of α and X. We see that $A_R L/W$ increases with decreasing α (lower C_L), and increases with increasing X. In order to discuss the function f, which is not so intuitive, we need to see how C_D depends on α for a Thom rotor mounted on a realistic multihull yacht. In chapter 4, we saw how the section characteristic c_d is transformed via the Lanchester-Prandtl equations for finite aspect ratio. There is no direct equivalent to this process for rotors, however we have seen experimentally how rotor characteristics vary with aspect ratio and fence radius ratio ; the Thom configuration presumably has characteristics that are more or less aspect ratio independent. In order to take the parasitic drag of the hull and superstructure properly into account, we need to define the net drag coefficient of everything above the water

$$C_D = (A_R C_{D0} + A_p C_{Dp})/AR \tag{7-24}$$

where C_{D0} is the drag coefficient of the rotor alone, A_p is the parasitic area of the hull and superstructure, and C_{Dp} is the drag coefficient of the hull and superstructure ($C_{Dp} \approx 0.3$). For soft sails, $0.1\ A_s \le A_p \le 0.25\ A_s$. For wingsails, $0.2\ A_s \le A_p \le .5\ A_s$. For rotors, being so compact, $0.8\ A_R \le A_p$

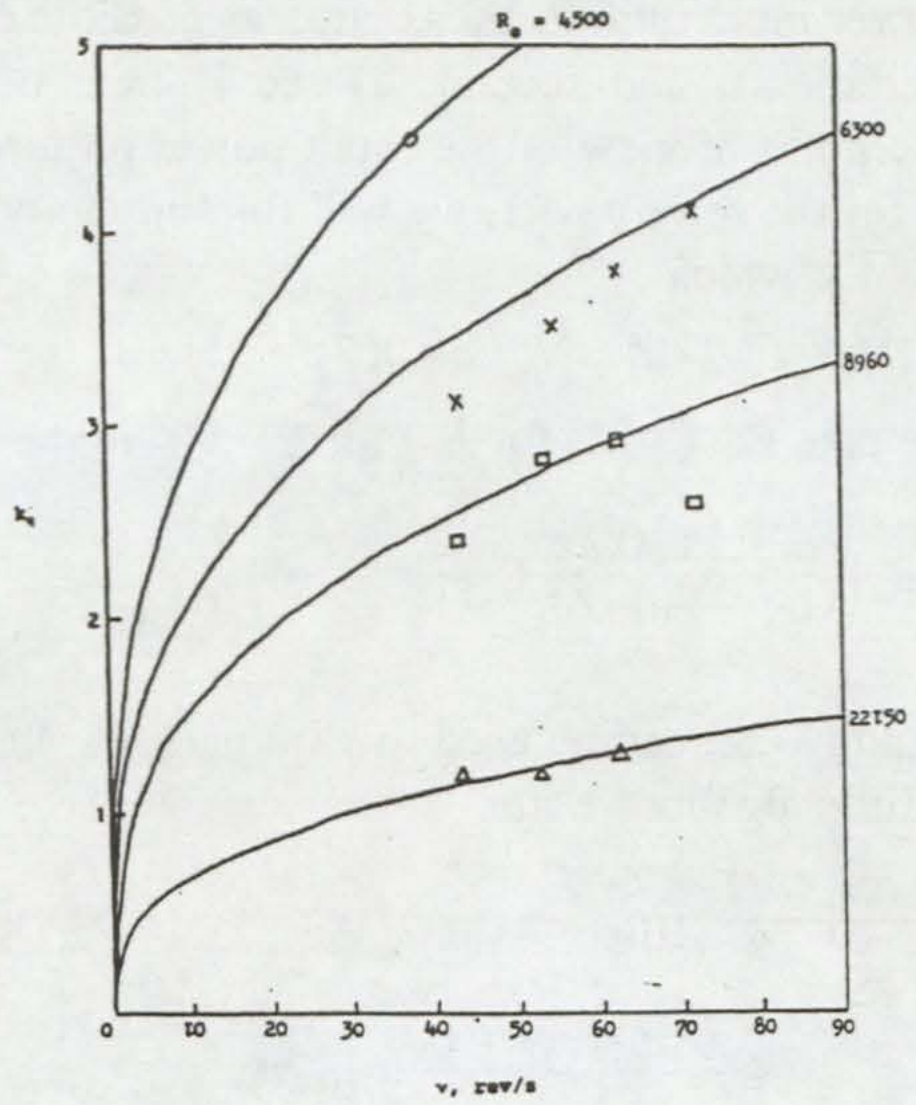

Fig. 7-13. Curves of torque coefficient kq calculated using Eq. (7-18) on which are plotted Thom's experimental points.

v rev/s	a = v/V	Re	kq
88.6	4.6	4500	4.5
62.6	7.5	4500	5.2
72.3	8.6	4500	5.2
43.4	3.6	6300	3.1
55.4	4.6	6300	3.5
62.6	5.2	6300	3.8
72.3	6.1	6300	4.1
43.4	2.6	8960	2.4
53.3	3.3	8960	2.8
62.6	3.7	8960	2.9
72.3	4.3	8960	2.6
43.4	1.0	22150	1.2
53.0	1.3	22150	1.2
62.6	1.5	22150	1.3

Table 7-1. Torque coefficients from Thom [7-9]

f

X α	2.50	4.00	5.50	7.00
0.50	.304	.217	.171	.141
0.75	.364	.261	.206	.170
1.00	.397	.286	.226	.186
1.25	.414	.299	.237	.195
1.50	.421	.306	.243	.199
1.75	.422	.309	.246	.201
2.00	.420	.309	.247	.201
2.25	.415	.308	.246	.201
2.50	.409	.307	.245	.199
2.75	.403	.304	.243	.198
3.00	.395	.301	.242	.196

$A_R L/W$

X α	2.50	4.00	5.50	7.00
0.50	.343	.167	.106	.083
0.75	.725	.342	.216	.170
1.00	1.20	.547	.343	.274
1.25	1.75	.771	.479	.386
1.50	2.37	1.01	.620	.505
1.75	3.07	1.25	.763	629
2.00	3.86	1.50	.910	.758
2.25	4.75	1.76	1.06	.893
2.50	5.78	2.04	1.21	1.03
2.75	6.97	2.32	1.36	1.18
3.00	8.39	2.61	1.52	1.33

Table 7-2 Tabulation of f and A_R L/W as a function of α and X for γ = 90° and $A_R = A_p$.

$\leq 1.2\ A_R$. Thus the more compact the rig, the higher the inherent L/D has to be in order that the ratio not be spoiled by parasitic drag. Figure 7-14 gives a tabulation and plot of the net L/D for a Thom rotor mounted on a yacht for which $A_R = A_p$. We see that $\alpha < 2.5$ does not give adequate L/D, nor does $\alpha > 8$. The choice in this range $2.5 \leq \alpha \leq 8$ is dictated by the power available and the rotor size limitations. The rule of thumb to keep in mind is that for a given force output, it takes less input power to turn a large rotor slowly (low α) than to turn a small rotor rapidly. Using the data of Fig. 7-14, we can now survey the function $f(\alpha,X)$ in Eq. (7-23). We can see that f increases monotonically with decreasing α, and we find that f initially increases with increasing X and has a weak maximum for $1.75 < X < 2$. A tabulation of f and A_RL/W as a function of α and X is given in Table 7-2.

The power output of the rotor to propulsion can be calculated using the hull drag relation Eq. (2-6) as

$$P_p = 8.78 \times 10^{-5} (W/L) V_B^3 \qquad (7\text{–}25)$$

in horsepower, with V_B in knots. Then, using Eq. (7–23), we find for the power output to power input ratio

$$P_p/P_R = 6.46\ [W/(L\lambda)]^{0.62}\ f^{2.47}\ V_B^{0.53} \qquad (7\text{–}26)$$

for which the dominating factor is f. Now let us look at three widely varied examples of the application of rotors to see how the method works in practice.

The first is a human-powered proa, for which we will assume L = 20 ft, W = 300 lbs. Since input power is very limited, we must maximise f above all other considerations. We therefore choose $V_B/V_T = X = 1.25$ and $\alpha = 2.5$ from which we find A_RL/W (hence A_R) and f with the use of table 7–2. We will assume that the Thom fencing configuration is essentially independent of aspect ratio and so we are free to use a suitable low value of λ, say 3 (λ comes in multiples of 0.75) This gives $V_B/P_R^{0.405} = 19.4$ (V_B = 19.4 knots for 1 hp input); the rotor is 2ft 11in in diameter and 8ft 10in tall. It has the same power as a $105ft^2$ conventional sail.

Dropping our limitation to $\gamma = 90°$, we use Eq. (2–21) and a generalised version of Eq. (2–23) to ascertain the performance of our pedal-driven rotor-proa on all courses. In Fig 7–15, we present a polar plot of performance in 8, 12, 16 knots of true wind. These curves assume a constant $\alpha = 25°$; the performance dead down wind could actually be improved by not pedalling at all since the drag at $\alpha = 0$ is larger than the drag at $\alpha = 2.5$. With a pedal-powered rotor, it is of even greater interest to

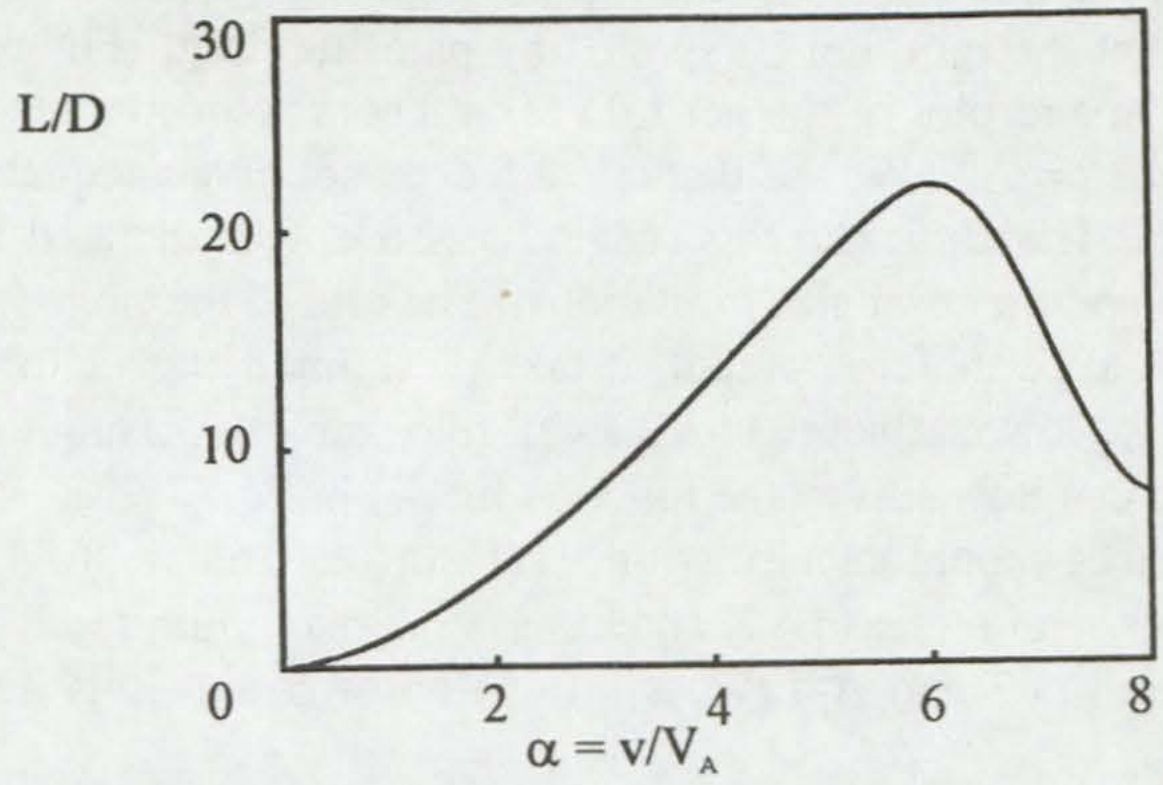

α	0.50	1.00	1.50	2.00	2.50	3.00	3.50	4.00	4.50	5.00	5.50	6.00	6.50	7.00	7.50	8.00
C_L	0.75	1.70	2.80	4.30	6.00	7.80	9.70	11.7	13.8	15.9	18.1	20.0	21.8	23.6	25.0	26.3
C_{DO}	1.17	1.05	0.95	0.84	0.75	0.67	0.60	0.55	0.51	0.50	0.49	0.63	0.97	1.59	2.45	3.64
C_D	1.47	1.35	1.25	1.14	1.05	0.97	0.90	0.85	0.81	0.80	0.79	0.93	1.27	1.89	2.75	3.94
L/D	0.51	1.26	2.24	3.77	5.71	8.04	10.8	13.8	17.0	19.9	22.9	21.5	17.2	12.5	9.09	6.68

Fig. 7–14. Lift and drag coefficients and their ratio for a Thom rotor mounted on a realistic multihull.

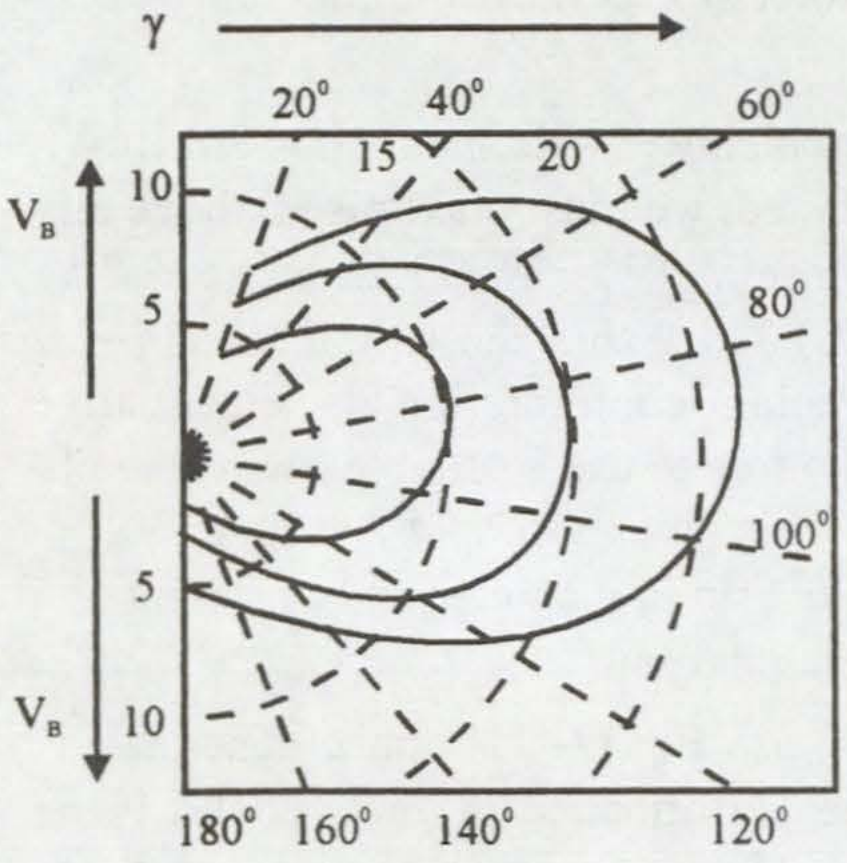

Fig. 7–15. Polar plot of boat speed versus course angle γ for 8, 12 and 16 knots of true wind for the pedal-powered rotor-proa.

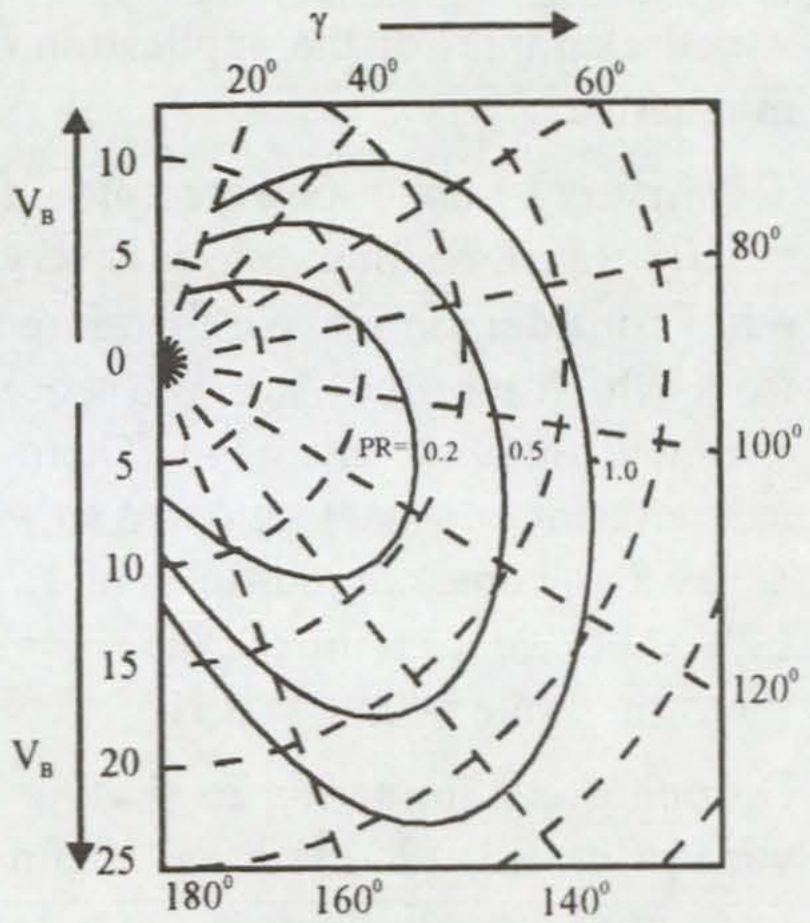

Fig. 7–16. Polar plot of boat speed versus course angle g for a constant rotor power input of 0.2, 0.5 and 1hp for the pedal-powered rotor-proa.

use our generalised version of Eq. (7–23) to plot V_B curves of constant input power: 0.2 hp, which an average fit person can deliver for an hour or more; 0.5 hp, which the average person can sustain for a minute or two; 1hp, which an Olympic cyclist can deliver for a 1-minute burst. These curves are shown in Fig. 7–16. With the proa configuration and a compact rotor with low centre of effort, none of the speeds in Fig. 7–15 and 7–1 6 are limited by righting moment. We see as one might expect, that pedalling to windward is hard work owing to the large values of V_A and consequent high rotor speeds. Very high speeds can be attained on a broad reach with modest power input if there is enough wind available. On such a course, about 35 times more power is delivered to propulsion than is required for input. A pedal-powered rotor-proa of this type is shown in Fig 7–17.

Obviously , human pedal power is an attractive as a means of supplying the rotor. For larger craft, what about electric power in the form of a DC motor? This is continuously variable in speed and easily reversible, which is required for a rotor power plant. The problem is that electric motors are only about 35% efficient and are very heavy for their power out put. The same problems that are at present being addressed for electric automobiles also apply to electric rotor power. for canal boats with electric power, the rotor may offer a means to multiply the power output with some help from the wind. For offshore work we are stuck with the weight problem, and the fact that one cannot plug into the mains for an overnight charge.

What about using a windmill to generate the needed power? Using the windmill equations of chapter 5, we can show that the required windmill area A_1 is typically of the order of several times larger than the rotor area A_R, and the windmill drag is several times that of the rotor. Thus windmill power for rotors is not an attractive proposition.

This leaves the obvious, if somewhat distasteful, option of using a modern light turbo-diesel to drive a closed loop hydraulic pump-motor system, which in tern drives the rotor. Hydraulics allow the speed to be varied continuously from full speed in one direction through zero to full speed in the other direction. One must then ask if, from the point of view of fuel consumption, trans-ocean voyaging is a viable possibility. On the assumption of a diesel power source consuming one gallon of fuel per hour per 40 horsepower, we can calculate the miles sailed per gallon of fuel used as

(7–27)

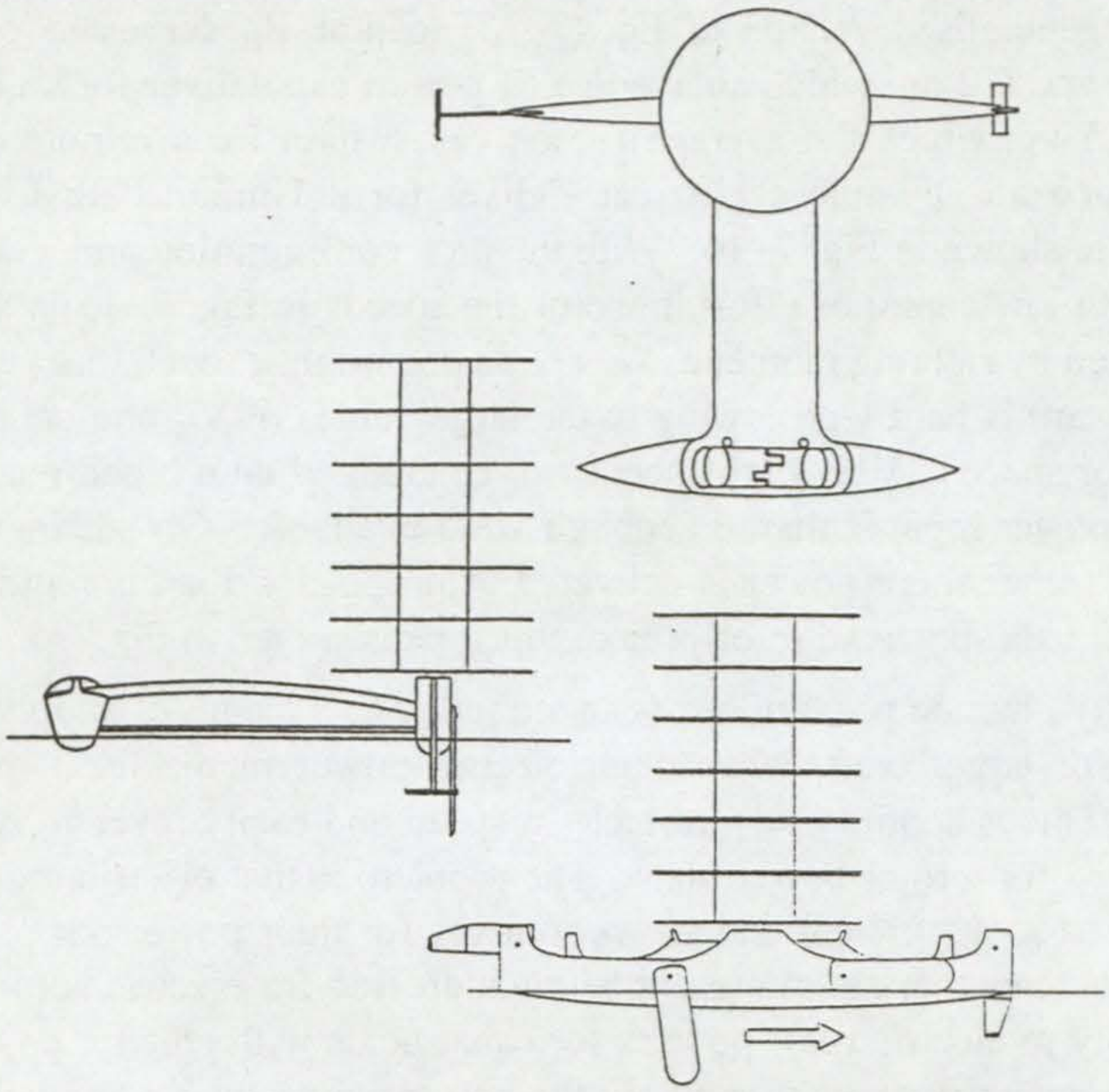

Fig. 7–17. A pedal powered rotor-proa of the type described in the text

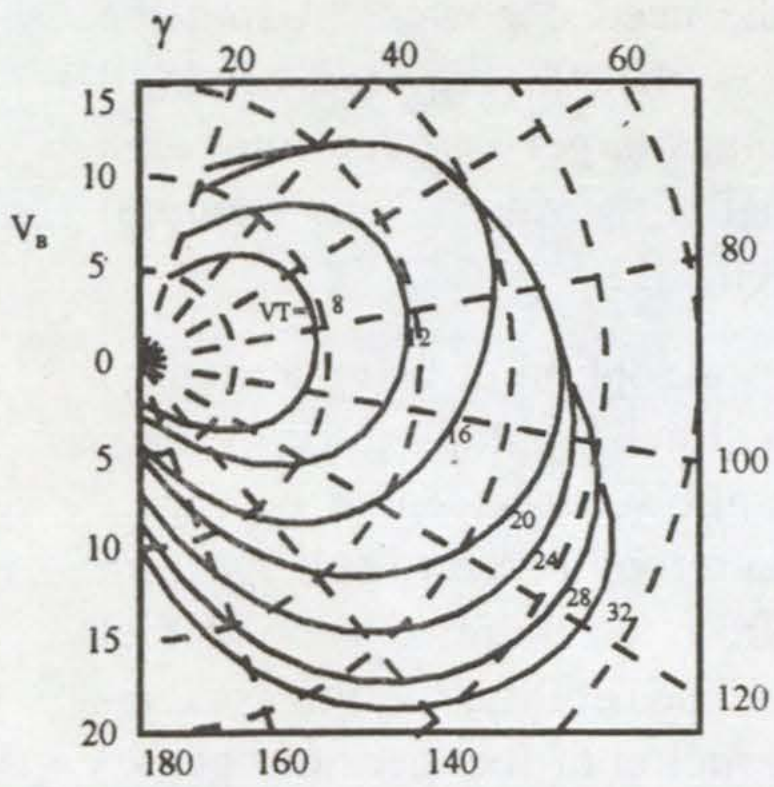

Fig. 7–18. Polar plot of boat speed versus course angle γ for various true wind speeds for the 50-foot catamaran described in the text.

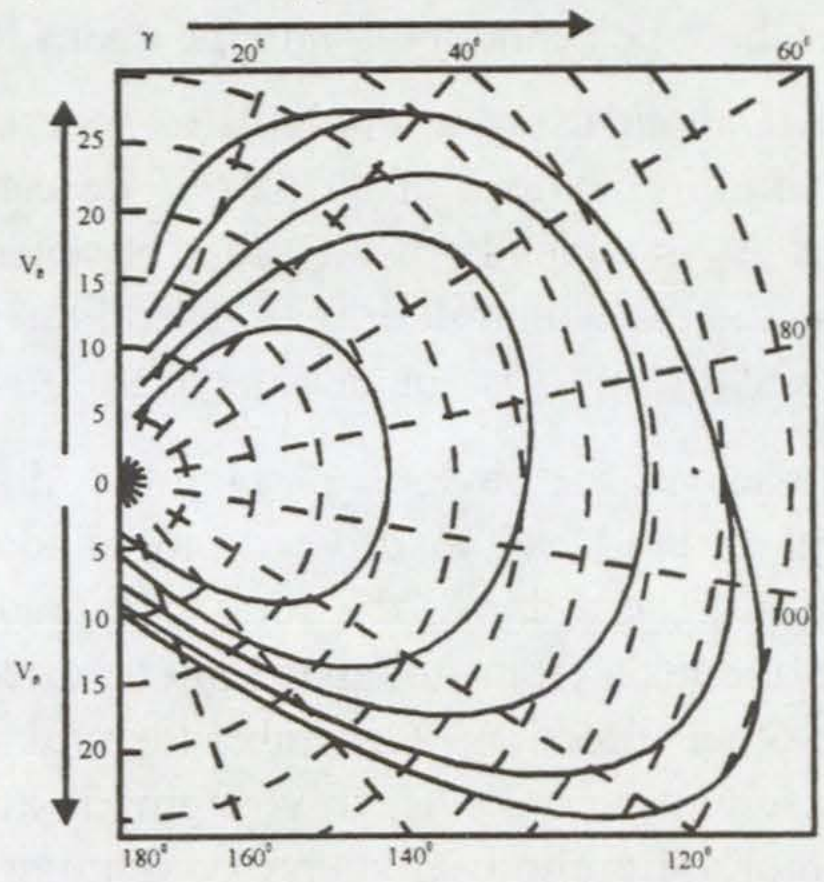

Fig. 7–19 Polar plot of boat speed versus course angle γ for various true wind speeds for the 120-foot proa described in the text.

where V_B is in knots and W and L are in pounds and feet respectively. Again, we see that the function f is the dominant factor. In the light of these observations, we consider a second example: a 50-foot cruising catamaran with lavish accommodation, such that the displacement is not less than 24,000 pounds. Can the use of a rotor on this yacht give high performance? Let us require X = 1.25 at $\gamma = 90°$, which would certainly not be possible with any reasonably sized conventional sail rig. Further, we select $\alpha = 7.0$ and $\lambda = 4.5$ in order to keep the rotor small and the centre of effort low. In 10 knots of wind, this yacht will make12.5 knots at $\gamma = 90°$ and will do 37 nautical miles for each gallon of diesel fuel consumed. The rotor will be about 29 feet tall and 6.4 feet in diameter, equivalent to a conventional windward sail rig of almost 3000 ft^2. The performance polar for this example, assuming a beam of 29 feet, is shown in Fig. 7–18. Here we see, as with the wingsail, a deficiency in sailing dead down wind owing to the inability to generate high drag. One does better by slowing the rotor down as $\gamma = 180°$ is approached in order to benefit from increased C_D at low rotational speeds. If it is convenient to do so, tacking down wind is certainly in order. Overall, the rotor has a clear performance advantage over soft sail rigs and wing sails.

Finally, we will let our imagination roam free and postulate a 120-foot Pacific flying proa with a displacement of 18,000 pounds. For this racer, we will specify X = 2.5 at $\gamma = 90°$ and α =7.0, $\lambda = 4.5$ for which the rotor is 26.4 feet tall with a diameter of 5.86 feet., equivalent to a soft rig of about 2,500ft^2. The fuel consumption in 10 knots of wind on a beam reach is 28 miles per gallon at a speed of 25 knots. since the centre of effort is so low owing to the compactness of the rotor, we can keep the overall beam and the weight to lower figures than would have been possible with a conventional rig or wing sail. Assuming b = 45 ft, h = 26 ft [see the definition in Eq. (2–10)], we can plot the performance polar. this is shown in Fig. 7–19; note that Figs. 7–15, 7–16, 7–18 and 7–19 have all been plotted to the same scale. This boat should sail in the 20 - 40 knot range most of the time and will require less than 250 gallons of diesel fuel for a typical voyage of 5000 miles.

Let me address a few practical points in closing. For values of $V_b/P_R^{0.405}$ approaching 20, the rotor can be operated by human pedal power. Cost considerations probably rule out the use of rotors with diesel-hydraulic power systems on boats of less than 35 feet or so. The cost of the hydraulics in 1994 was about $7000 at the 20 hp level, however the cost increases only slightly as we go up in power handling capacity. The rotor

must be rigid, and in order to avoid the weight and expense of cored composite construction, the best bet is probably inflatable rotors. Preliminary inquires with inflatable dinghy manufacturers indicates that inflatable rotors will cost less than sails. If you further consider the savings in spars, rigging, winches, etc, you see that rotors may be the most cost effective alternative to soft sails. Several rotors of various sizes could be carried and deflated rotors could easily be stowed away.

This chapter has been longer and more detailed than the wingsails and wind turbines chapters. Rotors, particularly Thom rotors, are less familiar and require greater analysis for understanding. At this writing, a Thom rotor boat has not yet been built. There is certainly room for experimentation. It would be good to have independent confirmation of Thom's C_L and C_D measurements, although they can be judged to be reliable since he had been making such measurements for more than ten years when the work with which we are concerned was done. I have assumed that each segment of the rotor is effectively isolated from the others, hence the coefficients should be aspect ratio independent. This assumption might br tested by starting with a rotor of aspect ratio 12 (Thom's value) and then removing one segment at a time to see if the coefficients change. Another experiment worth doing is to gradually reduce the fence diameter, starting with the canonical value $k = 3$, and see for each value of k at what value of α does C_D begin to increase.

Finally, it would be well to make tests of my power relation, Eq. (7–20), for which I already have some confirming data. I would be happy to contribute support and consulting anyone who would be interested in developing these ideas.

8 HYDROFOIL APPLICATIONS

in which we evaluate hydrofoil application to pitch and roll stabilization, seakeeping, and performance enhancement

In the last chapter, we discussed the function of hydrofoils that exert their forces entirely in the horizontal plane for steering and leeway resistance: boards and rudders. In this chapter, we will address ourselves to hydrofoils having dihedral angles (the angle between the hydrofoil and the water surface) other than 90 degrees. As with wingsails and keels, our first task is to obtain a set of Lanchester-Prandtl equations with which to convert section characteristics to realistic lift and drag coefficients for hydrofoils.

The lift force exerted at right angles to the velocity vector $-V_B$ is

$$F_L = \tfrac{1}{2}\rho_h V_B^2 A_F C_L \qquad (8\text{-}1)$$

where AF is the area of the foil. A foil of infinite length operating in an unbounded medium would have a lift coefficient

$$c_l = 2\pi\phi_T \qquad (8\text{-}2)$$

where ϕT is the angle of attack in radians measured from the angle of zero lift. This ideal lift coefficient is reduced by various factors. The first of these is the proximity of the free surface.

In a bounded fluid, the low pressure on the upper surface of he foil not only lifts the foil, it also distorts the free surface above the foil such as to reduce the pressure differential and hence decrease the lift. The perturbation of the water surface manifests itself as a transverse wave. The surface proximity effect can be taken into account by including two correction terms. The first correction describes the lift lost owing to pressure relief. This is similar to the interference suffered by the lower wing of a biplane. The correction is made by multiplying the lift slope 2π by a factor[8-1]

$$K = \frac{[4h/c]^2 + 1}{[4h/c]^2 + 2} \qquad (8\text{--}3)$$

where h is the depth of immersion and c is the chord length. This expression is plotted in Fig. 8-1. Note that the loss is only 5 percent or so at a depth of one chord, but then increases rapidly with decreasing depth, reaching a limiting value of 50 percent as $h \rightarrow 0$. The foil has then become a planing surface with a lift curve slope of π for infinite span.

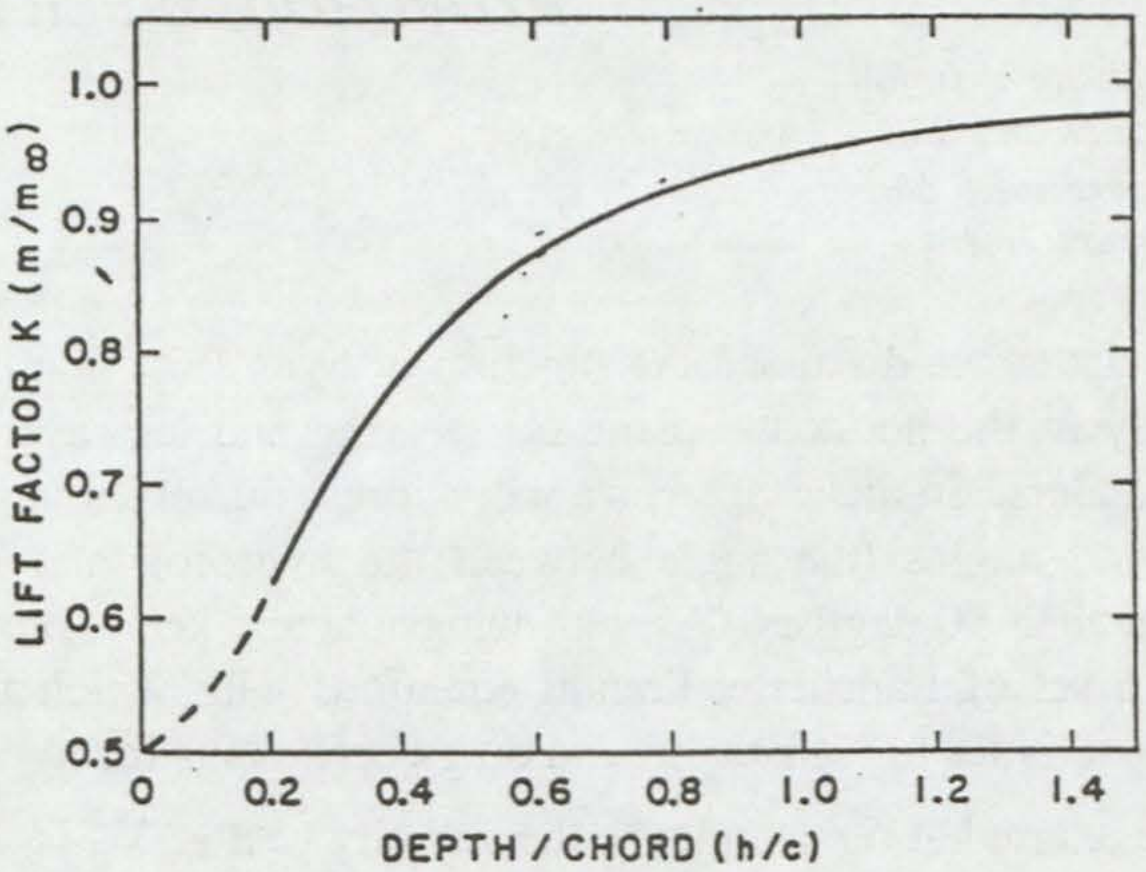

Fig. 8-1. Lift loss factor K owing to the proximity of the free surface.

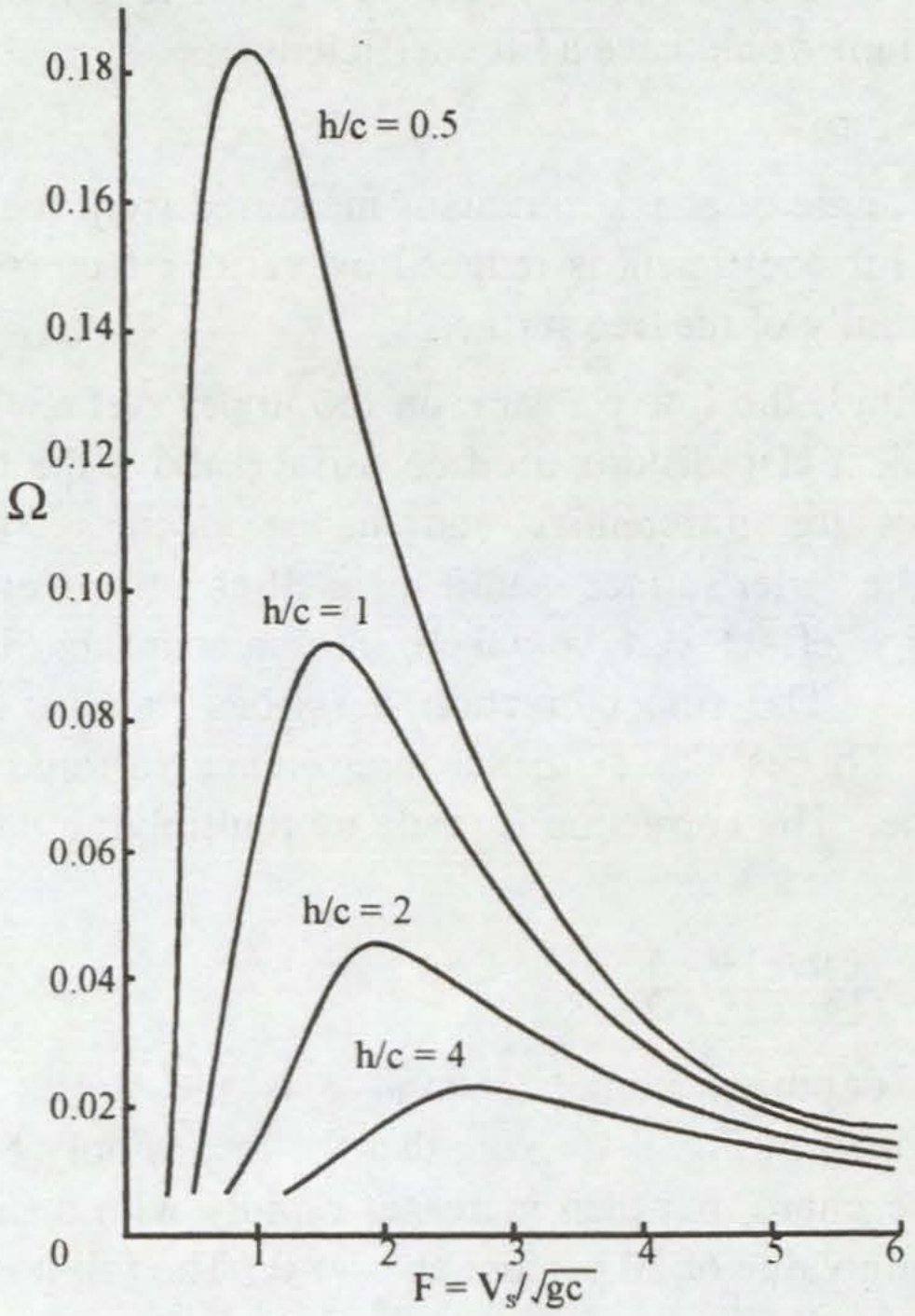

Fig. 8-2. Free surface wave function.

The tilt of the lift vector due to the foil-generated wave is taken into account by an inverse additive slope term[8-2]

$$\Omega = \frac{\exp\{-h/[cF^2]\}}{2F^2} \qquad (8\text{–}4)$$

where F is the Froude number defined on the basis of the chord

$$F = V_B/\sqrt{gc} \qquad (8\text{–}5)$$

This function is plotted in Fig. 8-2 for several values of h/c. In all practical cases the peak of these curves occurs at a boat speed that is well below the hydrofoil liftoff speed. Thus hydrofoils pass through the wave "hump" with relative ease at low speed, which is one of their virtues. This description breaks down when the hydrofoil is operated in shallow water. The maximum speed of a gravity wave in water of depth d is $(gd)^{1/2}$. For boat speeds exceeding $(gd)^{1/2}$, the wave train cannot keep pace and a more complex theory is required.

Just as in airfoil theory, a hydrofoil of finite span is subject to lift loss and induced drag as a result of the vortex system at the tip. A foil of aspect ratio λ and elliptical spanwise loading has an induced lift angle ϕ_i and drag C_{Di} given by

$$\phi_i/C_L = C_{Di}/C_L^2 = (1 + \sigma)/(\pi\lambda) \qquad (8\text{-}6)$$

where $\sigma = 0$ for airfoils and

$$\sigma = \frac{\lambda}{\lambda + 12h/c} \qquad (8\text{–}7)$$

for hydrofoils[8-3]. Again, the effect here is one of biplane interference. This factor is plotted in Fig. 8-3 as a function of depth/effective span and accounts for the diverging lateral waves associated with the trailing vortices of a finite-span foil. This correction applies only for high Froude number; two-dimensional theory gives a reasonable estimate at low speeds.

For modest aspect ratios, deviation from the assumed elliptical planform can be accounted for by multiplying the ideal slope 2π by a correction factor

$$E = (1 + 2/\lambda^2)^{-1} \qquad (8\text{-}8)$$

The flow velocity that generates lift is perpendicular to the span. If foils with a sweep angle ξ are used, then the two-dimensional lift slope must be multiplied by $\cos\xi$. This same sort of correction is also necessary for dihedral. The angle of attack is defined in the vertical plane and is therefore decreased by a factor $\cos\theta$, where θ is the dihedral angle.

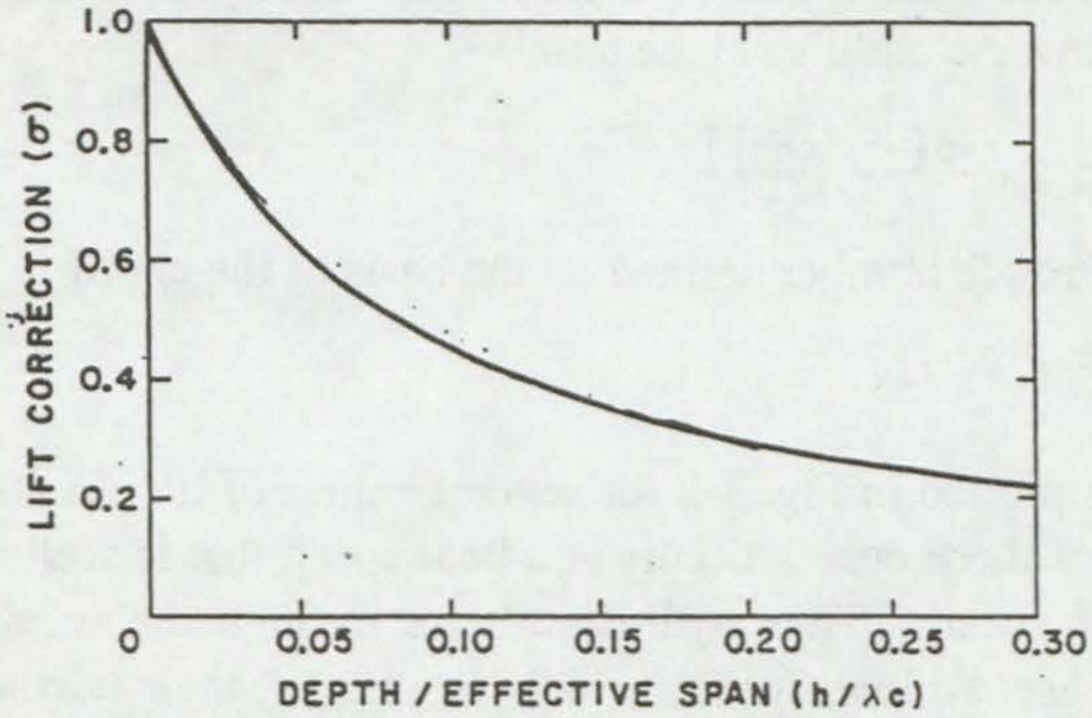

Fig. 8-3. Lift correction for finite aspect ratio.

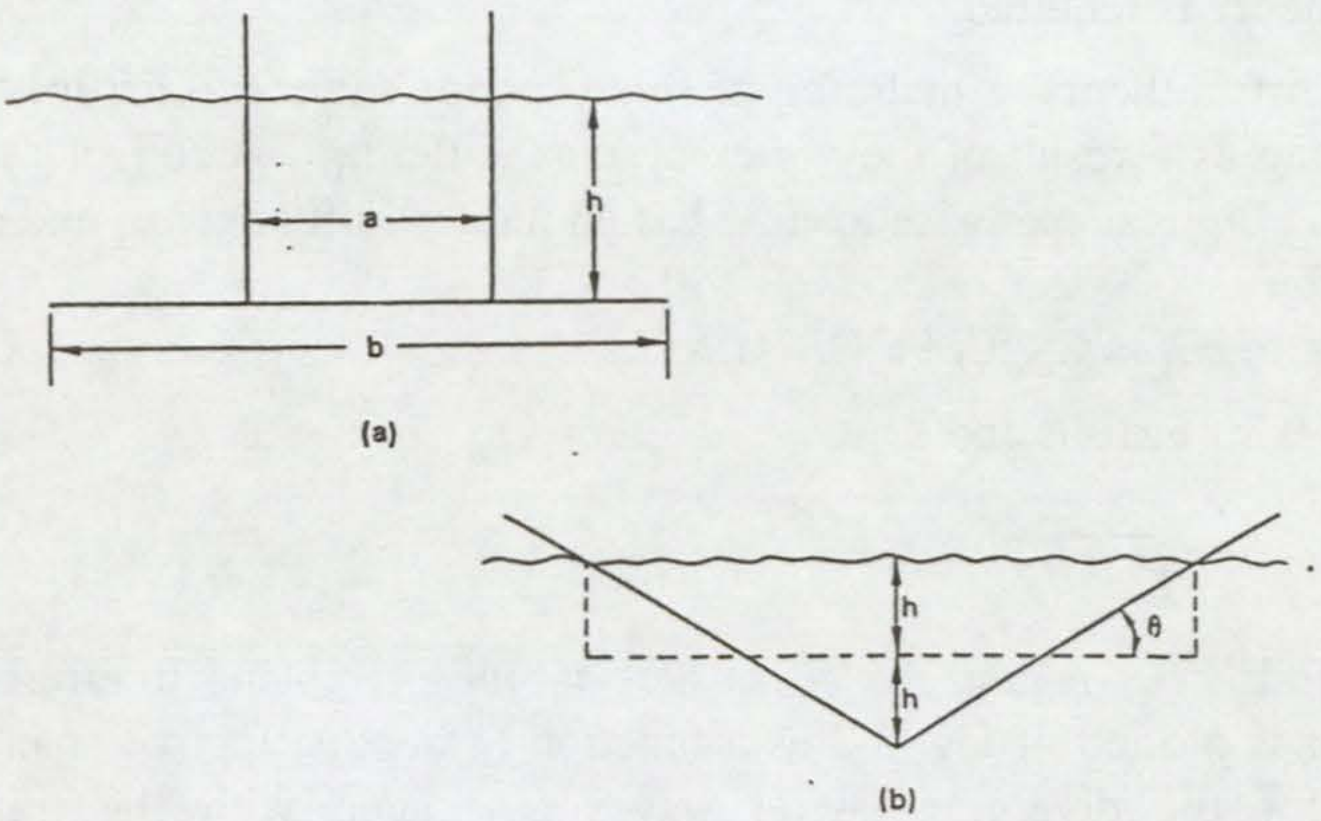

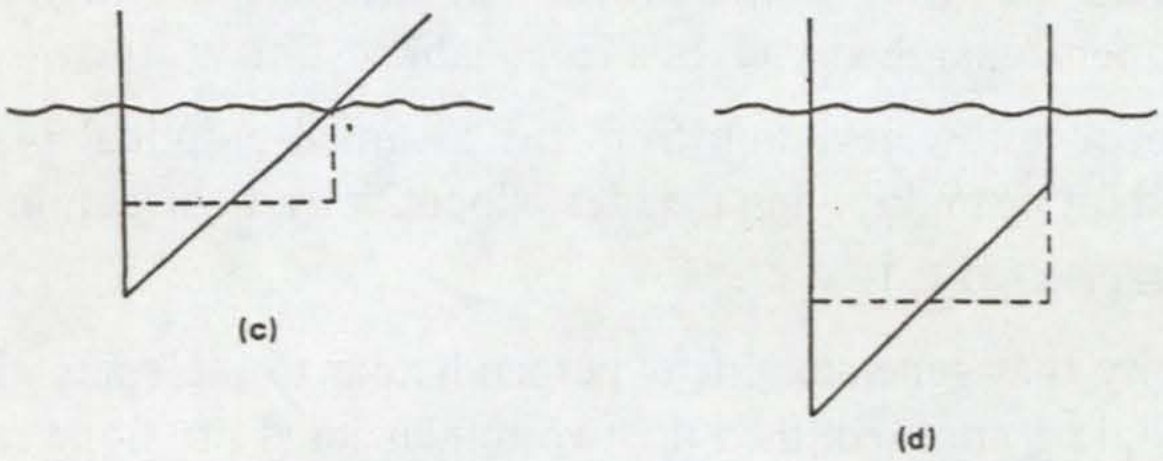

Fig. 8-4. Equivalence of dihedral foils to a horizontal foil - vertical strut combination for purposes of determining aspect ratio.

The definition of aspect ratio for hydrofoils is a bit more involved than for airfoils owing to the presence of struts and, for surface-piercing foils, the air-water interface, both of which inhibit spanwise flow. In Fig. 8-4a, we show a horizontal hydrofoil of span b supported by two struts separated by a distance a. The effective aspect ratio for this configuration is well approximated by

$$\lambda = (b/c)[\ 1 + (a/b)^3(h/b)] \tag{8-9}$$

For a T-foil having a single strut, a $\rightarrow$ 0 and $\lambda \rightarrow$ b/c as expected. For a V-foil as shown in Fig. 8-4b, Eq. (8-9) is applied to the equivalent configuration shown in dashed lines and one finds

$$\lambda = (b/c)(1 + h/b) = (h/c)(1 + 4\ \mathrm{ctn}\theta) \tag{8-10}$$

The aspect ratios for the asymmetric dihedral foils shown in Fig. 8-4c and 8-4d are similarly evaluated.

Collecting the contributions from Eqs. (8-2) to (8-4) and (8- 6) to (8-8), the hydrofoil lift coefficient modified by finite depth and aspect ratio is approximately

$$C_L = (2\pi\phi_T\lambda)/\left(\frac{\lambda/K + 2/\lambda}{\cos\xi\ \cos\theta} + 2[\pi\lambda\Omega + 1 + \sigma]\right) \tag{8–11}$$

Only for large Froude number, high aspect ratio, and deep submergence does this equation reduce to the simple expression

$$C_{L0} = 2\pi\phi_T[\lambda/(\lambda + 2) \tag{8-12}$$

most often used by hydrofoil experimenters.

The drag coefficient for the hydrofoil, excluding struts, is given by[8-3]

$$C_D = c_d + C_L^2[\Omega + (1 + \sigma)/(\pi\lambda\ )] \tag{8-13}$$

where c_d is the section drag coefficient. In the absence of experimental data, c_d may be estimated by using the empirical formula

$$c_d \approx 0.004\ (1 + 1.2\tau/c) + 0.11\ (c_1 - C_L)^2 \tag{8-14}$$

where τ/c is the thickness-to-chord ratio.

The strut drag is estimated as the sum of three terms. the body of the strut has a drag that can be approximated using Eq. (8-14). If the strut has a weather-cocking fairing such that it exerts no horizontal lift, then only the first term of Eq. (8-14) need be taken. The junction of the strut with the foil gives rise to drag effects that depend critically on the fillet or fairing used. The best source of data on this topic is Hoerner[8-4]. A torpedo shape at the junction often works well. Finally, a spray drag arises at the water

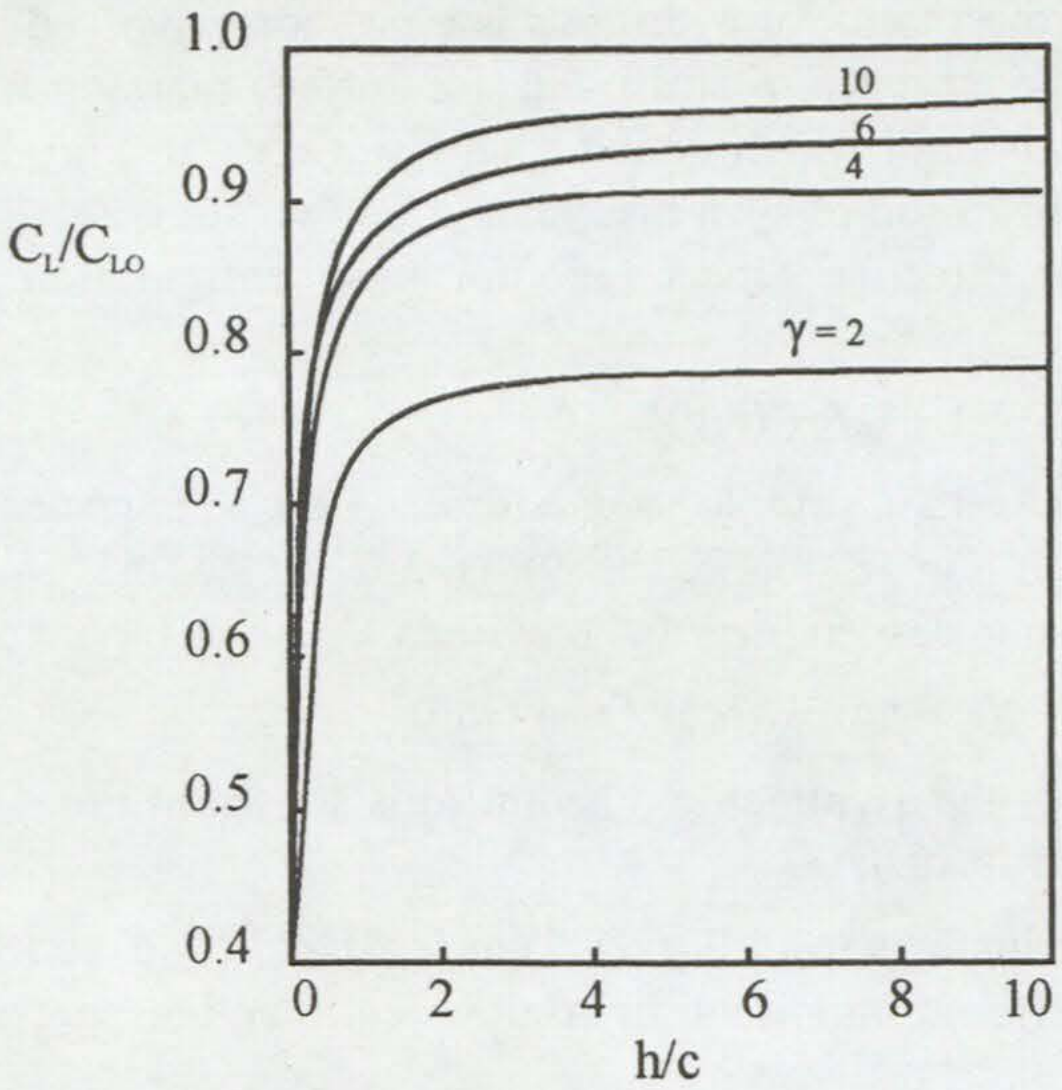

Fig. 8-5. Ratio of corrected lift coefficient for hydrofoils to C_L for an unbounded medium as a function of proximity to the free surface.

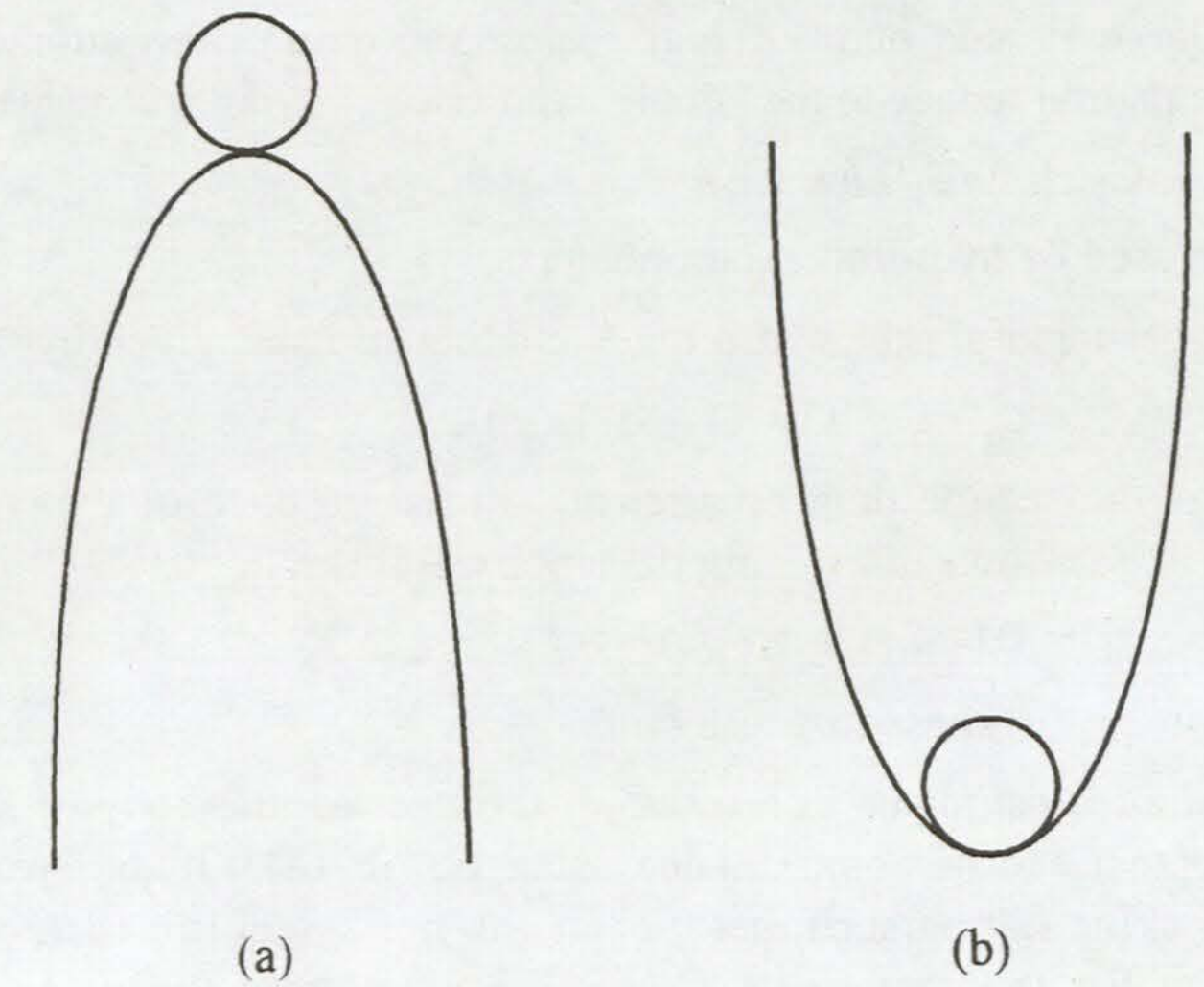

Fig. 8-6. Illustrating the distinction between unstable (a) and stable (b) equilibria.

surface; for sections with sharp leading edges a drag coefficient of 0.02 can be taken based on the product of chord and thickness as the reference area. The same term should be applied to determine the spray drag for surface-piercing foils.

In order to show the magnitude of the refinement of Eq. (8-11) over Eq. (8-12), we plot the ratio C_L/C_{L0} as a function of h/c for various values of λ in Fig. 8-5. Since Ω involves V_B as well as h/c, we have made the simplifying assumption of a hydrofoil with lift coefficient given by Eq. (8-12) lifting a constant weight. Hence, using Eq. (8-1) with $A_F = bc = \lambda c^2$

$$W = \tfrac{1}{2}\rho_h V_B^2(\lambda c^2)2\pi\phi_\tau[\lambda/(\lambda + 2) \qquad (8\text{-}15)$$

If we set W = 500 lb, c = 6 inches, $\phi_T = 4°$ for an admittedly arbitrary example, we get for the Froude number - aspect ratio relationship

$$F = \frac{94.6\sqrt{\lambda + 2}}{\lambda} \qquad (8\text{–}16)$$

and we can then write for the ratio C_L/C_{L0}

$$C_L/C_{L0} = \frac{\lambda + 2}{\lambda/K + 2/\lambda + 2[1 + \sigma + \lambda\pi\Omega]} \qquad (8\text{–}17)$$

It is this equation that is plotted in Fig. 8-5. We see that the correction is significant for shallow foil immersion and modest aspect ratios, both of which may be encountered in actual hydrofoil operation.

The chief application of hydrofoils is to exert lift to raise the hull or hulls partly or wholly clear of the water. How do the foils 'know' their altitude with respect to the free surface? In answering this question, we are concerned not only to see how an equilibrium vertical altitude is established, but also to question whether or not the equilibrium is a stable one. To illustrate the point, we show two simple equilibria in Fig. 8- 6: a ball at rest on top of a hill (a), and a ball at rest in a valley (b). If the ball on top of the hill is perturbed, then it will roll down the hill, never to return. Thus equilibrium (a) is unstable. On the other hand, if the ball in the valley is perturbed, then it will oscillate about its equilibrium position and, as the oscillations damp out, will return to rest at the bottom of the valley again. We say that equilibrium (b) is stable. In a sailing boat subject to a spectrum of wind gusts and wave conditions, perturbation is the rule and all equilibria must be stable.

Hydrofoil systems are of two types, classified according to how they deal with the altitude control problem. The first is surface-piercing foils, which

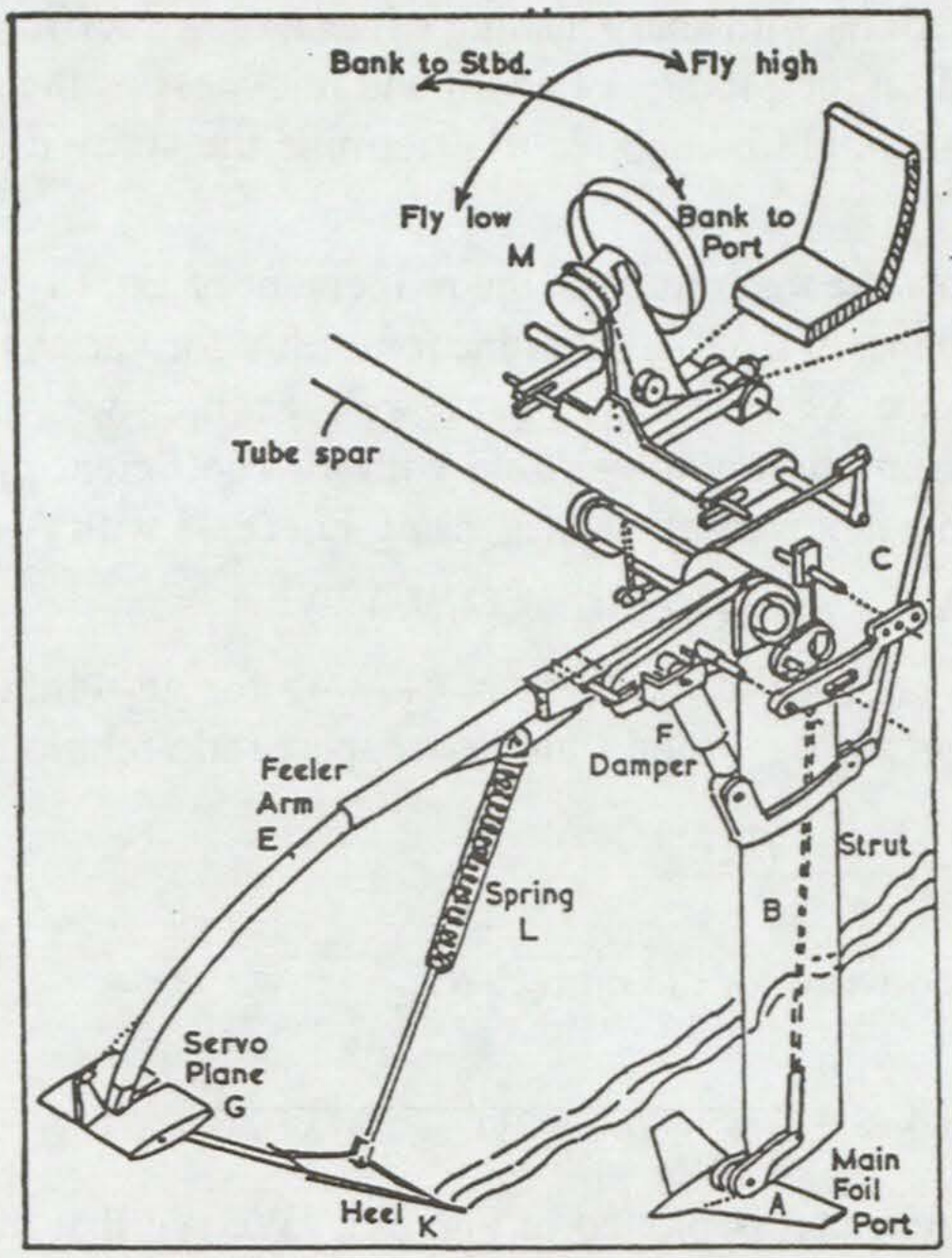

Fig. 8-7. The Hook Hydrofin system for controlling fully immersed foils.

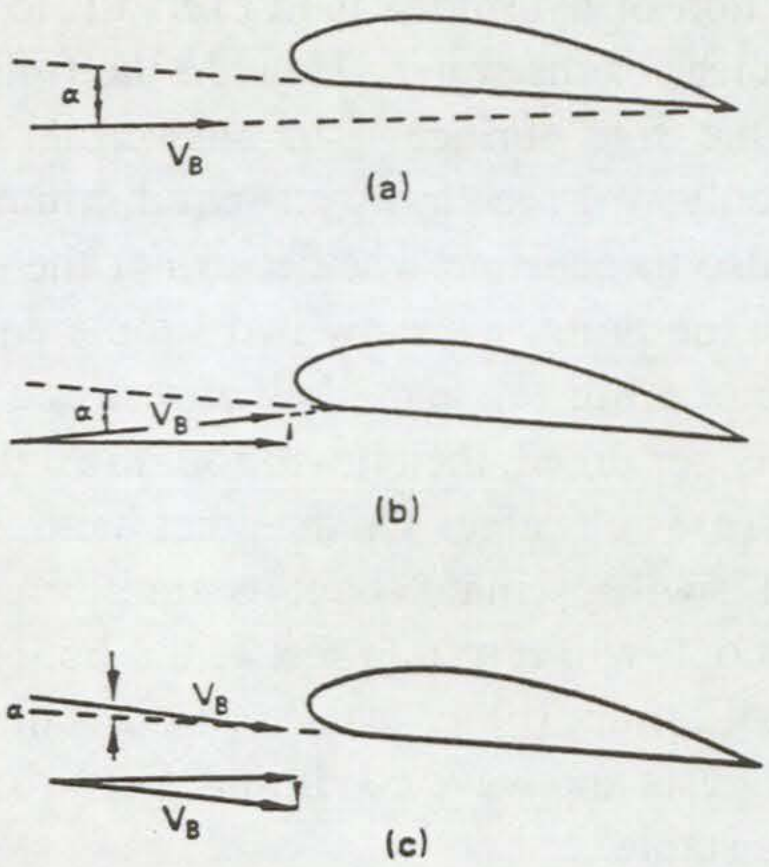

Fig. 8-8. Rate-dependent damping of vertical displacement perturbations by induced changes in angle of attack.

are simple and have some obvious advantages for the wide range of operational speeds encountered by sailing craft. Fully immersed foils have their own advantages, such as the elimination of the ventilation problem. Fully immersed foils foils can respond to a vertical displacement perturbation and restore the original flight altitude in either of two ways.

First, we can have horizontal foils operating very near the surface where, as we have seen, lift is a sensitive function of depth. This is called the Alexeyev System after the Russian engineer who developed it for large passenger vessels navigating Russian rivers and canals[8-5,6]. In this case, the foils themselves are the surface sensing device, as in the case of surface-piercing foils. The Alexeyev system is only applicable to craft operating in sheltered waters, and would be unworkable in any sort of sea.

The second type of fully immersed foil employs a surface- sensing feeler to send messages through a simple or complex linkage to change the angle of attack of the forward foils. The hydrofin system developed by Christopher Hook is an early example of this type[8-5]. The hydrofin, shown in Fig. 8-7, is a complex mechanism that amounts to an aircraft-type control system combining elevators and ailerons with a damper system to differentiate small waves from large ones so that the small ones can be ignored and the large ones contoured. For ocean-going yachts, the Hook system is probably too heavy and complicated. A much simpler system is used by Greg Ketterman in his Trifoiler where a surface-sensing plate on a springy arm raises or lowers the bow of the outrigger to which the foil is rigidly attached by a strut. The crossbeam-outrigger attachment joint has a springy pivot to accommodate the pitching of the outriggers[8-7]. The Trifoiler has operated successfully in a light chop, but may not be able to cope with ocean sailing. Dr. Sam Bradfield's HS21T uses a trailing flap on the main foils to control altitude. A wand senses the water surface and communicates with the flap through a control rod[8-8]. This seems quite reliable, but it, like the Ketterman and Hook systems, may be limited in the amplitude and frequency of waves that can be accommodated.

The outlook for surface-piercing hydrofoils as applied to ocean-sailing yachts may be better. To a first approximation, the lift exerted by a hydrofoil at a given speed varies linearly with its immersed area (vertical displacement) and with the angle of attack ϕ of the water onto the foil. In Fig. 8-8a, we see a hydrofoil experiencing a flow with angle of attack ϕ. If a downward displacement occurs, the hydrofoil sees an additional component of fluid velocity from below. This is interpreted as an increase

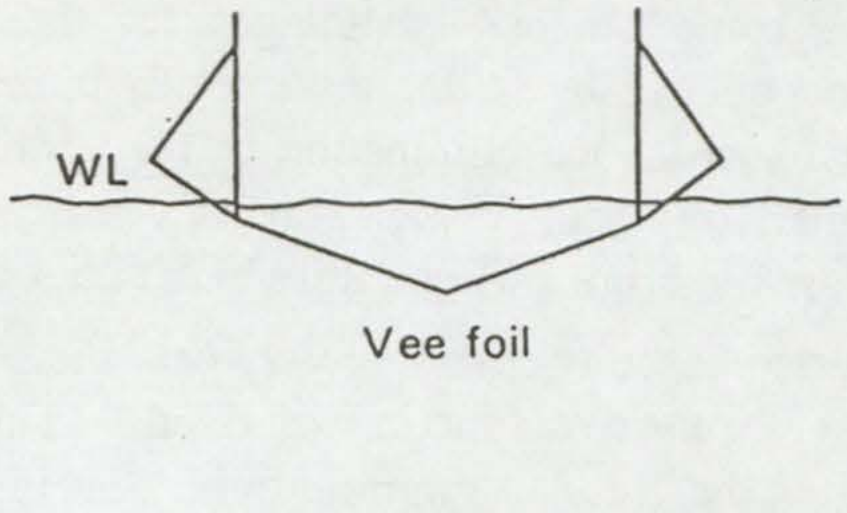

Fig. 8-9. Monoplanar and multiplanar surface-piercing hydrofoils.

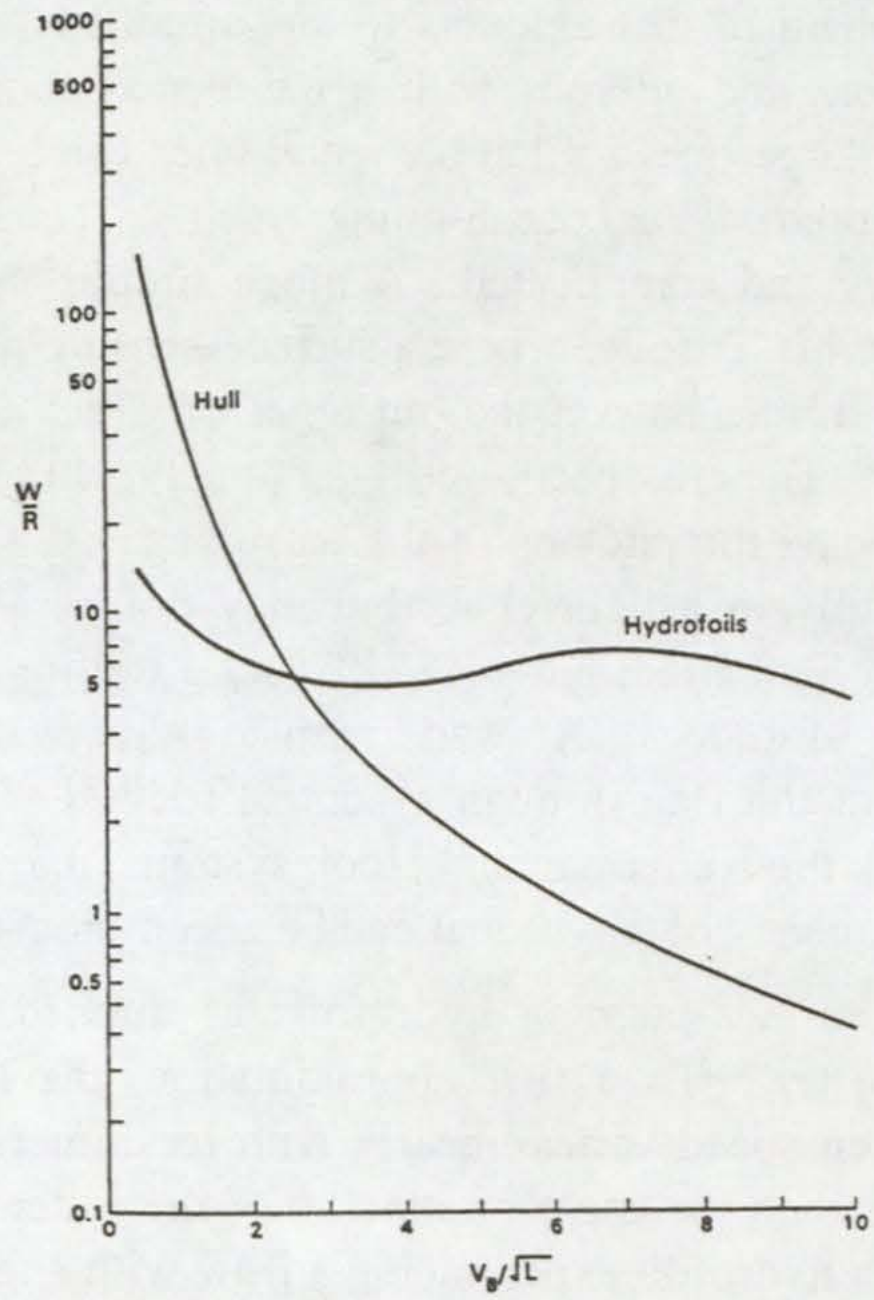

Fig. 8-10. A comparison of the lift/drag characteristics of fine hulls and hydrofoils capable of lifting them.

in the angle of attack as shown in Fig. 8-8b. If the displacement is upward, the effect is a reduction in í and the foil tends to lose lift in opposition to the perturbation (Fig. 8-8c). The effect is entirely analogous to that described in chapter 7 for yawing stability. The hydrofoil resists the vertical displacement with a force proportional to both the displacement and the rate of displacement. The rate of displacement correction is the only one available to fully immersed foils unless they or their flaps are controlled by surface sensors. For surface-piercing foils stabilization is powerfully augmented by the automatic variation of foil area. If a perturbation depresses the foil below its equilibrium waterline, the action of the increased area tends to restore the equilibrium, while the change of apparent angle of attack owing to the rate-dependent correction tends to damp the motion and prevent overshoot.

Surface-piercing hydrofoils may be monoplanar or ultiplanar as shown in Fig. 8-9. For smooth water sailing somewhat off the wind, the monoplanar foil works quite well, however for offshore sailing, the multiplanar or ladder foil should be preferred. The large reserve of unimmersed foil in the ladder arrangement can exert high lift as the foil enters a wave. The monoplanar foil is generally used in power vessels designed to operate foil-borne only over a narrow range of speeds. In sailing, our power source is highly variable and we must be able to operate foil-borne over a wide range of speeds. In order to see what determines this range, we must compare the lift-to-drag characteristics of a low-D hull of a type appropriate to advanced multihulls to the lift-to-drag characteristics of a set of hydrofoils capable of lifting this hull. These curves are plotted in Fig. 8-10 as a function of $S = V_B/\sqrt{L}$. We see that the buoyancy/resistance ratio for a good hull is greater than the lift/drag ratio of hydrofoils up to a value of $S \approx 2.2\text{-}2.4$. The length of the hull used in this calculation is 25 feet, so takeoff speed should be about 12 knots purely on the basis of optimal performance. Hook has done a similar calculation for power boats comparing hydrofoil s with several hull forms[-5,p.148], all 75 feet in length. He too finds a takeoff speed of 12 - 14 knots if the hull is of the displacement type. Thus, for very light air sailing, we should arrange to retract the foils and sail hull-borne, deploying the foils when the wind allows sailing speeds in excess of 10 knots. For the yachts that we contemplate, most ocean sailing in winds of 8 knots or more will be on the foils.

Now let us look at another aspect that shows the superiority of ladder foils. Figure 8-11 shows the motion of individual elements of water as a wave passes through from left to right. The orbits are circular with a diameter

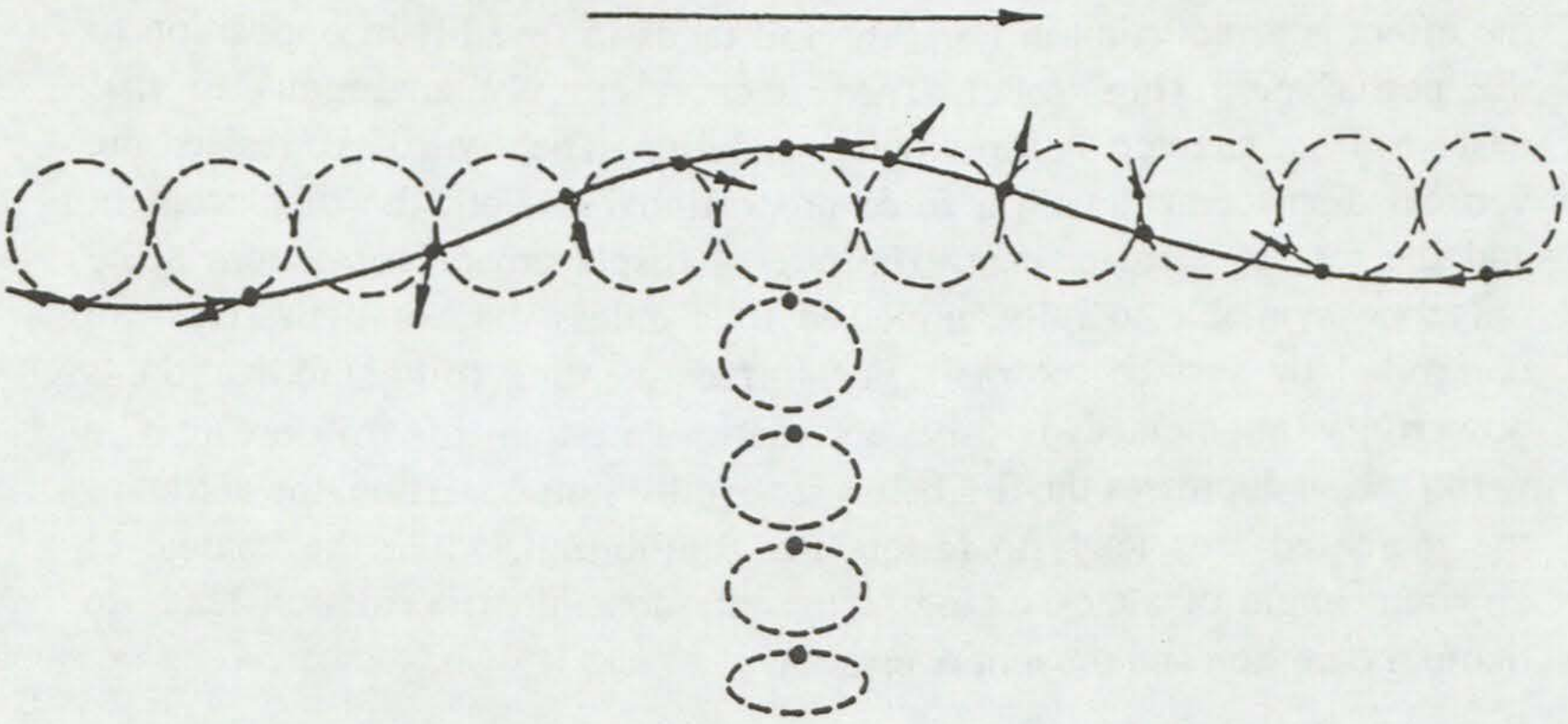

Fig. 8-11. Water particle orbits under wave action.

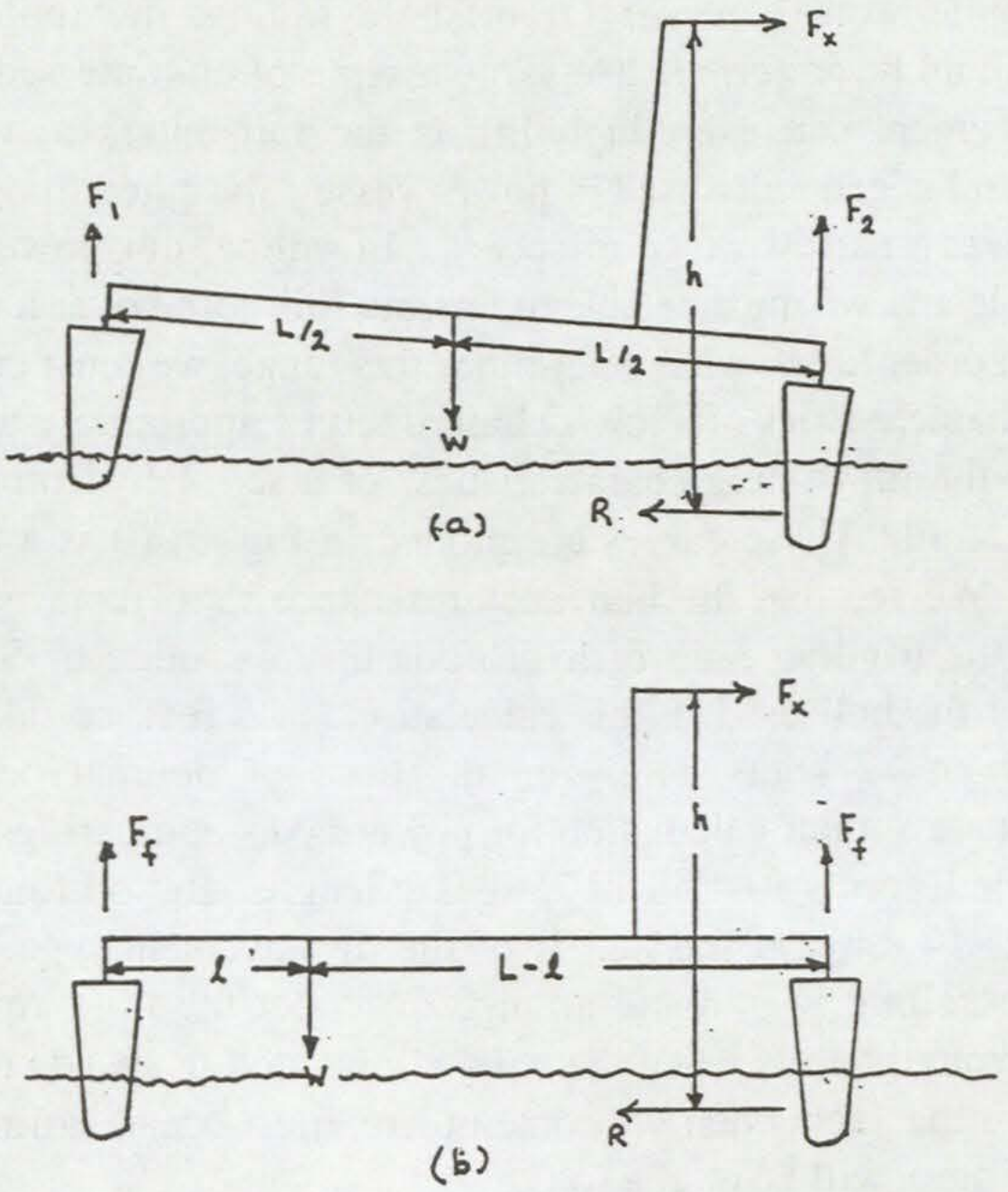

Fig. 8-12. Pitching moment compensation by (a) increased immersion of the front foil and consequent reduction of the angle of attack, and (b) by shifting the weight aft.

equal to the height of the wave at the surface. As depth increases, the orbits are flattened into ellipses, tending to a shuffling back and forth at greater depth. Now consider a hydrofoil-borne craft sailing to weather against the wave motion. Since the water on the front of the wave is rising, the foil sees this as an increase in angle of attack and the lift increases. The hydrofoil therefore tends to climb the wave rather than hold a constant altitude. On the back of the wave, the water is falling. This is interpreted as a decrease in angle of attack, lift decreases, and the boat tends to contour the back side of the wave as well. In a following sea, the situation is unfortunately reversed. If a foil-borne yacht moves downwind fast enough to overtake the waves, it will then tend to plow into the back side of the wave as the apparent angle of attack on the foil decreases. A monoplanar foil operating at low angle of attack would be sorely tried by this situation, however the ladder foil would likely cope owing to its reserve of previously unimmersed foil area. In operating a surface-piercing foil, the curved side near the air-water interface may develop a pressure less than atmospheric. A cavity can be formed and air may be sucked down from the surface leading to a loss of lift. We discussed this phenomenon of ventilation in chapter 7 with regard to leeboards and pointed out that if the foil or strut is given a slight forward sweep angle ξ, then surface water encountering the member has an upward component of velocity that tends to cancel ventilation.

We have said a good deal about vertical stability, but the picture is not complete without the inclusion of the pitching moment and stabilization of pitching perturbations. In Fig. 8- 12, we show schematically a hydrofoil-borne craft with front and rear hydrofoils that must not only lift the weight W of the craft, but must also cope with the pitching moment owing to the forward component of the sail force Fx a distance h above the center of effort of the foils. If we assume the foils to be identical and set at the same angle of attack, then in Fig. 8-12a where the center of gravity is located half way between the foils, the pitching moment can only be resisted by deeper immersion of the bow foil. This results in a bow-down attitude that reduces the angle of attack onto all the foils and results in deeper immersion for both front and rear foils. This puts the bow foil in a rather delicate position where a further pitching perturbation may cause the angle of attack to decline to the point where lift is lost altogether, or to the point where the entire load transfers to the bow foil and pitch equilibrium can no longer be maintained. The vertical force equilibrium and pitching moment equilibrium for case (a) are given by

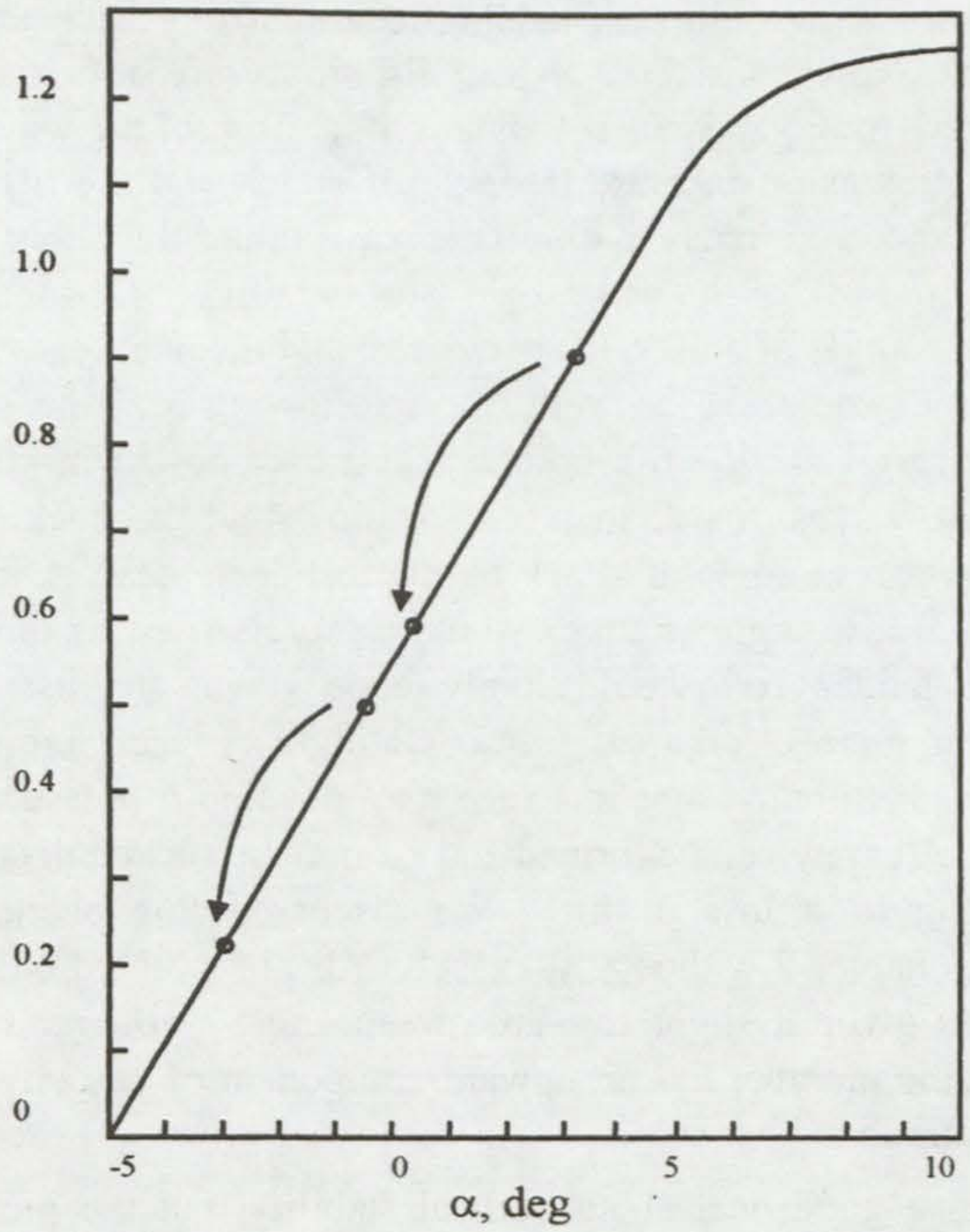

Fig. 8-13. Stabilization of pitching moment by operating the bow foil at a higher angle of attack than the stern foil.

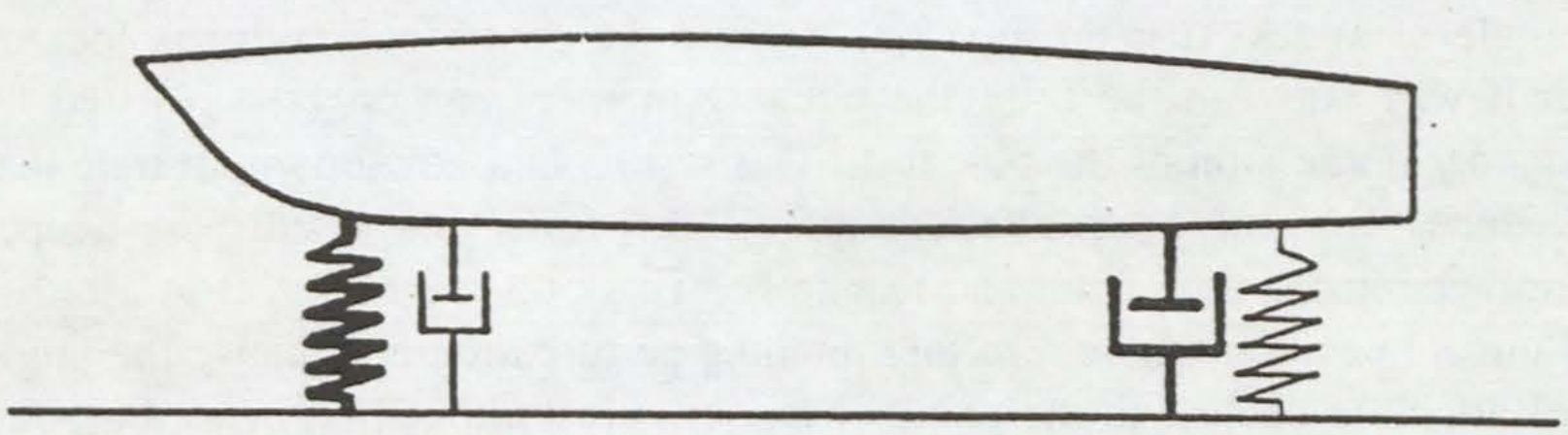

Fig. 8-14. Spring-damper analog for pitch stabilization.

$$F_1 + F_2 = W \tag{8-18}$$

and

$$F_x h + \tfrac{1}{2} F_1 L = F\tfrac{1}{2}_2 L \tag{8-19}$$

from which we find for the hydrofoil lift forces

$$F_1 = \tfrac{1}{2}(W - 2F_x h/L) \tag{8-20}$$

$$F_2 = \tfrac{1}{2}W + 2F_x h/L) \tag{8-21}$$

When F_x increases to $\tfrac{1}{2}WL/h$, then all of the weight of the craft is being carried on the forward foil and a pitchpole is immanent. In Fig. 8-12b, we have transferred the center of gravity aft so that the craft is level ($F_1 = F_2 = F_f$) for some value of F_x. The equilibrium equations are now

$$2F_f = W \tag{8-22}$$

$$F_f \ell + F_x h = F_f(L - \ell) \tag{8-23}$$

which holds for

$$F_x = \tfrac{1}{2}W(L - 2\ell)/h \tag{8-24}$$

For F_x less than this value, the craft trims bow up. As soon as F_x exceeds the value given by Eq. (8-24), then you are back in the position of case (a). With a small hydrofoil daysailer, crew shifts forward or aft can trim the craft, but for the ocean- sailing yachts that are the focus of this book, crew shifts cannot accomplish the purpose.

The trick that provides pitch stability is to operate the bow foil at a higher angle of attack than the stern foil. In Fig. 8-13 we show a typical lift curve. Suppose at equilibrium the front foils are operated at $\phi = 4°$ for a lift coefficient of 0.9, and the rear foils are operated at $\phi = 0°$ for a lift coefficient of 0.5. If a gust depresses the bow so that the angle of attack onto both front and rear foils is reduced by 3 degrees, then the front foil lift coefficient falls from 0.9 to 0.6, a loss of 33 percent, while the rear foil lift coefficient falls from 0.5 to 0.2, a 60 percent lift loss. Thus, by operating the bow foil at a higher angle of attack, a bow-down perturbation will always cause the stern to lose lift faster than the bow. Thus the stern will settle rapidly to recover equilibrium by greater immersion. This causes the angle of attack onto all the foils to increase. The increased boat speed owing to the gust and the recovery of the former angle of attack on the bow foil combine to stimulate the recovery. In this way, the equilibrium is stabilized. In order that the lift-to-drag ratio of the foils not be too low as a result of operating the bow foil at higher than optimum C_L, the center of

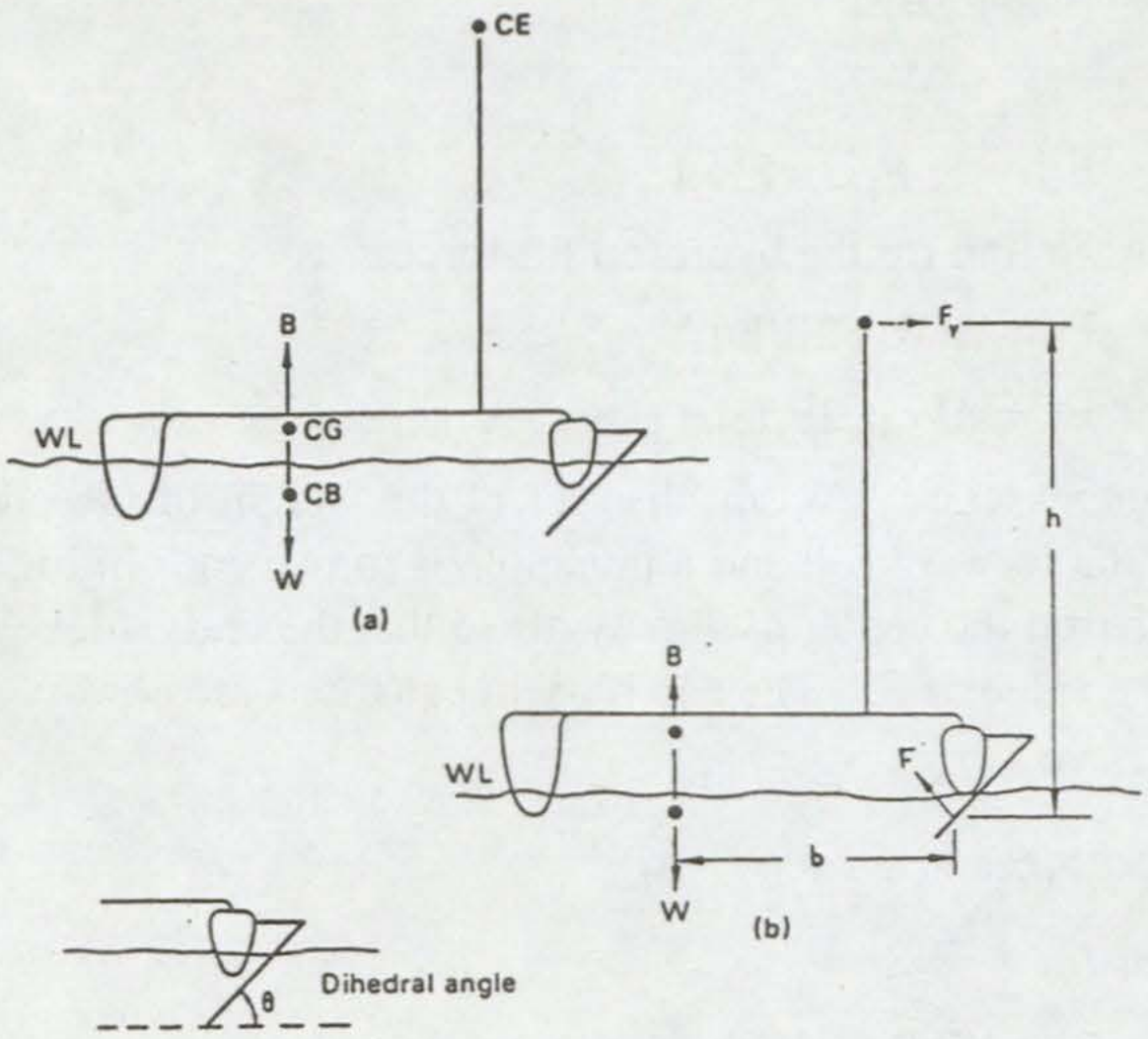

Fig. 8-15. A multihull craft with a canted leeward hydrofoil in static and dynamic equilibrium.

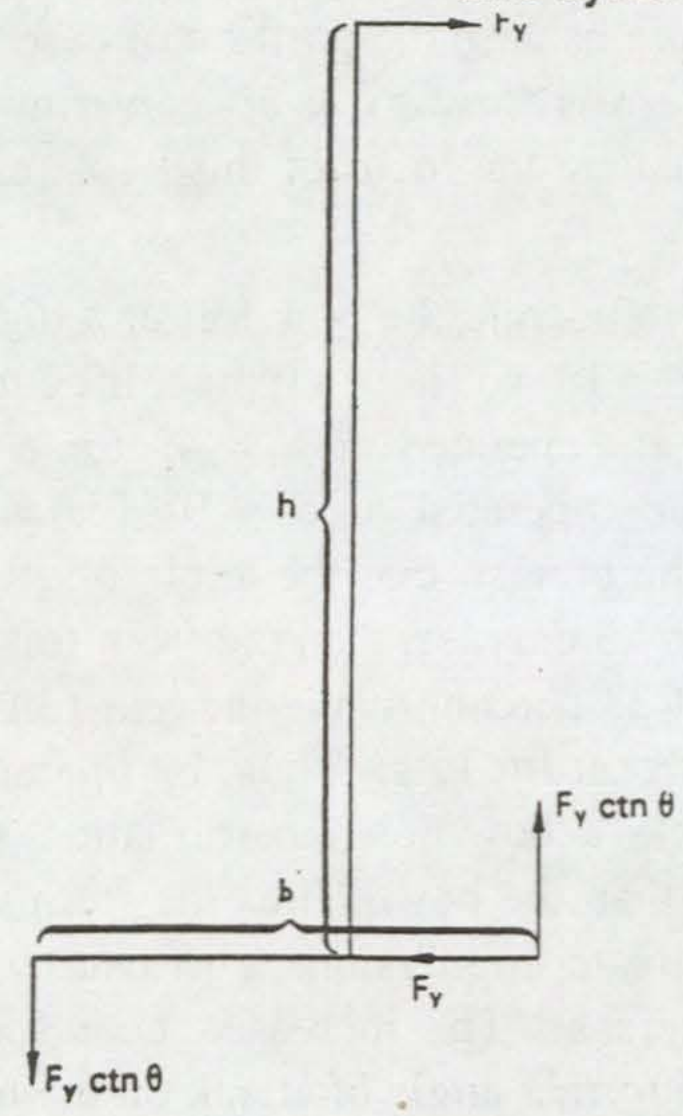

Fig. 8-16. Force diagram for multihull craft with canted hydrofoil to leeward at sub-liftoff speed

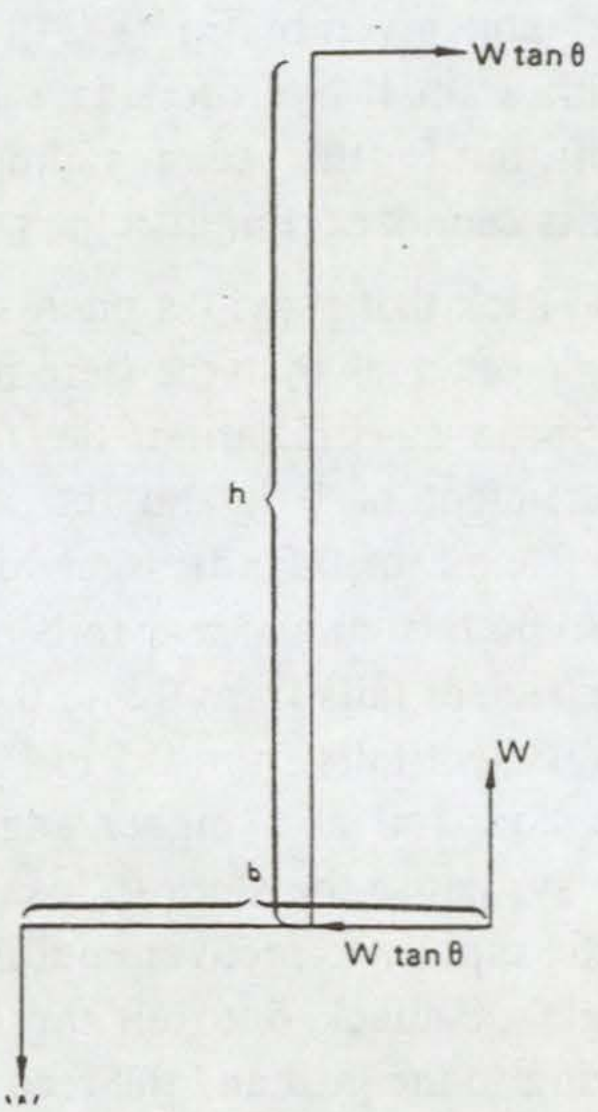

Fig. 8-17. Force diagram for multihull craft with canted hydrofoil to leeward at the point of liftoff.

gravity should be well aft. This reduces the loading on the bow foil and its contribution to the overall L/D of the entire foil system. The front foil therefore assumes more the role of a control surface (elevator) and less the role of a load carrier (wing). Thus we see that for hydrofoil systems in general, the canard configuration would seem to be preferred over the airplane configuration. George Chapman, for whom I have the greatest respect, disagrees with me on this point. He and Sam Bradfield are both concentrating their efforts on the airplane configuration. Neither of them has submitted convincing evidence that this configuration will cope satisfactorily with all aspects of ocean sailing, and until such evidence is forthcoming I will continue to believe the results of analysis and encourage development of canard foil systems.

In a canard configuration, the immersed area of the bow foil will be much less than that of the stern foil, however a large reserve area must be available to provide transient lift for recovery from gusts. In this way, a small-chord ladder foil in the bow operated at high angle of attack and low equilibrium load is combined with a large-chord biplanar foil in the stern operated at low angle of attack and high equilibrium load. Such a system is stable in its equilibrium altitude and fore-to-aft trim angle. This combination is analogous to a stiff spring suspension forward (high ϕ) with modest damping (small chord) and a weak spring aft (lowϕ) with strong damping (large chord) as shown in Fig. 8-14. That this same analogy was made in chapter 3 with regard to pitch stabilization of hulls.

Now let us turn from the longitudinal to the lateral and examine the question of roll or heeling equilibrium and stability. In Fig. 8-15, we see a multihull craft with a canted hydrofoil to leeward. In the (a) part of this figure, the craft is at rest and the only forces in effect are the weight W opposed by the hull buoyancy B operating along the same vertical line. In Fig. 8-15b, the boat is in motion at a constant speed and a state of dynamic equilibrium exists. The basis for leaving the buoyancy in the same vertical line as the weight is the assumption that the net heeling moment can be eliminated. Were this assumption not true, the center of buoyancy would move to leeward as the boat heels. A state of equilibrium is realized only when the vector sum of all the forces is zero. In addition, the moment of all the forces (torque) about any point must also be zero. Neglecting longitudinal forces, the nature of whose equilibrium we have already discussed, the vanishing of net forces implies

$$B = W - F\cos\theta \qquad (8\text{-}25)$$

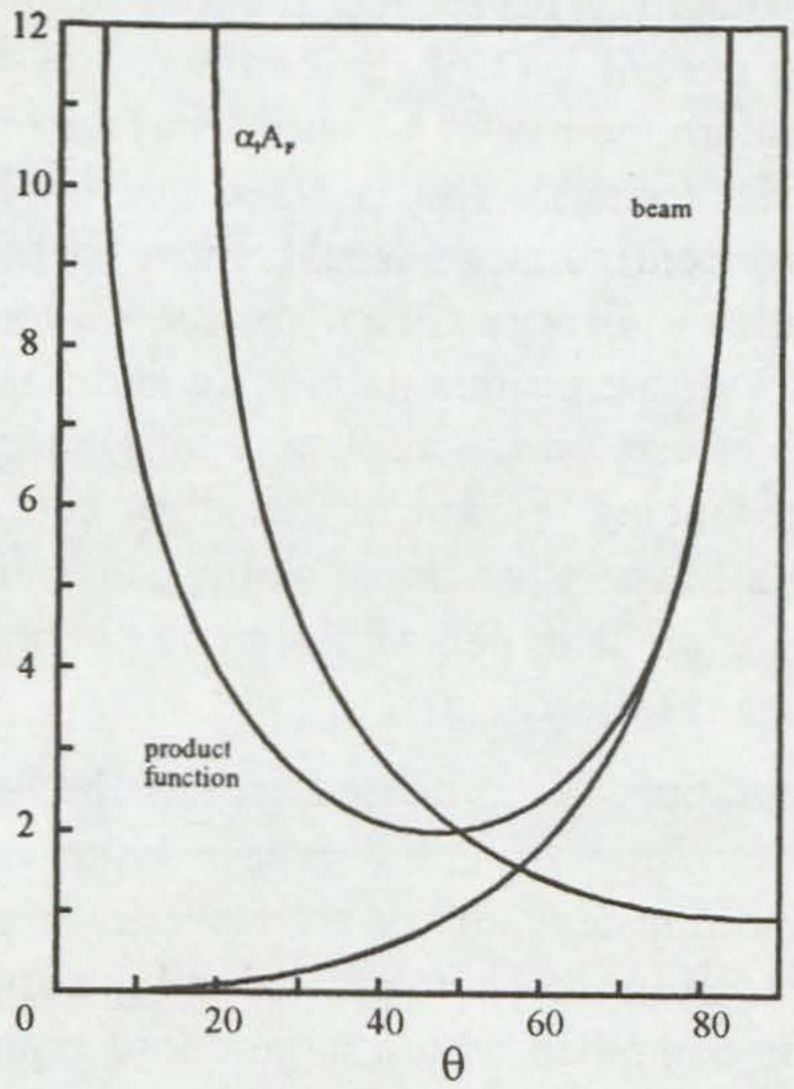

Fig. 8-18. Beam function tan , leeway - foil area function $(\sin^2)^{-1}$, and their product as a function of dihedral angle.

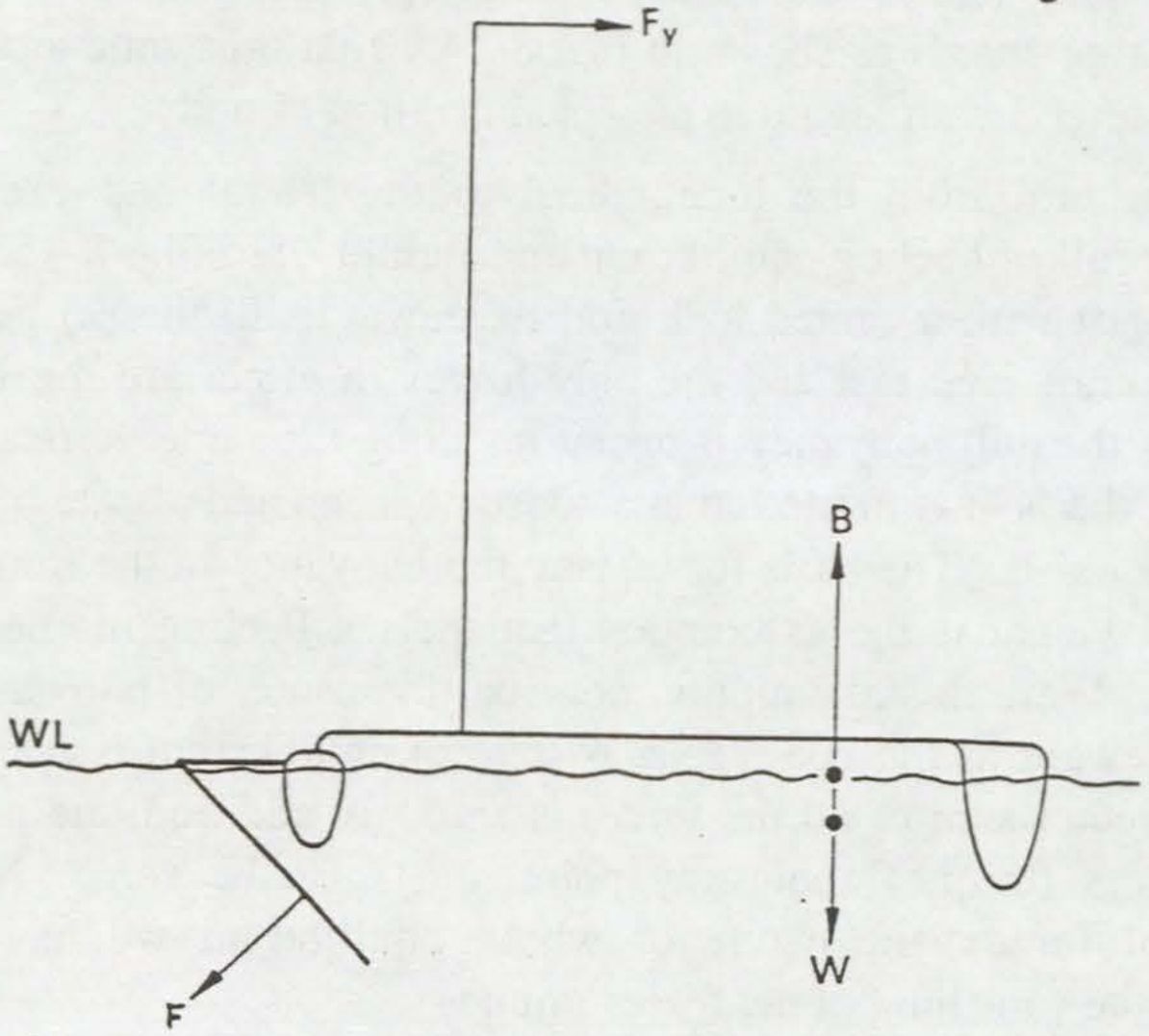

Fig. 8-19. Cancellation of heeling torque with the use of a canted depressing foil to windward.

and

$$F_y = F \sin\theta \tag{8-26}$$

where θ is the dihedral angle of the foil. Multiplying Eq. (8- 25) by $\sin\theta$ and Eq. (8-26) by $\cos\theta$ and adding, we find

$$B \sin\theta + F_y \cos\theta = W \sin\theta \tag{8-27}$$

or

$$F_y = (W - B) \tan\theta \tag{8-28}$$

Using Eq. (8-26), the vertical component of the hydrofoil force is

$$F \cos\theta = F_y \operatorname{ctn}\theta \tag{8-29}$$

and so, using Eq. (8-28), we can express the buoyancy as

$$B = W - F_y \operatorname{ctn}\theta \tag{8-30}$$

Thus our hydrofoil craft in dynamic equilibrium can be reduced to the force diagram shown in Fig. 8-16. By taking moments about any point on this figure and setting the sum of them equal to zero, we are led to an important relation

$$F_y(h - b \operatorname{ctn}\theta) = 0 \tag{8-31}$$

Since F_y does not vanish except in the trivial static case, the criterion for the vanishing of the heeling moment must be

$$b = h \tan\theta \tag{8-32}$$

This raises several questions having to do with the practical realization of heeling cancellation. First, how large can F_y be (or, equivalently, how much sail can be carried in a given wind) in order that Eq. (8-31) still be satisfied? The answer to this question is contained in Eq. (8-30). This equation describes the decrease of buoyant force as the hulls are lifted out of the water by $F_y \operatorname{ctn}\theta$, the vertical component of the hydrofoil force. As Fy approaches W tan , B approaches zero as the hulls lift out. At the point of liftoff, the force diagram given in Fig. 8-16 goes over into that shown in Fig. 8-17. The righting moment has now maximized at

$$N_{max} = bW \tag{8-33}$$

the same value that applies to a hull-borne multihull. Any further increase of F_y over W $\tan\theta$ will lead to a reduced righting moment and possible capsize. The virtue of the canted leeward hydrofoil arrangement, generally known as a Bruce foil after Edmond Bruce, is that (1) no heeling at all is experienced up to the point of liftoff, thus maintaining sail driving force (which falls off as the cosine squared of the heel angle) at a maximum, and

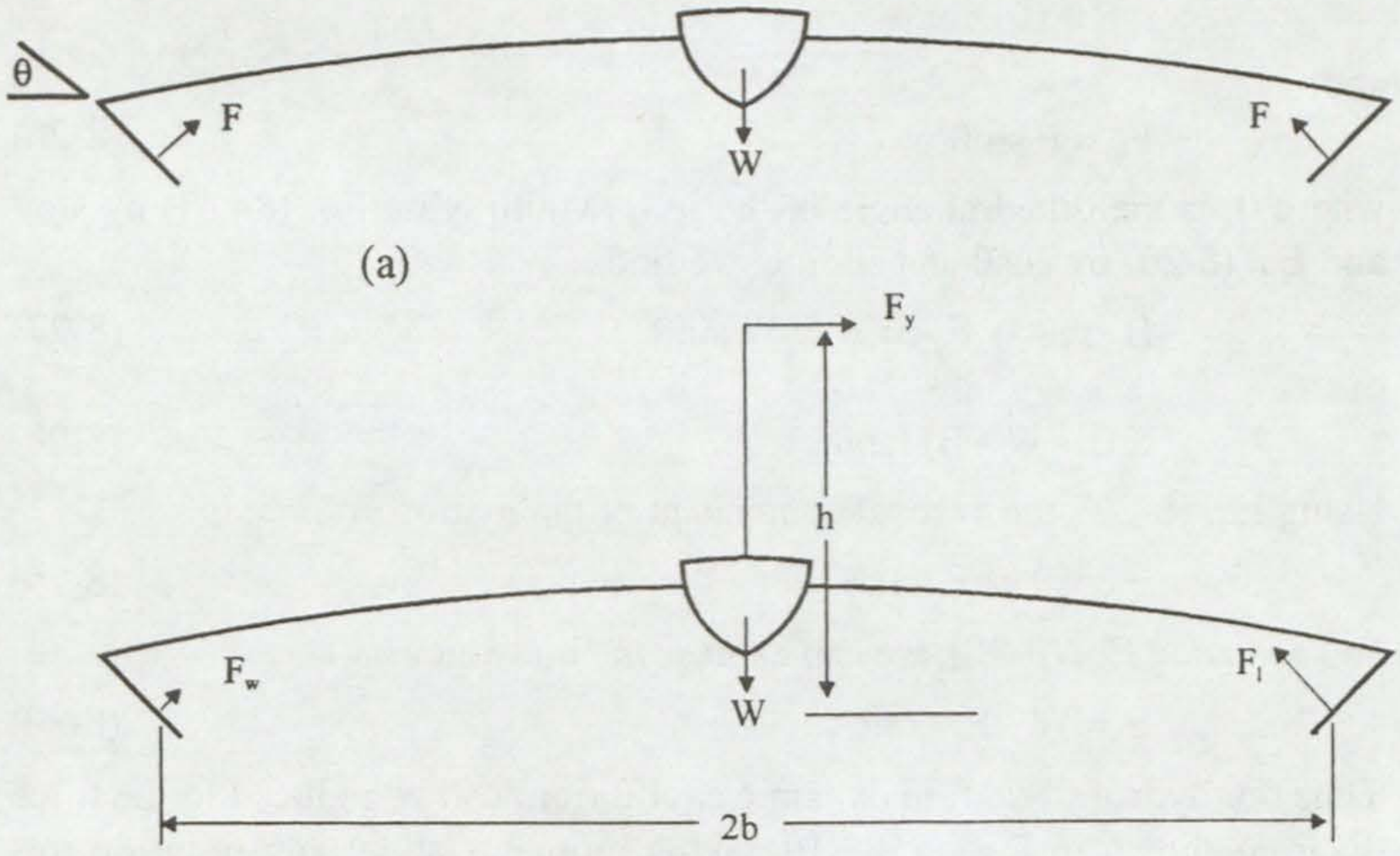

Fig. 8-20. Forces on a laterally symmetric hydrofoil system (a) without side force, and (b) with side force.

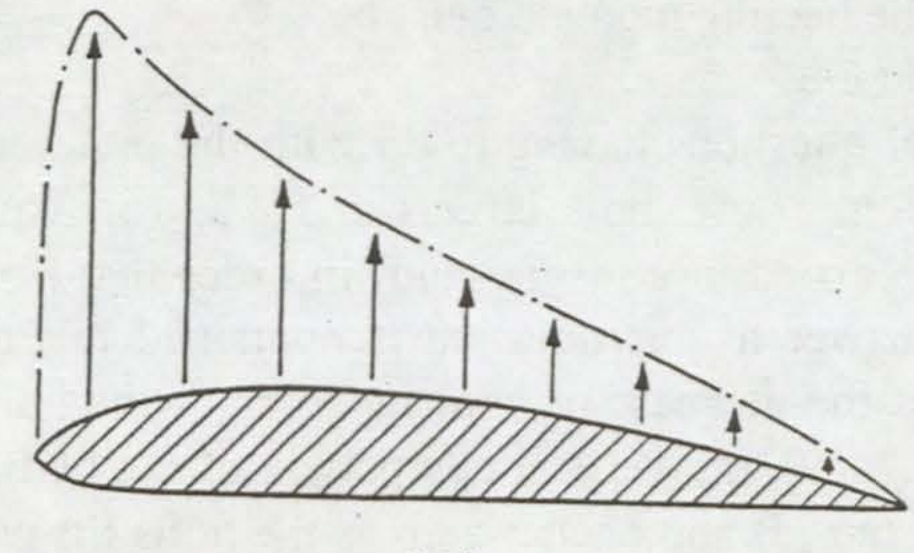

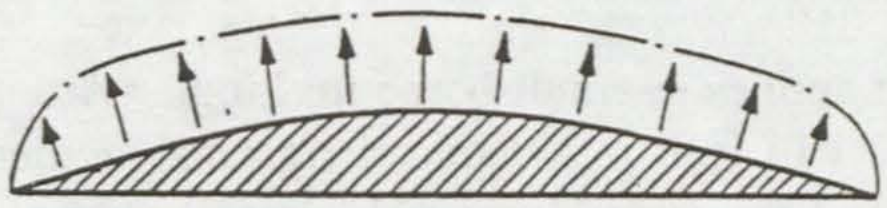

Fig. 8-21. Lift distribution for blunt (a) and ogival (b) sections at low angles of attack.

(2) the side force of the rig F_y is converted into vertical lift F_y ctnθ, thereby reducing the drag of the hulls.

The other practical question has to do with the appropriate value of dihedral angle θ. We see from Eq. (8-31) that this angle determines the beam of the boat, which is limited owing to the considerations of strength and weight. Too large a value of θ and the beam required for heeling cancellation is too large; too small a value of θ and the leeway angle and foil area necessary to generate a force F sinθ to oppose F_y becomes too large. We have seen from Eq. (8-32) that the beam is proportional to tanθ, the constant of proportionality being h, the height of the center of effort. We see from Eq. (8-26) that $F_y = F \sin\theta$, and since F is proportional to $A_F\phi_T$, the product of foil area and total angle of attack onto the foil, we find using the relation between leeway angle θ_l and angle of attack

$$\phi_l = \phi_T \csc\theta \tag{8-34}$$

that the product of foil area and leeway angle is proportional to $(\sin^2\theta)^{-1}$. In Fig. 8-18, we have plotted the functions tanθ (the beam function), $(\sin 2\theta)^{-1}$ (the leeway - foil area function), and the product of these two $\tan\theta/(\sin^2\theta) = (\sin\theta\ \cos\theta)^{-1}$ as a function of θ. These curves show a minimum in the product function $(\sin\theta\ \cos\theta)^{-1}$ at $\theta = 45°$, with the leeway - foil area function rising somewhat more rapidly toward small θ than the beam function rises toward large θ. Thus the practical range of dihedral angles is about

$$35° \leq \theta \leq 48° \tag{8-35}$$

with the final decision depending upon the details of the overall design.

It is also possible to cancel the heeling torque using a canted foil to windward that depresses rather than lifts the boat as shown in Fig. 8-19. There are two outstanding disadvantages to this arrangement, however. First, the hulls are being depressed and so the hull and hydrofoil drag is an increasing function of F_y. Second, and more important, the windward-depressing foil system is unstable. If a leeward foil pops out of the water owing to wave action, then the heeling torque acts to quickly reimmerse the foil. If a windward foil comes unstuck, the heeling torque is then uncountered by a windward depressing force and a rapid capsize may result. As a final comment on the question of hydrofoil heeling control and stability, we note that the analysis has so far been based on a laterally asymmetric or proa configuration. What about the application to laterally symmetric (trimaran or catamaran) configurations? In Fig. 8-20a we show a symmetric hydrofoil configuration being towed or motored at zero

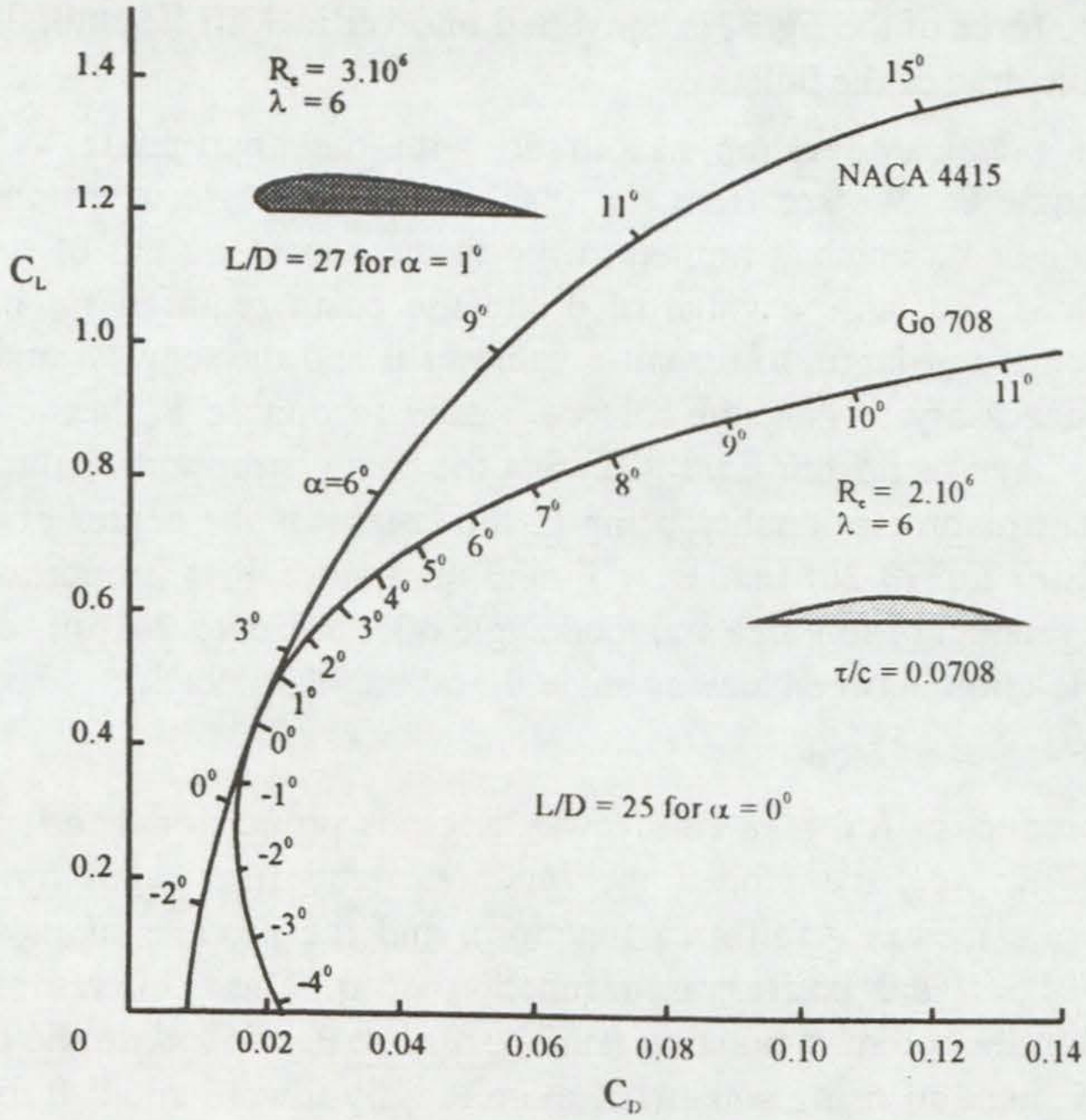

Fig. 8-22. Comparison of the characteristics of NACA-4415 and G"708 sections for an aspect ratio $\lambda = 6$.

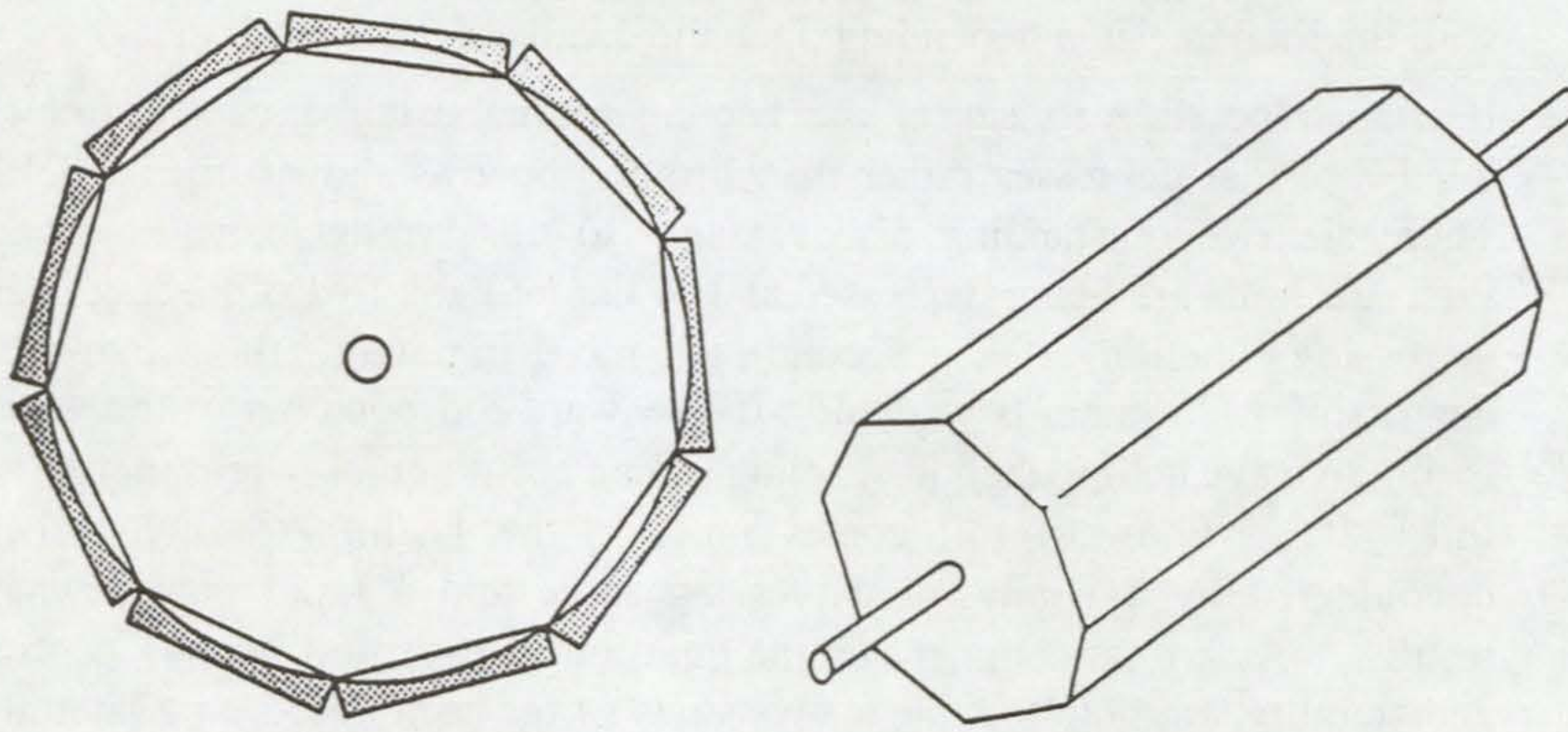

Fig. 8-23. A method for machining ogival foils.

leeway angle. Both the starboard and port foils are generating the same force. Equilibrium requires that

$$(F_p + F_s)\cos\theta = W \tag{8-36}$$

and

$$(F_p - F_s)\sin\theta = 0 \tag{8-37}$$

If the boat is under sail, then a side force F_y is present at the center of effort of the rig as shown in Fig. 8-20b. The boat will then develop a leeway angle such as to cause the foils to produce a net side force in opposition to F_y

$$(F_l - F_w)\sin\theta = F_y \tag{8-38}$$

where F_l is the force of the leeward foil and F_w is the force of the windward foil. The criterion for total heeling cancellation is that the line of action of the foils, the line of action of F_y, and the line of action of gravity must all pass through a single point. Unless a rig with very low center of effort is used (a rotor, perhaps) the line of actions of the hydrofoils is likely to cross the rig somewhat below the center of effort. In this case, the force differential between the two foils owing to leeway will be augmented by a difference in immersion as the boat heels slightly to leeward. By appropriate foil design, this heel angle can be held to a bare few degrees. This allowance of a modest amount of heel means that the leeway angle is reduced to a value less than that required for leeway alone to accomplish the heeling cancellation. Leeway angles for such symmetric configurations will generally be about 2°, half or less that required by a typical daggerboard. Finally, let us address the question of appropriate sections for hydrofoils. For surface-piercing foils, the drag at the surface is minimized by using a section having a sharp leading edge. Such sections have a rather even lift distribution when operated at sufficiently low angles of attack, and under these conditions are less prone to ventilation. If the foils are to be used on a proa, then the foil section should look the same from either direction. The likely choice for both reasons is an ogival section (flat on the bottom and a constant radius on the top). The lift distribution for a NACA-4412 section and an ogival section is shown in Fig. 8-21. The C_L versus C_D plot for these two types of sections is given in Fig. 8-22. We see that the simple ogival section gives away very little to the more sophisticated section in terms of maximum L/D. For angles of attack larger than the angle with which the upper surface of an ogival foil meets the lower surface (about 16° for a Gö708), flow separation occurs and the pressure distribution becomes peaky. For this reason, it may be worthwhile to give the leading and trailing edges a modest radius to extend the stall

phenomenon to higher angles of attack. In practice, the advantage of a truly blunt-nosed section is only realized for a deeply immersed foil, and then only if the foil can be made and finished to a standard normally unattainable by an amateur constructer. The ogival section, on the other hand, is easily made. For a Gö708 section, we take a cylinder whose cross section is an eleven- sided equilateral polygon (Fig. 8-23 shows a nine-dided example). Bar stock is mounted on each flat and the lot is chucked into a lathe and machined to a constant radius. For the Gö708 section, for which we have data, the radius/chord ratio is 1.7. High- strength aluminum or composite construction might be used.

With the outstanding exception of Dave Keiper's *Williwaw*[8-9], all sailing hydrofoil experimentation has been on day sailers, mostly with the emphasis on maximum speed in sheltered waters. In this chapter, I have deliberately restricted the discussion to hydrofoil systems capable of coping with heavy weather ocean sailing. In such conditions, the main advantages to the use of hydrofoils is seakindliness and enhanced seakeeping. The average day's run will very likely be somewhat augmented.

In writing this chapter I have solicited comments from men with vast experience of sailing hydrofoils: Dave Keiper whose emphasis is nearly identical with mine, George Chapman, and Sam Bradfield. I have seriously considered their comments, but have not accepted all of them. In particular, the theoretical evidence of superiority of the canard foil configuration seems strong, and none of my friends have been able to give me a convincing argument against it. Surface piercing foils are like*wise* no longer in fashion, but the fact remains that Dave Keiper's *Williwaw* sailed all over the Pacific on surface-piercing foils, so we know they work. For speed sailing the underwater lift-to-drag, or what George Chapman calls "hydro-load"[8-10], is superior for fully immersed foils. Whether these can be developed to cope with the full spectrum of ocean sailing conditions remains to be seen.

Some additional references on hydrofoils are given in [8-11 - 16].

in which we arrange the foregoing bits and pieces into laterally symmetric catamarans and trimarans

In preparation for writing this chapter, I reread Rob James' Multihulls Offshore[8-1], which I consider to be an excellent summary of the design factors for modern catamarans and trimarans. A review of this discussion, only some of which is applicable to the boats we envision, gives us a useful point of departure.

A trimaran, with all its accommodation and stores in the center hull, has a lower center of gravity than a catamaran. This low center of gravity, together with greater overall beam, gives the trimaran a higher ultimate righting moment than a catamaran[9-2], although the initial righting moment is lower owing to the easy initial submersability of the outriggers. Since the center hull is set down into the water unlike the wingdeck of a catamaran, the windage on a beam reach is less for the trimaran. Hard on the wind, the catamaran has the windage advantage. In light airs, the trimaran is essentially sailing on one hull and has a wetted area advantage of about $\sqrt{2} = 1.4$ over a catamaran of identical weight, prismatic coefficient, and length. As the wind pipes up, the wetted area advantage goes to the catamaran as the trimaran transfers ever more load onto its outrigger, which has high wetted area for its buoyancy. The wave resistance advantage, not a large factor in either case, is with the catamaran in both light and heavy airs. The trimaran has an accommodation advantage over a catamaran only in the very smallest sizes. Otherwise, the catamaran offers much larger and more useful accommodation space. Trimarans, running on two dissimilar hulls with different longitudinal center of buoyancy locations are less pitch prone than catamarans. On the other hand, catamarans are generally cheaper to build than trimarans and are safer in extreme conditions where heaving-to is the only option. Catamarans were developed for ocean racing later than trimarans because of the structural problem of spar and rigging strains on cross beams that also have to contend with the wracking strains imposed by two hulls trying to pitch independently. For conventional sloop rigs with the need for high forestay tension, the problem of mounting a rig "in mid air", so to speak, is formidable and solutions adequate for ocean racing awaited the development of high-tech composite engineering.

With these points of comparison between conventional cats and tris in

mind, let us see what the conclusions of the earlier chapters of this book contribute to the discussion. First, we note that wingsails and rotors, the only valid alternative rigs that we have considered, do not impose staying strains or mast compressional loading on the structure. The alternative rigs can and should be operated remotely from an inside helm station below and in front of the rig. The rig should operate within the perimeter of the boat, especially the wingsail, which is not demountable. Both rigs appreciate minimum heel angles, especially the Thom rotor with its large diameter fences that would shadow the rotor if the rig were to experience much heel angle at all. In the chapter on rudders and boards, the most important insight is that bow rudders are a natural for multihulls [9-3]. Bolger, whose idea this is, finds that if he takes two identical monohull daysailers, one with a stern rudder and one with a bow rudder, the one with the bow rudder is <u>always</u> faster by a fairly considerable margin. There are two problems with bow rudders, however[9-4]. The boat with its rig and board in the stern and rudder in the bow refuses to come about! This problem can be relieved by retracting the board or allowing it to weathercock as the boat comes about. The other problem is keeping a bow rudder in the water when going to windward in choppy conditions. The answer to both problems is a small sail in the bow in effect a canard yawl rig, where the foresail acts as a balancer and control surface, an aerodynamic bow thruster to drive the bow through the wind in a tack, and an air rudder to take over when the hydro rudder is aerated. I have designed and sailed a bow-steered catamaran and feel strongly that Phil Bolger's bow rudder deserves to be developed.

The hydrofoil chapter of my earlier book was fairly good for the 1970's, but needed a lot of updating for the present book. We see that hydrofoils can 1) eliminate the pitching instability, 2) stabilize heeling at $\theta = 0°$, 3) increase the speed of the boat by lifting the hulls entirely out of the water, and 4) contribute greatly to seakeeping and seakindliness. One should tend to be cautious in including too many radical ideas in one boat design, but fortunately we have an outstanding piece of test data to reassure us that hydrofoils are highly advantageous for ocean sailing.

In 1978, I wrote that the only flying hydrofoil craft to have successfully crossed oceans was David Keiper's *Williwaw*. In 1995, this is still true. Keiper's boat had no secret design features; it made a straightforward application of ladder foils to a trimaran configuration, designed and built as a flying hydrofoil craft. *Williwaw* was 31 feet, 4 inches overall, with an empty weight of about 2400 pounds, of which the aluminum hydrofoils accounted for about 400 pounds. She had a loose- footed sloop rig of 380

square feet. The hydrofoil configuration was neither canard nor airplane. There was a ladder with three horizontal rungs at the stern, which doubled as the rudder. The bow foil was a fairly lightly loaded monoplanar Vee-foil, highly braced with struts. Each outrigger mounted a canted ladder with a dihedral angle of 35 degrees. The photo in Fig. 9-1 shows *Williwaw* with its foils retracted. The heeling torque is compensated at a heel angle of 5 to 10 degrees, which suffices to lift the windward dihedral foil mostly clear of the water. When sailing, the foil configuration is a sort of reverse proa with the windward foils on either end of the hull 26 feet apart, and a single canted ladder foil to leeward, 10 feet from the symmetry axis of the other two. In practice, this configuration works wonderfully well under a wide variety of conditions[9-2].

Williwaw's conception began in 1963. She was built in 1966 and first became foil-borne in April, 1968. Her first offshore sea trials in the Pacific were in May, 1969. In September of 1970, Williwaw made a 16 day passage from Sausalito, California to Kahului Harbor, Maui, Hawaii under less than ideal conditions. Since then, Williwaw has crossed the Pacific, cruising more than 20,000 miles in all conditions between California and New Zealand. *Williwaw* was destroyed at anchor by storm waves at Hanalei Bay, Kauai, Hawaii on 15 October, 1977. The experience gained with *Williwaw* showed that hydrofoils give a much better ride than hulls and eliminate pounding, quick motions, snap rolls, control problems in heavy seas, and are much easier on the crew as regards fatigue and motion sickness.

Williwaw was designed to lift off at V_B = 12 knots in a wind $V_T \geq 13$ knots. At liftoff, the horizontal projection of the hydrofoil area was about 12 ft^2. The sections were NACA 16-510 with 6 inch chord. The leeway angle was very small except in gusts. The original outriggers each had a buoyancy of about 20 percent of the whole. This was increased first to 40 percent and then to 60-70 percent of the loaded weight. As a result of the experience gained, Keiper now feels that 100 percent buoyancy in the outriggers would be more appropriate. The bow foil had a forward sweep angle of 10 degrees and the lateral foils had a forward sweep angle of 14 degrees in order to discourage ventilation.

In spite of a mediocre rig, *Williwaw* was fast, having a top speed of about 22 knots at sea, and close to 30 knots in flat water and strong wind. Figure 9-2 shows Williwaw foil-borne at sea. Figure 9-3 shows Keiper's conception for a 40-foot version of *Williwaw*. David Keiper is a true

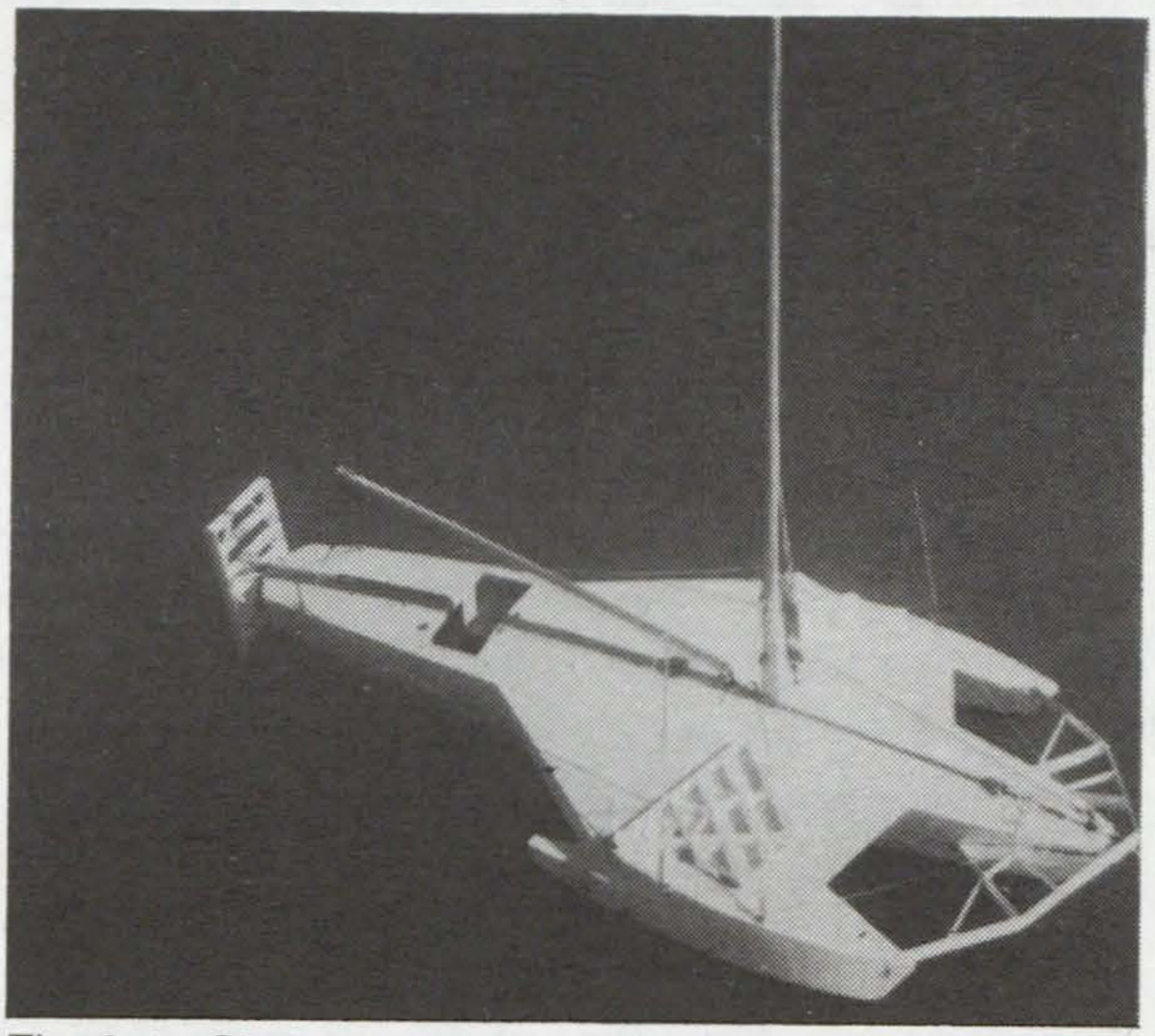

Fig. 9-1. Showing *Williwaw* with all four foils retracted.

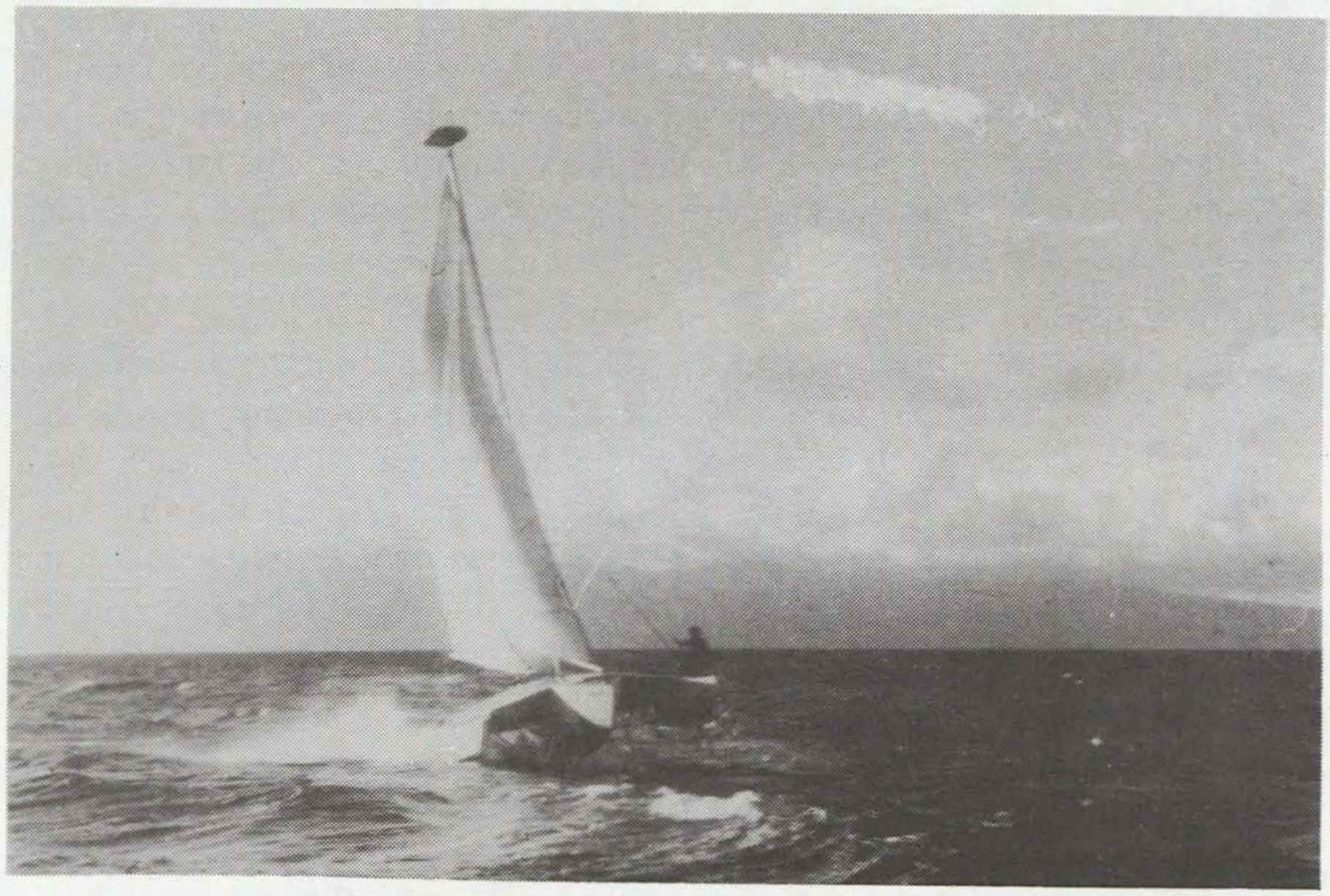

Fig. 9-2. *Williwaw* foil-borne at sea.

pioneer and an important figure in the development of multihull ocean yachts for the twenty-first century [9-5-8]. It is hard to argue with such experience and success, however we see in Fig. 9-3 that Keiper favours rather short full outriggers of modest buoyancy. I would contend that there will eventually come conditions where one cannot sail and the only thing to do is to heave-to. Keiper's storm strategy was to leave the foils set. This lowered the center of gravity and the foils tended to stick the boat to the water so wind gusts could not flip it. In conditions where wave-induced capsize is a problem, you do not want the boat stuck to the water, but rather free to slip and slide on steep wave fronts. In any case, I feel that the hull configuration should be optimal for avoiding wave- induced capsize. This configuration is a trimaran with high- buoyancy outriggers, or, better yet, a catamaran[9-1]. In modern designs, trimaran outriggers are approaching a length and buoyancy where they are indistinguishable from catamaran hulls. At this limit, the difference between cats and tris is the center structure: catamaran wingdeck as opposed to trimaran center hull.

Excess catamaran side windage is caused by the need to allow adequate wave clearance in the wingdeck to minimize slamming. This problem is alleviated to some extent by not extending the wingdeck all the way into the bows. Another design technique that lowers the sole of the deck saloon is to incorporate a Vee-shaped nacelle, a non-slamming shape, in the bottom of the wingdeck. Prout use this approach in several of their successful designs. Figure 9-4 shows my 61-foot *Gaïa* design in which all of the accommodation is contained in a 12 foot wide center pod with a hollow-Vee bottom profile that comes to within four inches of the static waterline. If we are going to be doing all of our serious sailing foil-borne, as seems reasonable, then the wingdeck water clearance problem that so complicates catamaran design can be alleviated by lowering at least the aft part of the wingdeck, or by going to a trimaran center hull with thick connecting beams like the Horstman or Macouillard designs. The only consideration is then weight and frontal windage. In this way, with the use of foils, the distinction between catamarans and trimarans is almost totally erased. It all boils down to performance expectation and accommodation choice. One may design a racer with minimal accommodation in a small center pod, or one may produce a luxurious cruiser with full-width deckhouse and accommodation in the aft one third of the hulls. The compromise imposed by the relative advantages and disadvantages of traditional cats and tris no longer apply.

We have seen that the beam of a conventional trimaran is greater than that

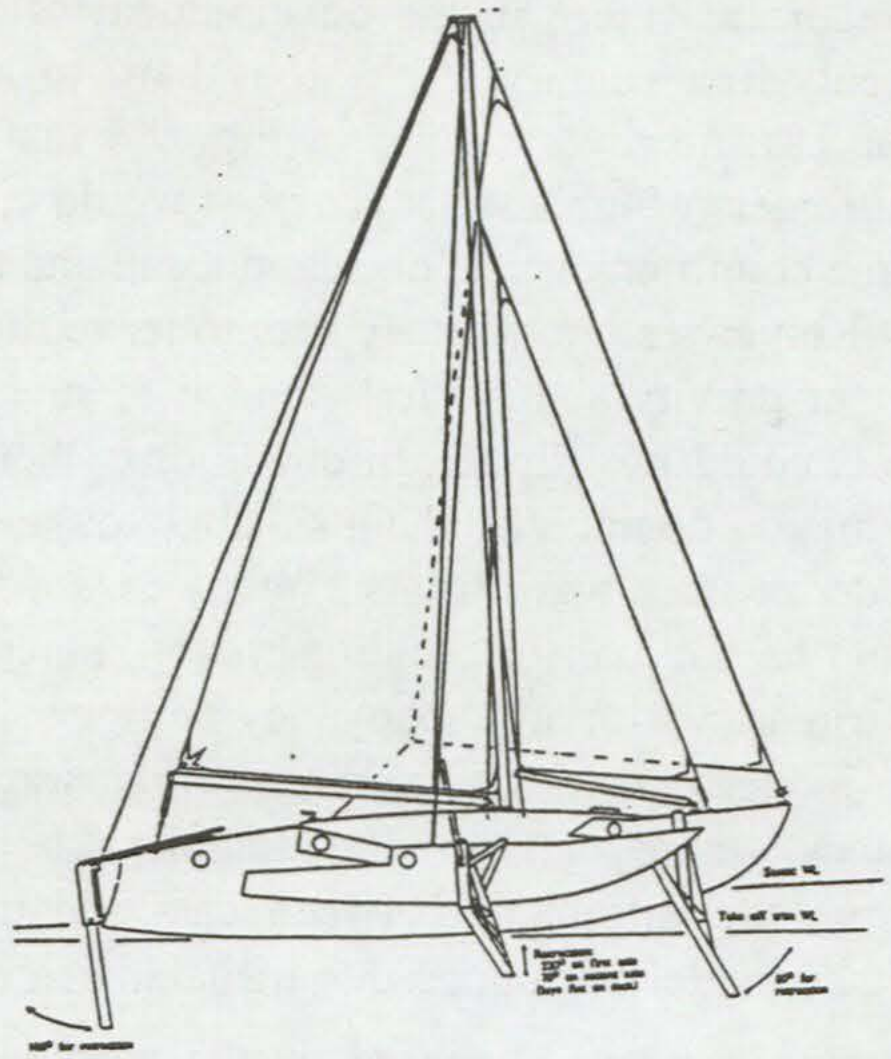

Fig. 9-3. Profile of Keiper's conceptual design for a 12-metre hydrofoil trimaran cruiser.

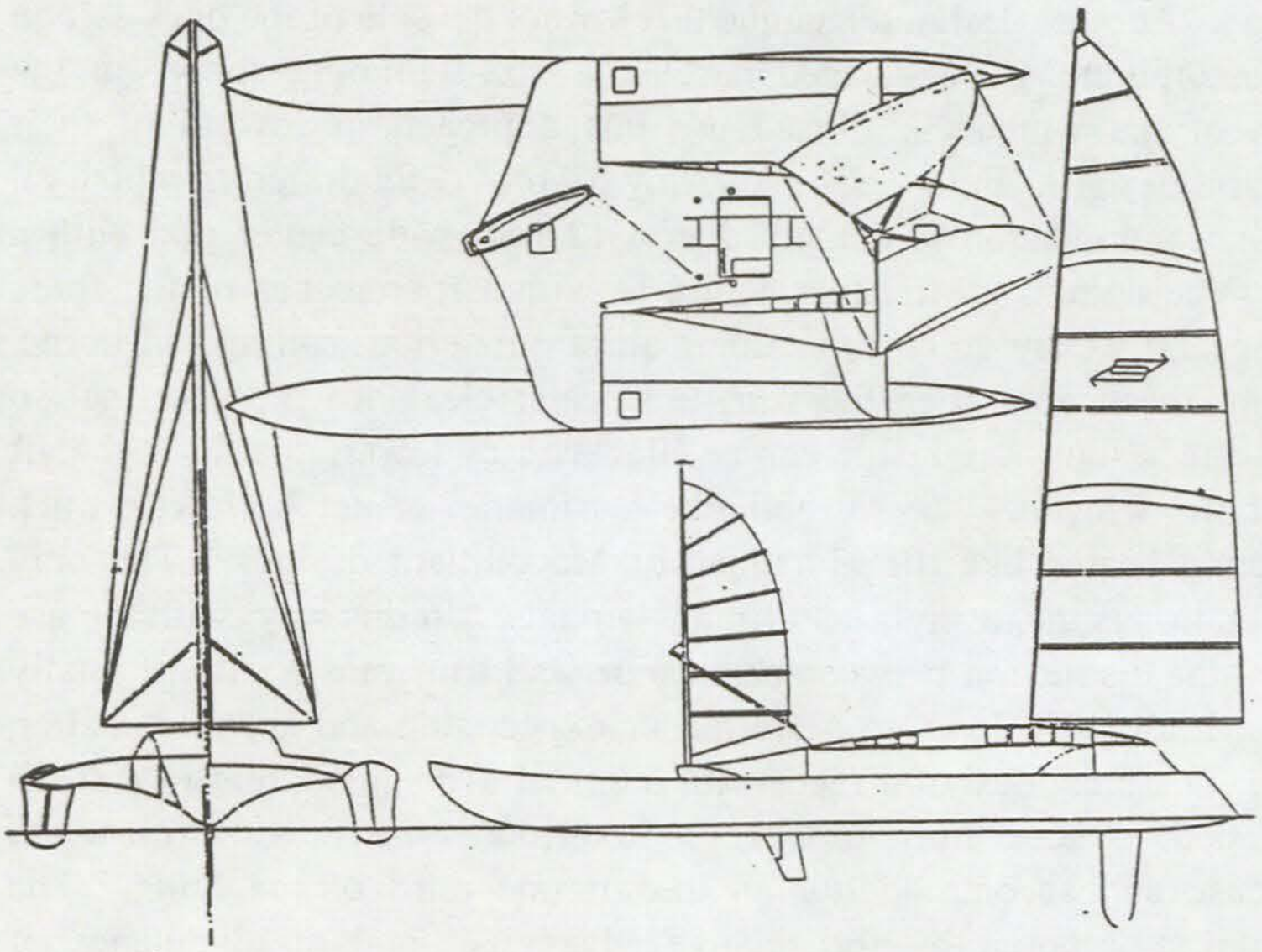

Fig. 9-4. Gaïa, a canard catamaran with accommodation only in the center pod.

of a catamaran owing to the presence of the center hull in the tri. Part of the decision as to how much beam to design has to do with not trading off lateral righting moment for longitudinal righting moment. It also has to do with having adequate strength in the beams without adding too much weight and hence exceeding the point of diminishing returns. With the distinction between cats and tris all but removed, we can probably contemplate a centreline-to-centreline beam of about 65 or 70 percent of the overall length for yachts in the 60 foot size range.

In my earlier book[9-2], I showed that the bending strains are the most severe ones that a cross beam experiences. This strain is given by

$$\sigma_{max} = Wl/h/I \tag{9-1}$$

where W is the weight of the boat, l is the length of the beam, h is the half-depth of the beam, and I is the a real moment of inertia given by

$$I = (2/3)a\,[h^3 - (h - \tau)^3] \tag{9-2}$$

for a hollow rectangular beam of width a, skin thickness τ. For $h >> \tau$ as seems likely, Eq. (9-2) reduces to

$$I \approx 2ah^2\tau \tag{9-3}$$

and Eq. (9-1) can therefore be written as

$$\sigma_{max} = \tfrac{1}{2}Wl/(ah\tau) \tag{9-4}$$

The weight of the beam is given approximately by

$$W_B = 2l(a + 2h)\tau\upsilon \tag{9-5}$$

where υ is the weight density of the beam skin (specific gravity times 62.4 lb/ft^3). Eliminating the skin thickness τ from Eq. (9- 5) by use of Eq. (9-4), we find

$$W_B/W = l^2(\upsilon/\sigma_{max})(a + 2h)/(ah)$$

or

$$l = \{(W_B/W)(\sigma_{max}/\upsilon)\,[ah/(a + 2h)]\}^{1/2} \tag{9-6}$$

This is a very interesting and useful formula. The quantity (σ_{max}/υ), wholly a function of the material of which the beam is constructed, has the dimension of a length. From Table 3-1 of[9-2], we find that (σ_{max}/υ) is about 32,000 feet for mahogany beams, almost the same for aluminum at 39,000 feet (but aluminum has lousy fatigue properties), 61,000 feet for glass cloth in polyester, 133,000 feet for Kevlar in epoxy, and a whopping 262,000 feet for carbon fibre in epoxy. Since the geometrical term ah/(a + 2h) is proportional to L, the boat length, for otherwise similar boats, we see that beam length can only increase as $\sqrt{L}$. This agrees with our observations

of nature where large animals are stocky and small animals are slender. Now let us put all this together. In Fig. 9-5 we show a 60-foot ocean cruiser with moderate accommodation. Steering is by a lightly loaded bow ladder foil that retracts aft. The main lifter is a biplanar foil of about 40 degree cant angle mounted on beam extensions. These foils are hinged at the point of attachment to facilitate easy retraction. The outer hulls (or outriggers) are used only for light storage. The accommodation is entirely in the center hull with some extension into the beam (wing), which is about 4 foot, 6 inches thick at the root. The rig is a low aspect rotor in order that full heeling compensation be achieved.

In this way, hydrofoils and a stress-free automated rig combine to eliminate the main distinctions between cats and tris and allow us to contemplate hybrid symmetric multihulls to cover the entire performance-accommodation spectrum.

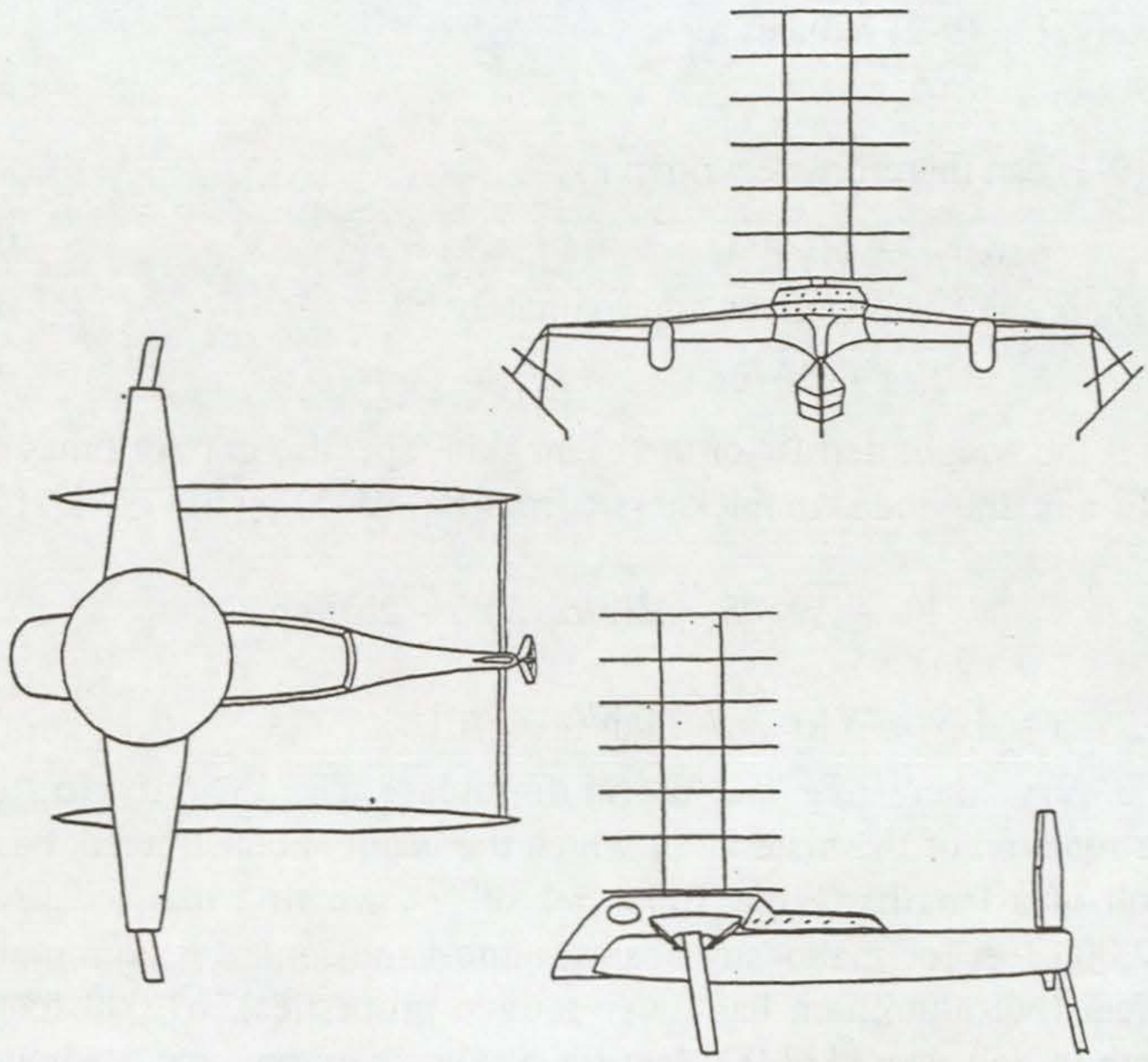

9-5 A symmetric multihull flying hydrofoil ocean cruiser

10 ASYMMETRIC MULTIHULLS

in which we take a critical look at proas and see that they may constitute the ultimate multihull configuration

In the last chapter, we had the advantage of well-developed multihull configurations, cats and tris, as our point of departure. In the present case, we do not have this advantage; proas have scarcely been developed at all. We have seen that trimarans and catamarans are symmetric laterally and asymmetric longitudinally, having a definite bow and stern like all "reasonable" boats. A proa, on the other hand, is symmetric longitudinally and asymmetric laterally, having no definite bow or stern, but a recognizable difference between its windward and leeward sides. This lateral asymmetry can be manifested in either of two distinct ways as shown in Fig. 10-1. At the top of this figure we see a trimaran. If we saw off the windward outrigger and beams, we get an "idealized" trimaran, a tri without the weight and aerodynamic drag of its windward members. This configuration is known as an *Atlantic proa.* If instead, one saws off the leeward outrigger and beams, the result is a *Pacific proa.* Examples of both have been built and have their adherents. These two types are so wildly different; how can they both be right? Let us examine each type in turn and see what are their advantages and disadvantages.

The Atlantic proa, typified by Newick's *Cheers*[10-1], designed and built for the 1968 OSTAR race in which it placed third, has one overwhelming advantage. Most of the weight: the accommodation, the rig, the stores, rudders, boards, etc are all in the windward hull, so the righting moment is maximized and the weight is minimized, which is exactly what a proa is all about. This optimization of power-to-weight ratio is not without cost, however.

First, the masts have almost no staying base to windward, so one is forced to use large-section free-standing masts that may compromise the efficiency of the sails and will certainly add weight and windage. On the plus side, the masts are probably buoyant enough and strong enough to stop a capsize aback at 100° - 120° where wave action or ingenuity may re-right the boat. This objection, which applied to *Cheers* is eliminated by the use of modern carbon fibre masts, which can be both light and slim, and by the use of double luff sails that wrap around the mast.

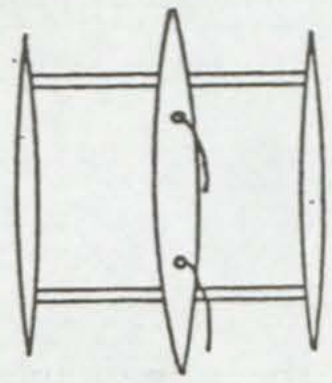

Trimaran

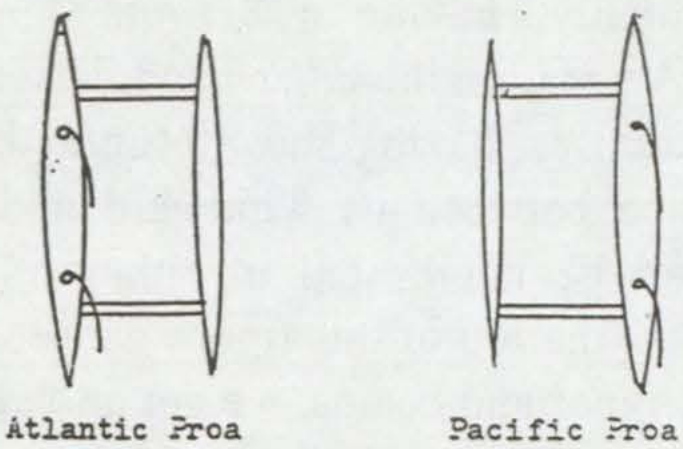

Atlantic Proa

Pacific Proa

Fig. 10-1. Defining Atlantic and Pacific proas in terms of a trimaran.

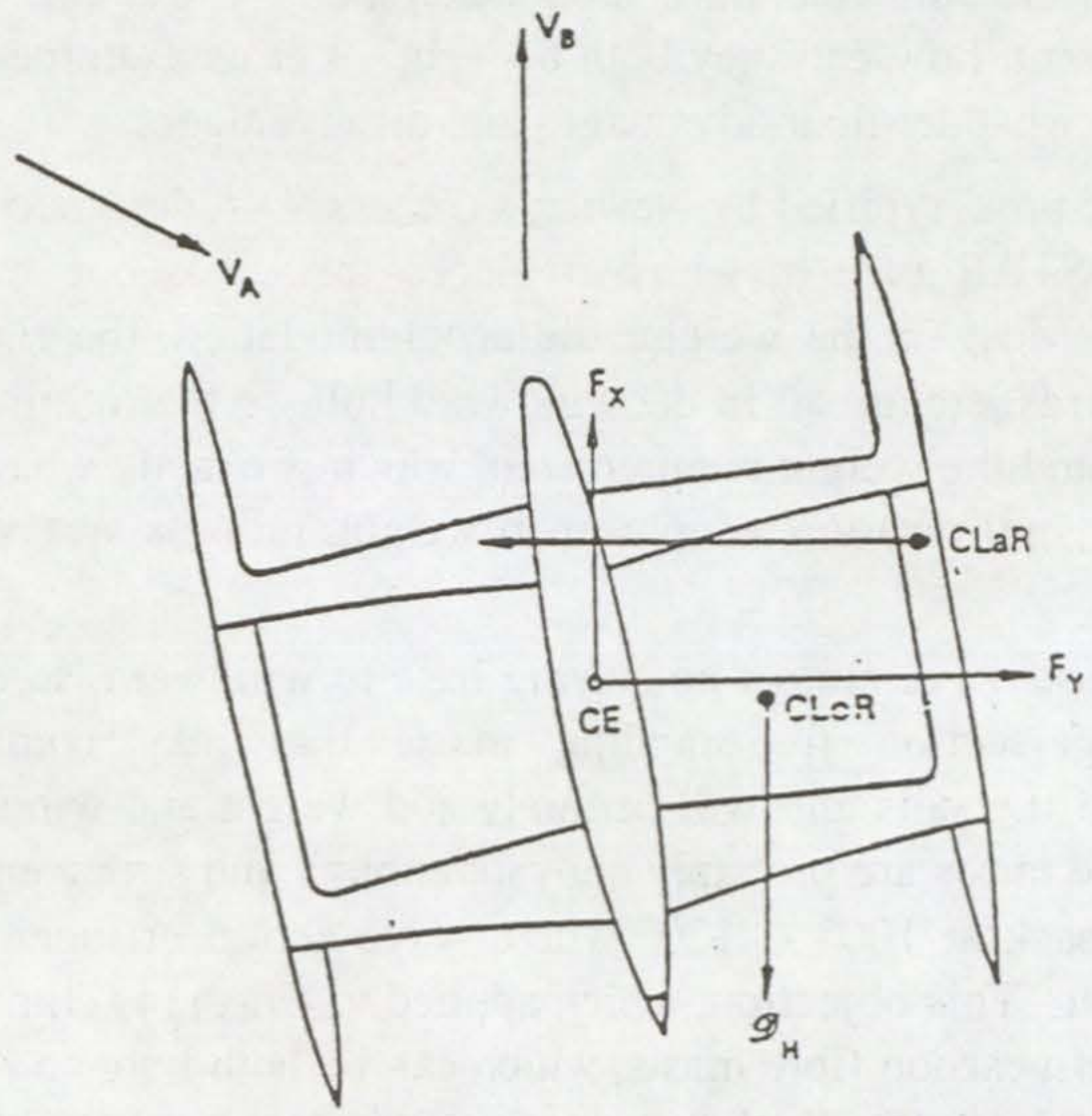

Fig. 10-2. Showing the balance of yawing torques on a trimaran.

The second problem with Atlantic proas is more severe. As shown in Fig. 10-2, a trimaran or catamaran must correct the lee helm that results when the lee hull or outrigger is driven deep into the water and the center of hydrodynamic resistance moves outboard of the center of effort of the rig. In a cat or tri, this correction is accomplished by locating the board somewhat ahead of the center of effort of the rig, so as to give a counter-torque to windward. Also, as we have seen, a trimaran outrigger is shaped so that its center of buoyancy moves forward as the outrigger is immersed, which has the effect of keeping the bows up and stabilizing the pitch instability. The proa, with its longitudinal symmetry, has a hard task to meet these obligations. Unless the center of lateral resistance can be moved forward as the speed increases, or the center of effort of the rig can be moved aft, there will be an ever-increasing lee helm. Newick solved these problems on *Cheers* by using a schooner rig whose center of effort is always aft of the mid point, and by using two daggerboards, one at either end of the windward hull, to adjust the location of the center of lateral resistance. This arrangement endowed *Cheers* with total inherent self-steering capability. *Cheers* is shown in Fig. 10-3.

The most worrisome problem for Atlantic proas arises from the fact that all of the windage is on the windward hull, an obviously unstable situation. An Atlantic proa, if left alone, will turn itself around and put the light outrigger to windward. It is then in position for a capsize, and indeed Cheers and almost all of its imitators have experienced such a capsize aback. In an attempt to relieve the problem, if not cure it, Cheers was modified to extend the accommodation to windward in a sort of pod or sponson (see Fig. 10-3) in order to catch a capsize at an angle from which the boat will recover. This is a weak fix and has only been marginally successful. The Pacific proa in its original Micronesian form[10-2] , Fig. 10-4, or as developed by Russ Brown[10-3], has its outrigger to windward and its accommodation, rig, rudders, and boards to leeward. In the Micronesian proa, the righting moment is supplied by a heavy solid log outrigger and a large agile crew,who can be sent scampering out to windward as needed. In Russ Brown's *Kauri,* there is provision for water ballast in the windward outrigger, however the usual solution is simply to back off. Brown's boats are light enough to move well with only modest righting moment. The Pacific proa configuration provides a very broad base for staying the mast, which can consequently have a small section. This encourages sail efficiency, and since the initial righting moment is modest, there is less structural strain imposed on the boat.

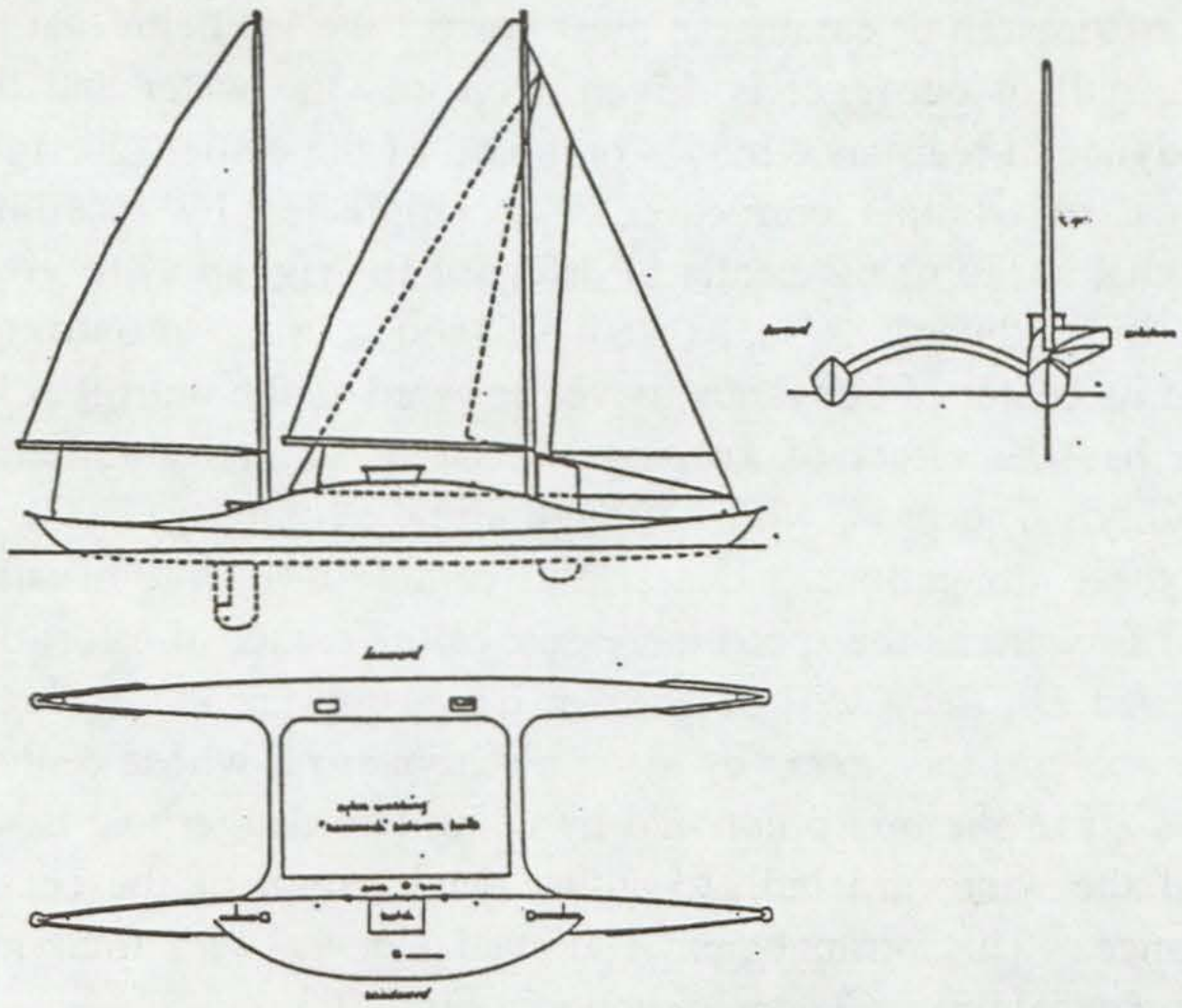

Fig. 10-3. Dick Newick's Atlantic proa *Cheers*.

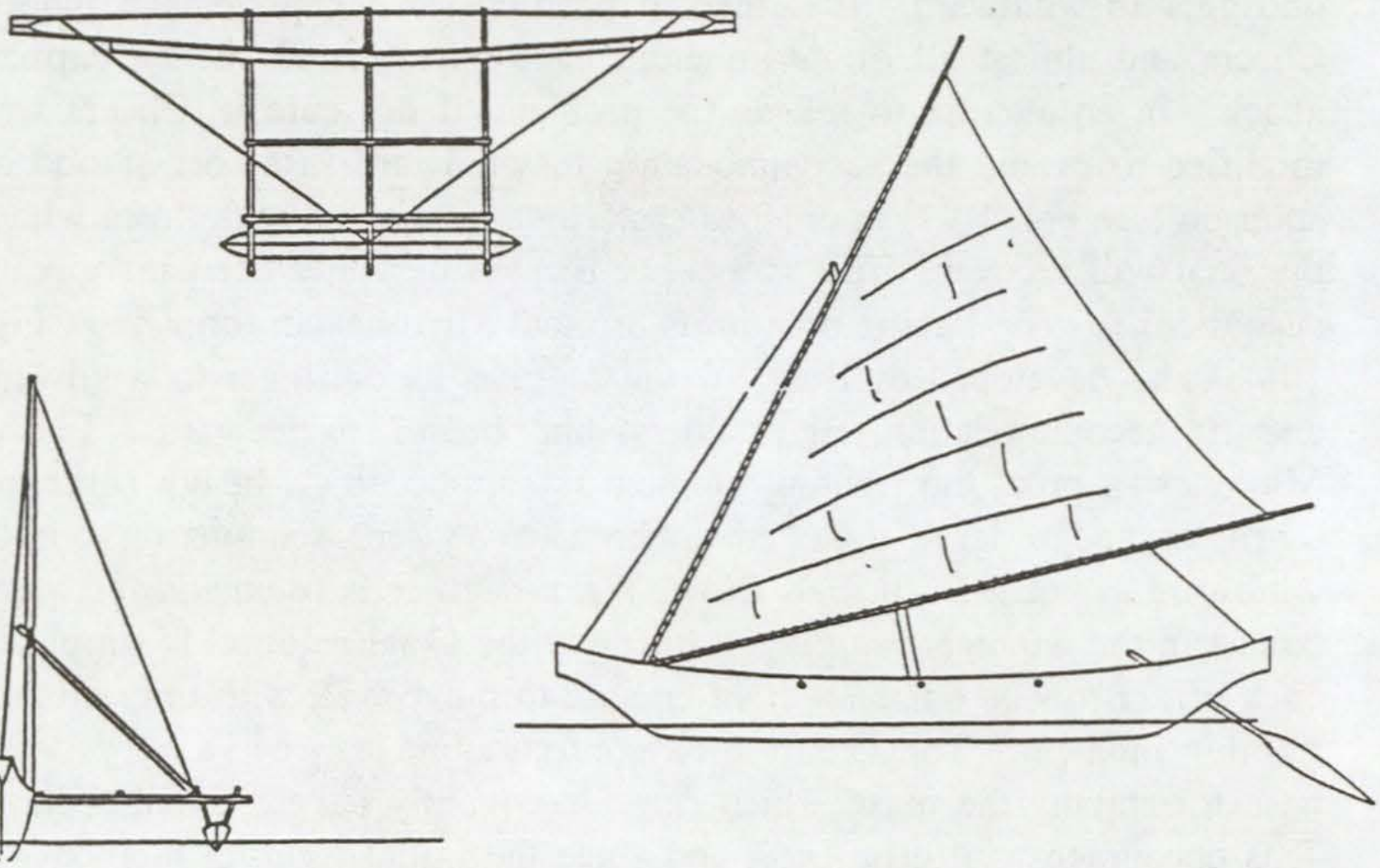

Fig. 10-4. The Micronesian Flying Proa.

As the windward outrigger leaves the water, all of the forces become concentrated in the same vertical plane. Unlike the Atlantic proa, the Pacific proa improves its helm balance as speed increases. By locating the center of lateral resistance aft of the center of effort, helm balance can be maintained with less effort than that required on the Atlantic proa.

The greatest virtue of the Pacific proa is that the windage is all on the leeward hull, so the boat naturally assumes the relationship with the wind that it was designed for. The greatest flaw of the Pacific proa for a modern yachtsman sailing shorthanded is the modest righting moment. Neither Atlantic nor Pacific proas as described will take care of themselves in extreme conditions. This is the greatest common flaw of both types and explains why there has been so little development work done.

In the last chapter, we found that with the application of alternative rigs and hydrofoils we could go a long way toward combining the virtues of cats and tris, and eliminating their vices. Can we do the same with Atlantic and Pacific proas, even before the introduction of hydrofoils and alternative rigs? The answer is yes, and I am surprised that no one has done it before. The greatest virtue of the Atlantic proa is that most of the weight is to windward where it provides righting moment. The outstanding feature of the Pacific proa is that the windage is to leeward and the boat is stable hands off. We can combine these virtues by locating the accommodation, stores, tankage, and such to windward in an aerodynamically clean hull, with sails, rudders, boards, and all other control surfaces to leeward. This arrangement combines the greatest virtues and eliminates the major vices of the other two types. A further advantage is that if you are caught aback, and the leeward (now windward) hull starts to lift, the accommodation hull with no appendages in the water will not act as a fixed axis for capsize, but will slide sideways as soon as the boards and rudders of the other hull clear the water. This type of modified Pacific proa may not only be the fastest hull-borne multihull possible, it may also be the safest. An example of this type is shown in Fig. 10-5. The sail is a wingmast sloop rig mounted on a balestron, quite similar to the rig used on *Elf Aquitaine II - Saab Turbo*. The daggerboard concept was suggested by Daniel Charles for Guy Devoux's proa Montpellier Languedoc Roussillon. The trunk is semi-circular; the board can be hauled to either end as shown in the figure. This scheme allows an asymmetric section with the leading edge always in the right direction and the center of lateral resistance appropriately aft of the center of effort. Bow trim and pitch stabilization require a modest application of hydrofoils. The two rudders are permanently deployed in

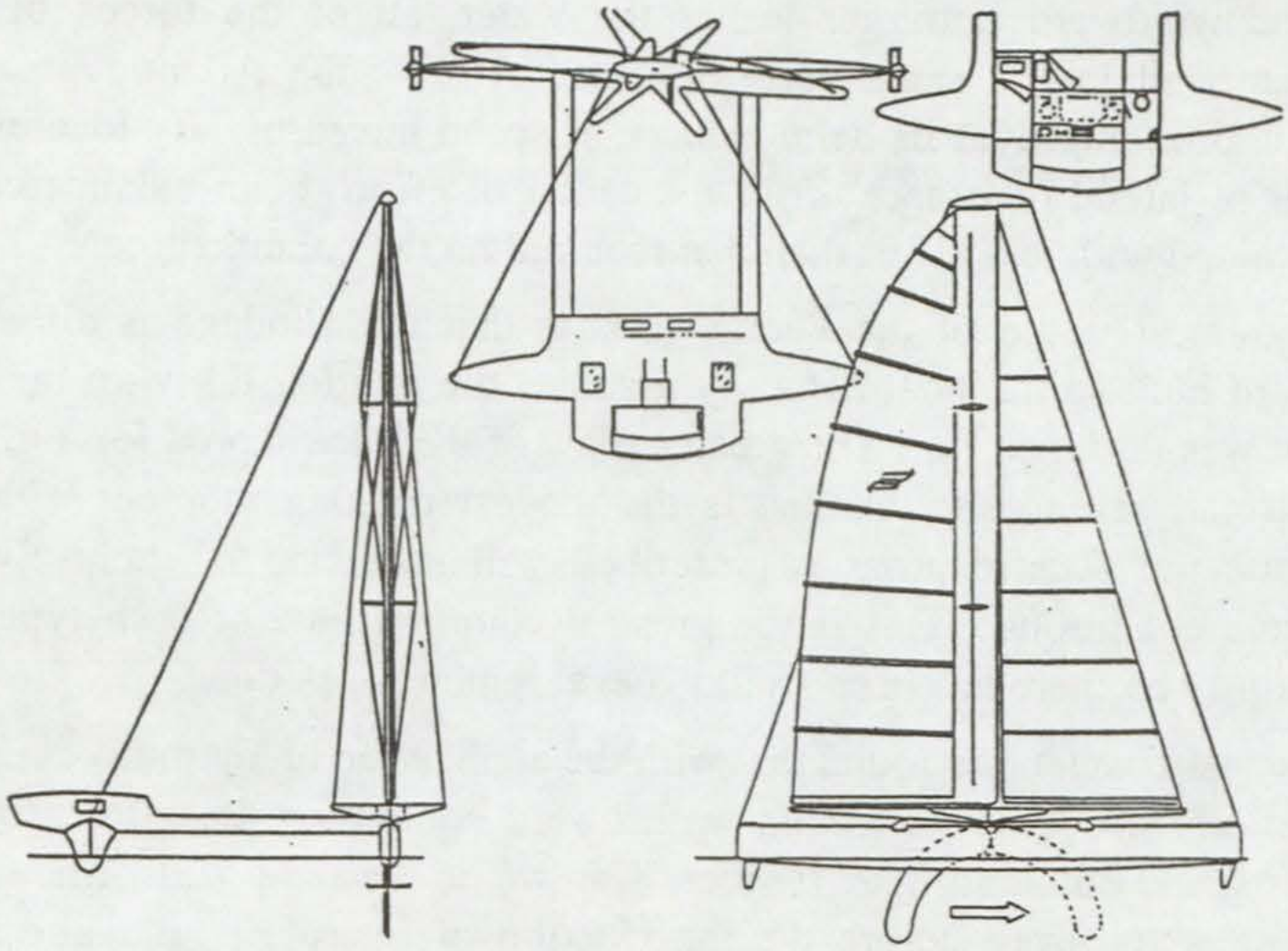

Fig. 10-5. A 36-foot modified Pacific flying proa.

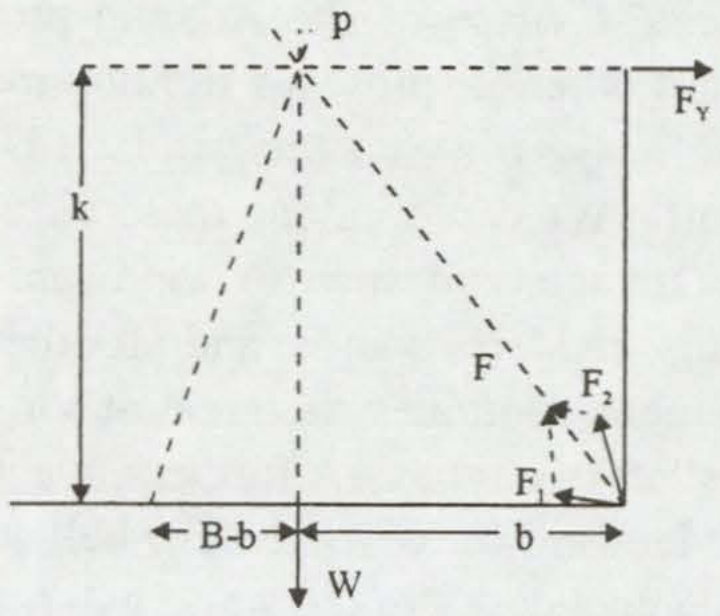

Fig. 10-7. A section view schematic of the hydrofoil proa forces showing total heeling compensation.

cases angled at 4° sweep so that the bow T-foil has 4° positive angle of attack and the stern foil has 4° negative angle of attack. The two rudders are turned 180 degrees on *shunting* (the term for changing ends; proas do not come about). Steering is by the bow rudder; the stern rudder can be clamped at an appropriate small angle to trim the boat. The windward hull has seawater ballast tanks in either end, so that one may choose to reef or ballast as the wind pipes up.

We now have a workable conventional proa configuration [10-4] (if any proa can be said to be conventional). Let us see what alternative rigs and hydrofoils can do for us. Clearly, the wingsail and rotor are both ideal for the proa application. Both have their center of effort coincident, or nearly

so, with the midplane, and both can be easily reversed for sailing in either direction. The trade-off is between the cost and height of the center of effort of the wingsail as opposed to the need for auxiliary power to turn the rotor. The requirement of being to sail in either direction imposes special conditions on a hydrofoil system. In Fig. 10-6, we show a schematic view of a hydrofoil system for a Pacific proa. The leeward hull has two identical canted foils at either end. The bow foil operates at an angle of attack ϕ and the stern foil operates at $-\phi$, thus reversal of direction does not entail adjustment of foil angles of attack, and the bow foil is always at the greater angle of attack as required by pitch stabilization considerations. The dihedral angles of the two leeward foils may differ; there is the means to vary these angles over a range of 15 degrees or so. There is also a central windward foil with force output F_3 and a fixed dihedral angle θ^3. This windward foil is operated at a 0° angle of attack so that it too need not be reset when the boat shunts. The sections of all foils must naturally be ogival in order to be longitudinally symmetric and to resist ventilation since forward sweep angles and the need to reverse them upon shunting are a complication we would rather do without. There is provision for water ballast in either end of the windward hull. By the use of ballast and/or smaller dihedral angle on the bow foil, the longitudinal trim can be maintained under any conditions. Figure 10-7 shows a schematic section of the hydrofoil system. If the net force from the leeward foils F and the force of the windward foil F_3 both pass through the junction of the line of action of the side force of the rig F_y and the weight W at the point P as shown, then clearly all torques about the point P vanish and the heeling is negated. The longitudinal situation is shown in Fig. 8-12.

The windward foil is, in theory, unnecessary as shown in the discussion of chapter 8. Stress consideration mandate a windward lifter, however. Figure 10-8 shows a 60-foot modified Pacific hydrofoil flying proa. The rig is a biplanar wingsail of 1150 square feet with wingsail air rudders at either end of the lee hull. The water rudders are used hull-borne and the air rudders are used foil-borne, the bow rudder steering and the stern rudder trimming in both cases. The dihedral angle on the forward lee foil is about 28o; this is increased to about 43° at the stern by means of a hydraulic ram acting against the lower point of contact of the struts with the beam extension. The angles of attack of the bow and stern foils are set at 2° and -2° respectively. In this way, the features of a stable and efficient hydrofoil system, capable of sailing in either direction, are incorporated into the proa design.

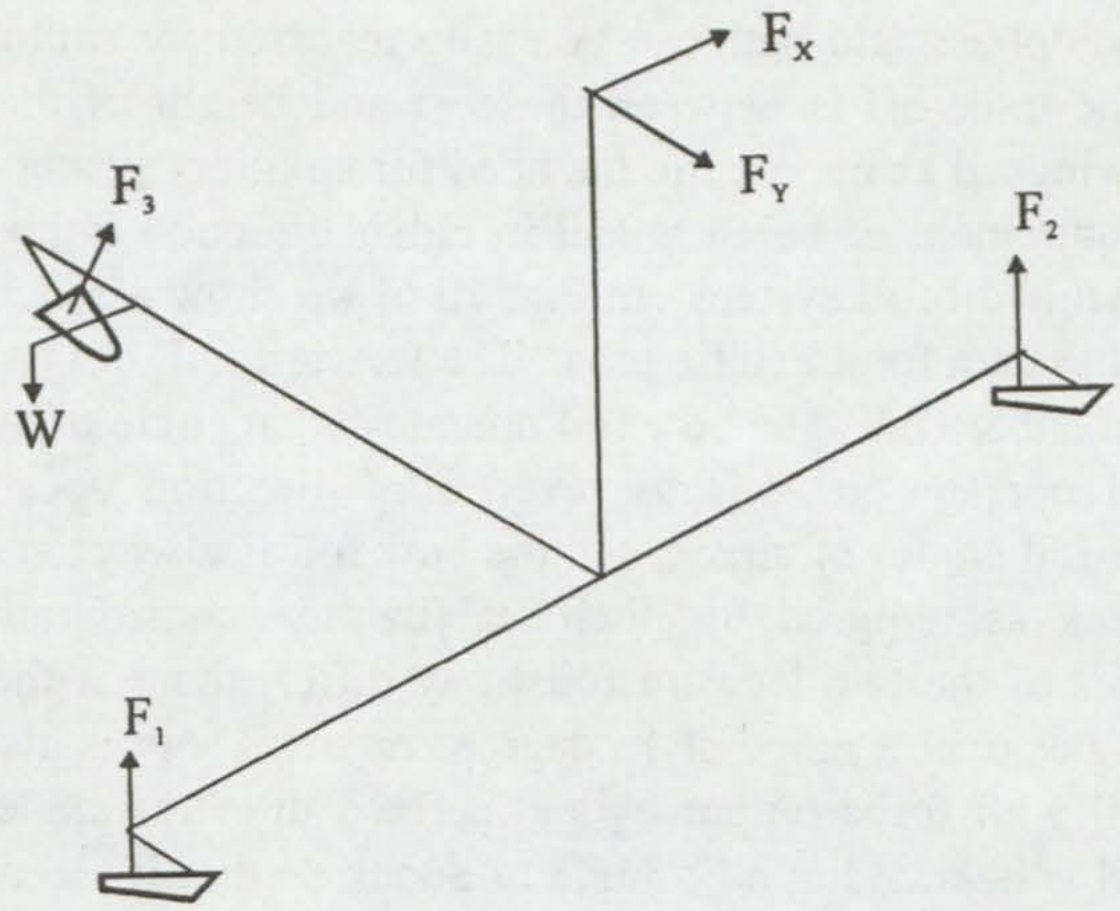

Fig. 10-6. An isometric view of the hydrofoil configuration and forces on a foil-borne Pacific flying proa.

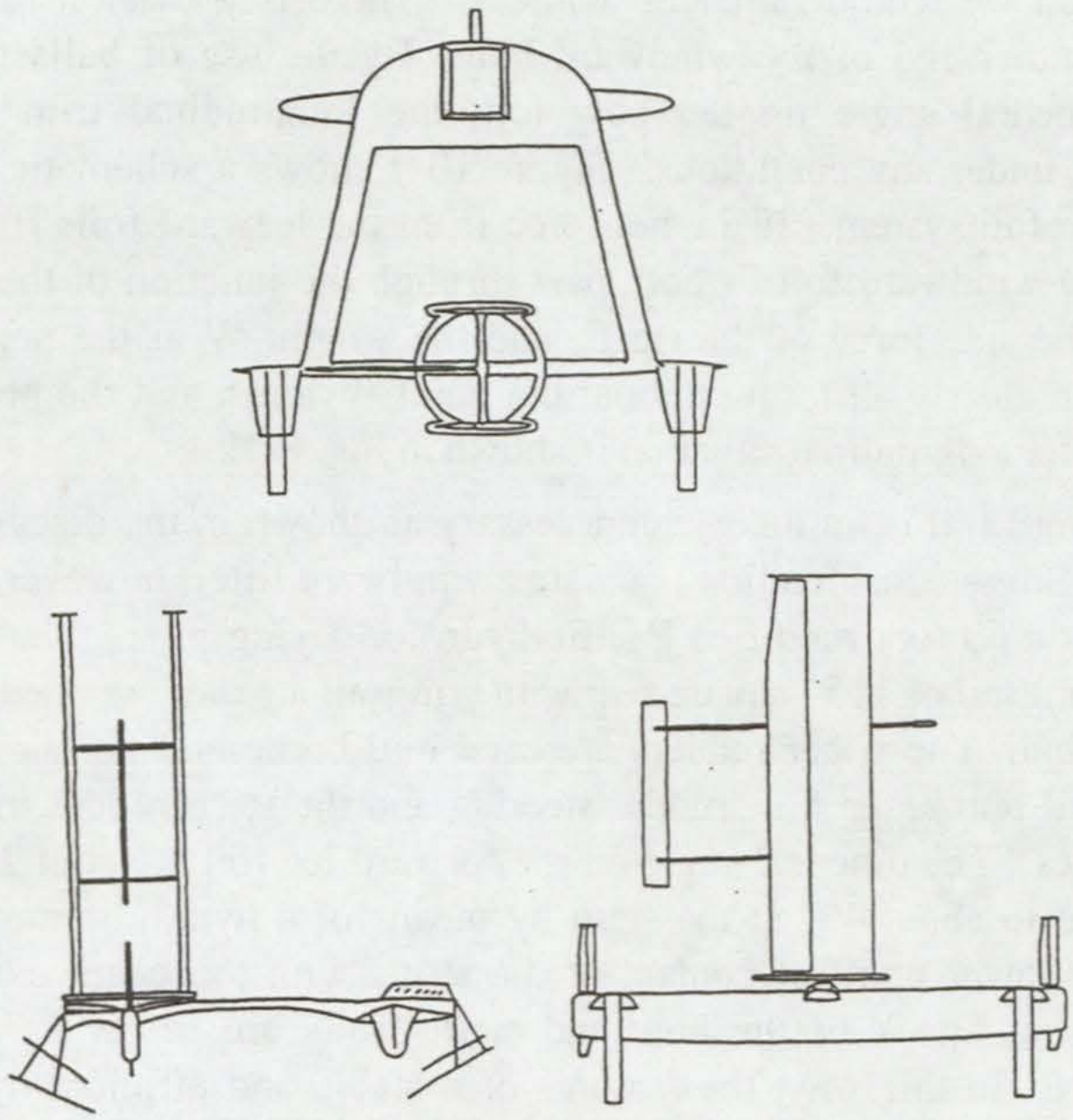

Fig. 10-8. A modified hydrofoil Pacific flying proa.

11 POSTSCRIPTS AND AFTERTHOUGHTS

in which we try to fill in some of the gaps and answer some of the obvious questions

In this book, we have examined the contribution that alternative rigs and hydrofoils can make to sailing in the twenty- first century. Our point of departure has been state-of-the-art multihull ocean sailing yachts. The rigs that we have discussed lend themselves to sailing with a degree of control and saving of physical effort that is not possible with conventional rigs with their enormous stay strains and sheet loads. Our emphasis on hydrofoils has been their application to promote seakeeping and seakindliness, rather than speed at any cost. The multihull ocean cruising yachts that we envision are *family* boats, capable of rapid and serene ocean passages with a small crew of people who need not be Olympic-class athletes.

In writing the book, certain questions and addenda have suggested themselves. Rather than go back and insert these into the appropriate chapters and pretend that they are not really afterthoughts, I have chosen to deal with them here.

Let us begin with chapter 2. The aim of this chapter was the derivation of Eq. (2-21) for $X = V_B/V_T$, which characterizes the light air performance of a hull-borne boat, and Eq. (2-22), which gives the maximum speed as limited by the righting moment. I would like to look at some limiting cases opf Eq. (2-21) with in mind a better understanding of this important formula. If, for simplicity, we take $\gamma = 90°$, then Eq. (2-21) becomes

$$X^4 - a^2(C_L - XC_D)^2(X^2 + 1) = 0 \qquad (11\text{-}1)$$

where $a = 0.119\,(A_s L/W)$. This equation is still somewhat messy to solve analytically. It is of interest to look at limiting cases, however. For small values of X, we find

$$X = \sqrt{0.119 C_L A_s L/W} \qquad (11\text{-}2)$$

If we take $C_L \approx 1.5$ as a representative example, then

$$X \approx 0.4\sqrt{A_s L/W} \qquad (11\text{-}3)$$

which is just the Kelsall-Shuttleworth formula[11-1]. In the limit of large X, Eq. (11-2) tends to

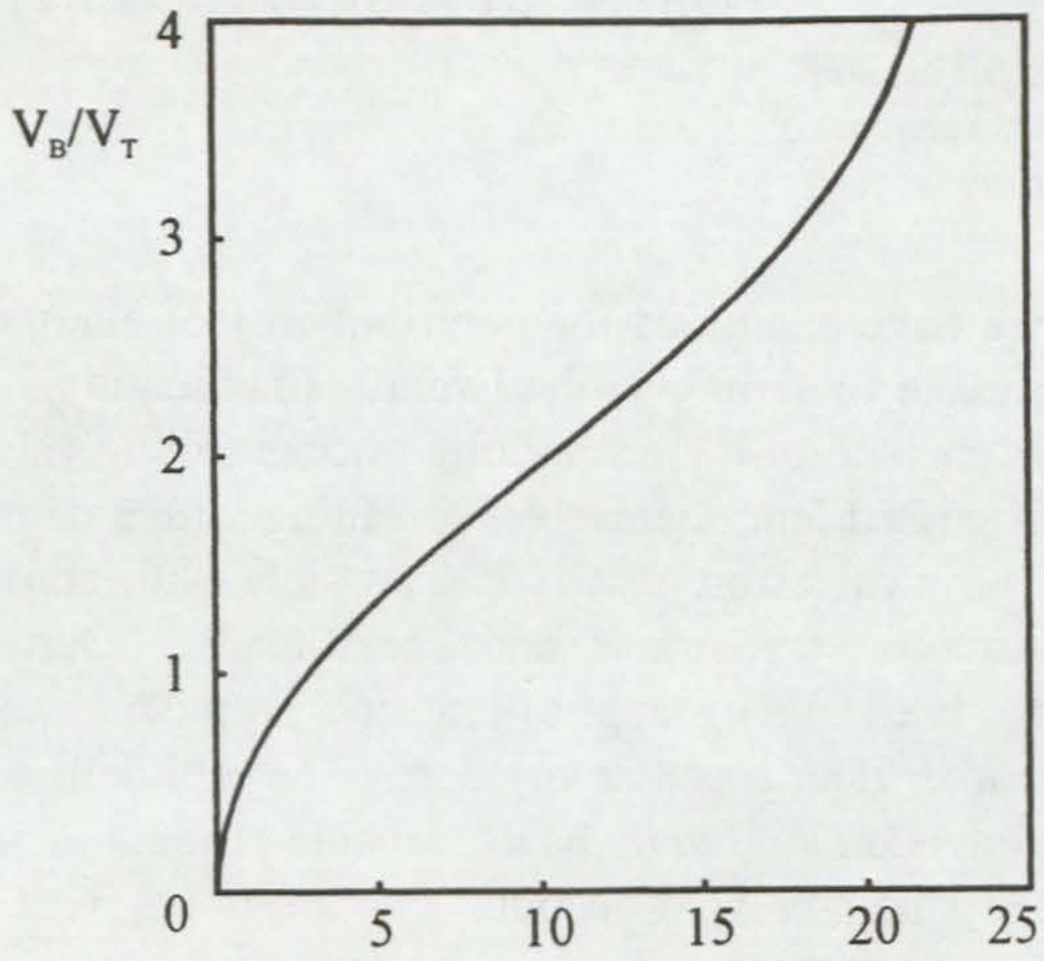

Fig. 11-1. $X = V_B/VT$ as a function of A_sL/W for $\gamma = 90°$.

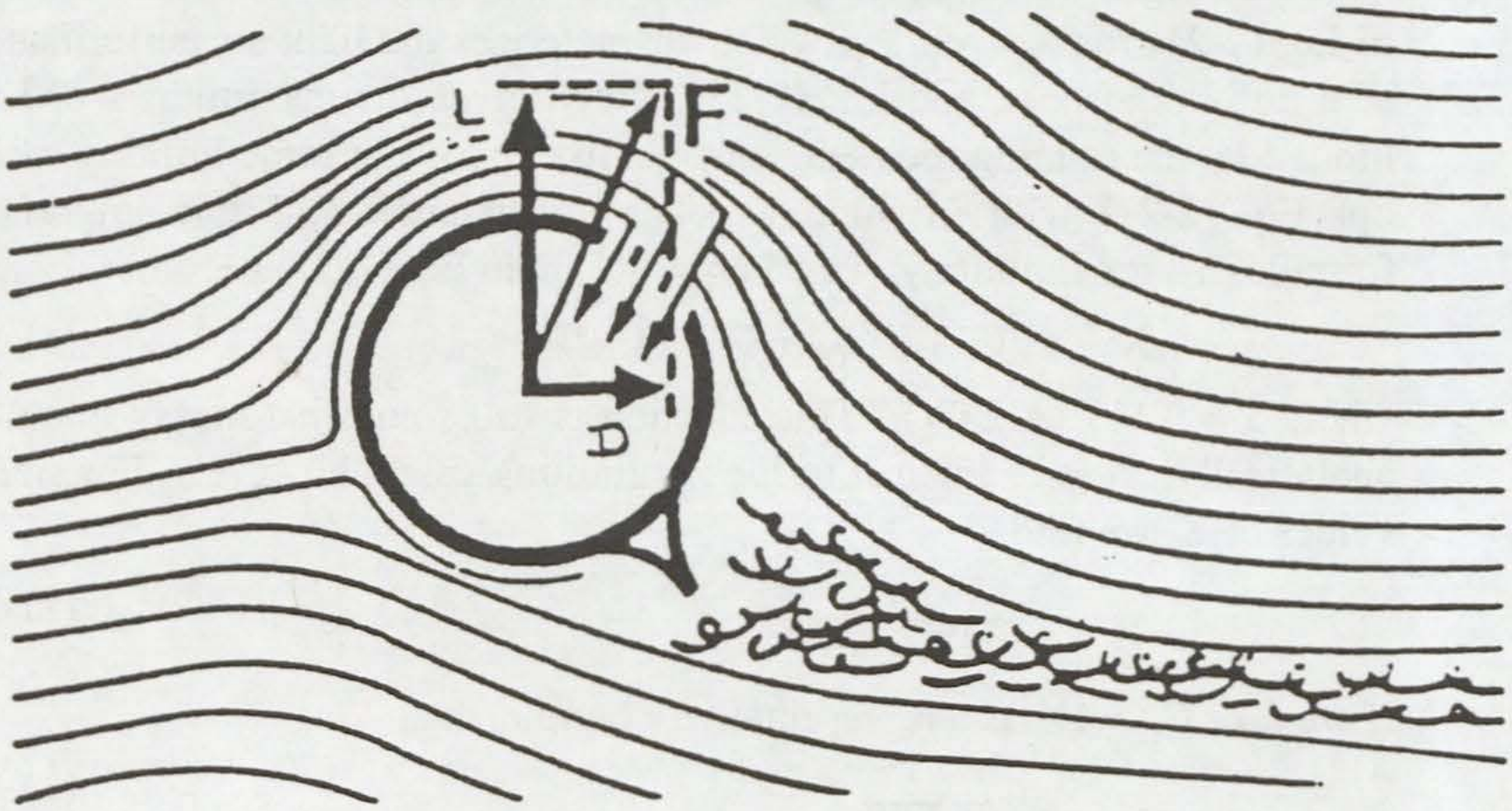

Fig. 11-2. The aspirated cylinder.

$$X = 0.119 C_L A_s L/W \qquad (11\text{-}4)$$

An exact solution of Eq. (11-1) showing the transition from square root dependence to linear dependence is shown in Fig. 11- 1. Here the choice of lift and drag coefficients is in agreement with the results of a study by Milgram[11-2]. In reviewing chapter 3 on hulls and outriggers, one further option that seems useful to me is to let the parameter α, defined in Eq. (3-20) as the eccentricity of the elliptical section be a function of distance along the hull x rather than a constant. In this way we would have the option to go from narrow deep sections in the bow to broad shallow sections in the stern. A linear function such as

$$\alpha(x) = (\alpha_1 - \alpha_0)x/L + \alpha_0 \qquad (11\text{-}5)$$

might suffice without complicating the evaluation of Eqs. (3-25) to (3-28) too much.

Chapters 4, 5, and 6 are concerned with alternative means to harness the wind for marine propulsion. We have considered the main alternatives to soft sail, however there is another possible candidate that might be mentioned, the aspirated cylinder[11-3]. This consists of a non-rotating vertical cylinder that generates lift by deflecting air through the cylinder (see Fig. 11-2). The development work was done by Lucien Malavard of the French Academy of Sciences and one of his colleagues, Bertrand Charrier (whose Ph.D. thesis on rotors is referenced in the rotor chapter). The results of this development was a sea trial by Jacques-Yves Cousteau on a 65-foot catamaran, *Moulin á Vent*. This cylinder, which was elliptical, featured two perforated vents running the length of the cylinder. A movable flap is positioned to cover one or the other of of the vents, depending upon which tack you are on. A 12 hp exhaust fan at the top of the cylinder draws air in through the vent and lowers the external air pressure on the open-vent side, thereby developing lift. The cylinder can be trimmed to an appropriate angle of attack to optimize sailing efficiency. In a sense, this amounts to a symmetric section wingsail with boundary layer modification capability. A British group at the Wolfson Unit of Southampton University have also worked on the idea, however in their case they inject air into the boundary layer on the windward side, rather than remove air on the leeward side. I do not have any data on lift and drag, hence I did not make a chapter on aspirated cylinders.

Now we come to the AeroRig, which looks at first sight to be only a small departure from a conventional sloop, but is truly a rig for the twenty-first century. This rig is also known as a balestron or swing rig (see Fig. 10-5).

Fig. 11-3. A Hirondelle Family catamaran with the AeroRig option.

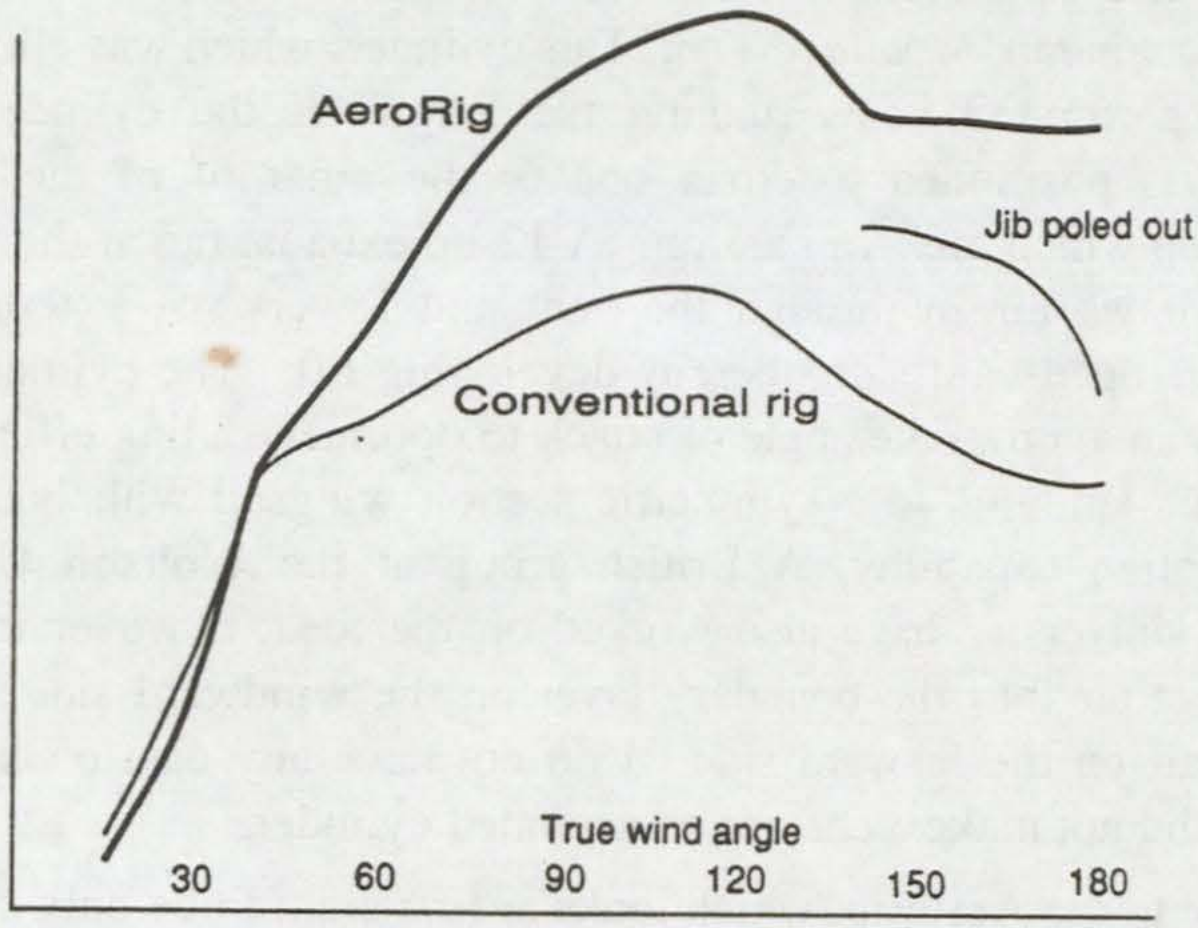

Fig. 11-4. The driving force of an AeroRig as compared to a conventional fully battened rig. Notice the improved performance off the wind.

The AeroRig is not new; model sailing boats have been built using this rig for a 100 years. Blondie Hasler experimented with it 30 years ago, and more recently, the rig enjoyed great success on *Elf Aquitaine II - Saab Turbo*, a French racing catamaran. In the late 1980's, Carbospars, Ltd. was founded in England to build and produce Ian Howlett's refinement of the concept. It is Carbospars' name for it, *AeroRig*, that is likely to stick.

The AeroRig mast is a tapered circular section spar of carbon fibre construction and is unstayed. The mast rotates freely, being stepped in a bronze/stainless thrust bearing on the keel (trimaran) or nacelle (catamaran) and passes through a Vestalyte collar bearing in the coachroof. The distance between the two bearings must be at least eight percent of the mas height, so not all existing multihulls can be retrofited with the AeroRig. The boom is rigidly attached to the mast and extends forward as well as aft of the mast, to provide a point of attachment for the jib tack and a sheeting position for the jib clew on a short curved transverse track. Thus, the spar configuration is an inverted asymmetric cross and the sail configuration, although it looks like a seven-eighths sloop rig, is, in effect, a balanced slotted lugsail. The net center of effort of the rig is just behind the trailing edge of the mast, mere inches aft of the pivot axis. Thus the load on the mainsheet, the only working sail control required, is very light. On a Hirondelle catamaran, the first production boat to offer the AeroRig, a simple 2:1 purchase suffices (Fig. 11-3).

Since the boom is rigidly fixed to the mast, which is free to rotate, the headsail is set in an ideal relationship to the mainsail, and this relationship is maintained regardless of the course that the boat takes with respect to the wind. Figure 11-4 shows the results of wind tunnel tests at Southampton. to compare the Aerorig with a conventional one. Hard on the wind the wind the forces are similar. As the apparent wind angle passes 40 degrees, the AeroRig begins to show its advantages, producing 33 percent more force at 120 degrees and 50 percent more force at 180 degrees (dead run). When the conventional rig uses a poled out jib, the AeroRig forces advantage is reduced to 33 percent. The AeroRig is able to maintain a much higher coefficient of lift at all angles exceeding 45 degrees.

With the AeroRig, the angle of attack of the apparent wind onto the rig is an optimal 22-30 degrees and the resulting aerodynamic force is more directed to propulsion and less to heeling than a conventional sloop rig for which the relationship between the jib and the mainsail is far from ideal when the boat is other than hard on the wind.

What is the AeroRig like to sail? Going to windward you have all the advantages of a modern sloop rig doing what it does best. In addition, there is no standing rigging to whistle and cause parasitic drag. Tacking the rig is just a matter of putting the helm over and walking to the other side of the cockpit. There are no winches to grind or headsails to haul over. The jib slot, which Carbospars have found by experiment should be about eight degrees on the average, can be fine tuned for wind strength by the use of stops on the transverse clew track. Similarly, such track stops could be used to lock the jib to windward so that the rig could be hove-to. In testing the rig, British sailing journalist Denny Desoutter's only criticism was that he did not see how the rig could heave to[11-4]. A simple track stop cures that objection.

Since, as we saw in Fig. 11-4, the AeroRig provides a greater portion of its aerodynamic force to propulsion and less to heeling, the wind strength for which reefing is advisable is higher and less critical than with the conventional sloop rig. The headsail is roller furled and the fully battened mainsail has a single-line slab reefing system. The reefing line goes forward to a single Spinlock jammer. The main halyard, spare halyard, and jib sheet run aft to a triple Spinlock jammer. Between the two boom-mounted jammers is the rig's only winch (on the Hirondelle adaptation). Reefing is not critical since the mast is tapered to a degree that allows gusts to be spilled by upper mast deflection while drive is retained lower down. As the gust passes, the entire rig comes back on line. In addition, one may feather the sheet, which is never very heavily loaded, by tightening up to the point where the sails just begin to fill. In sum, the AeroRig is much more "panic proof" in rising winds and gusts than a conventional rig.

Downwind, the sheet is let out until the boom is at right angles with the axis of the boat. The main and jib are thus fully exposed to the wind, now at 90 degrees to the rig. Specialist downwind sails are not needed and offer no advantage, except perhaps in the very lightest winds. The prospect of a gybe holds no fear at all. The rig can be sailed by the lee to a considerable degree and a gybe, when it occurs, is a gentle thing owing to the balancing action of the jib. Imagine the situation where you are on a run in heavy seas and a rising wind and you really need to reef. In a conventional rig with the sails pressed against the shrouds you either have somehow to claw the sails down or turn upwind, putting yourself abeam of the seas in so doing. With the AeroRig, you simply release the sheet. The rig then weathercocks with the boom 180 degrees around, and you are hove to downwind and may reef at your leisure from the security of the cockpit. As

this scenario suggests, sail may be hoisted with the boat on any course you like, even downwind, simply by allowing the rig to weathercock as the mainsail is raised.

In trimming the rig, tell-tales on the jib are very helpful. Alternatively, one may use a wind instrument with a close-hauled indicator that measures apparent wind direction not with respect to the axis of the boat, but with respect to the axis of the boom, in effect, angle of attack onto the rig which should be in the range 22-30 degrees for all courses except a run.

All of the advantages enumerated above add up to major convenience for the cruising sailor and to a degree of control unattainable in any other soft sail rig of which I am aware. As to performance, measurements carried out in Britian on two Hirondelles, one AeroRigged and the other a conventional sloop, showed that the AeroRigged boat with 15 percent less sail area was 45 percent faster to windward and nearly 60 percent faster on a broad reach in 8 knots of wind as compared with the conventionally rigged Hirondelle[11-5] (which is scrapping its sloop rig and is being refitted with an AeroRig). Denny Desoutter has written a follow-on to his 1993 article[11-6] and is convinced that the AeroRig will find a prominent place for itself on the sailing scene.

As a final comment on the AeroRig, I note that it would not be all that difficult to arrange for automatic sail trim. This could be done by adapting a robust wheel-type autopilot to rotate the rig, with apparent wind direction information supplied by a small wind direction indicator in the bow of the boat. It might be necessary in this regard to set the center of effort of the sail plan quite close to the pivot axis in order to keep the torque demanded of the sail trimming motor at a reasonable level.

The operation of such an automated AeroRig, a "cruise control" if you will, would be quite comparable to, but much simpler than, the wingsail described in chapter 4. Now let us see what sort of loose ends we have left in the hydrofoil chapter. It would be useful to make a comparison of the relative efficiency (as determined by lift-to-drag ratio) of an incidence controlled T-foil and a surface piercing foil. A good deal of thought about this has about convinced me that this is best left to experimental measurement. One thing we can do that is useful is to point the way to a version of Eq. (2-21) that predicts hydrofoil-borne values of $X = V_B/V_T$ for all course angles and all true wind speeds V_T. This problem is not inherently difficult, however it requires more hydrofoil drag data than we have at the present time. In Fig. 11-5, we show two curves that estimate

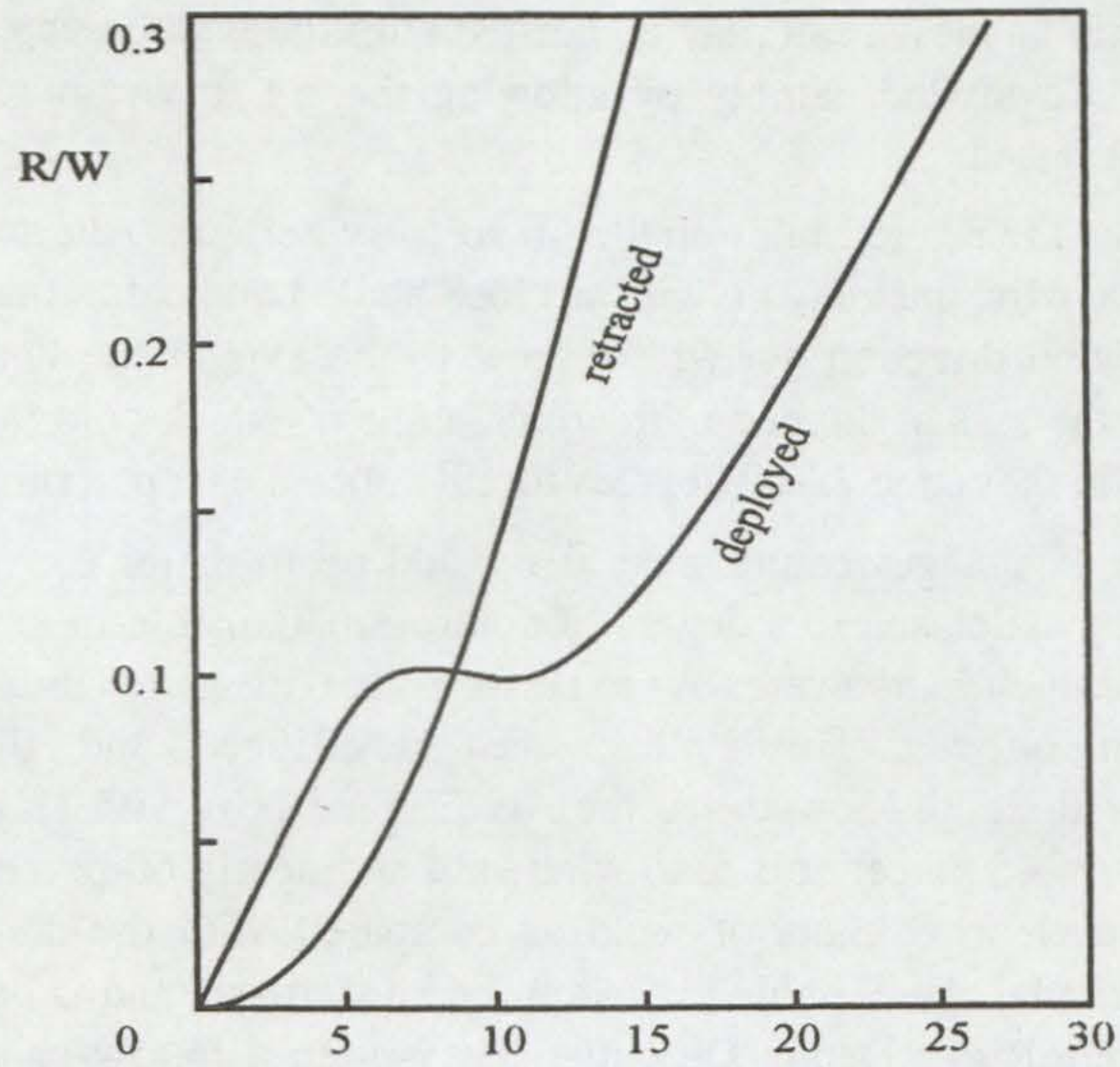

Fig. 11-5. Estimated R/W for *Williwaw* with foils retracted and deployed.

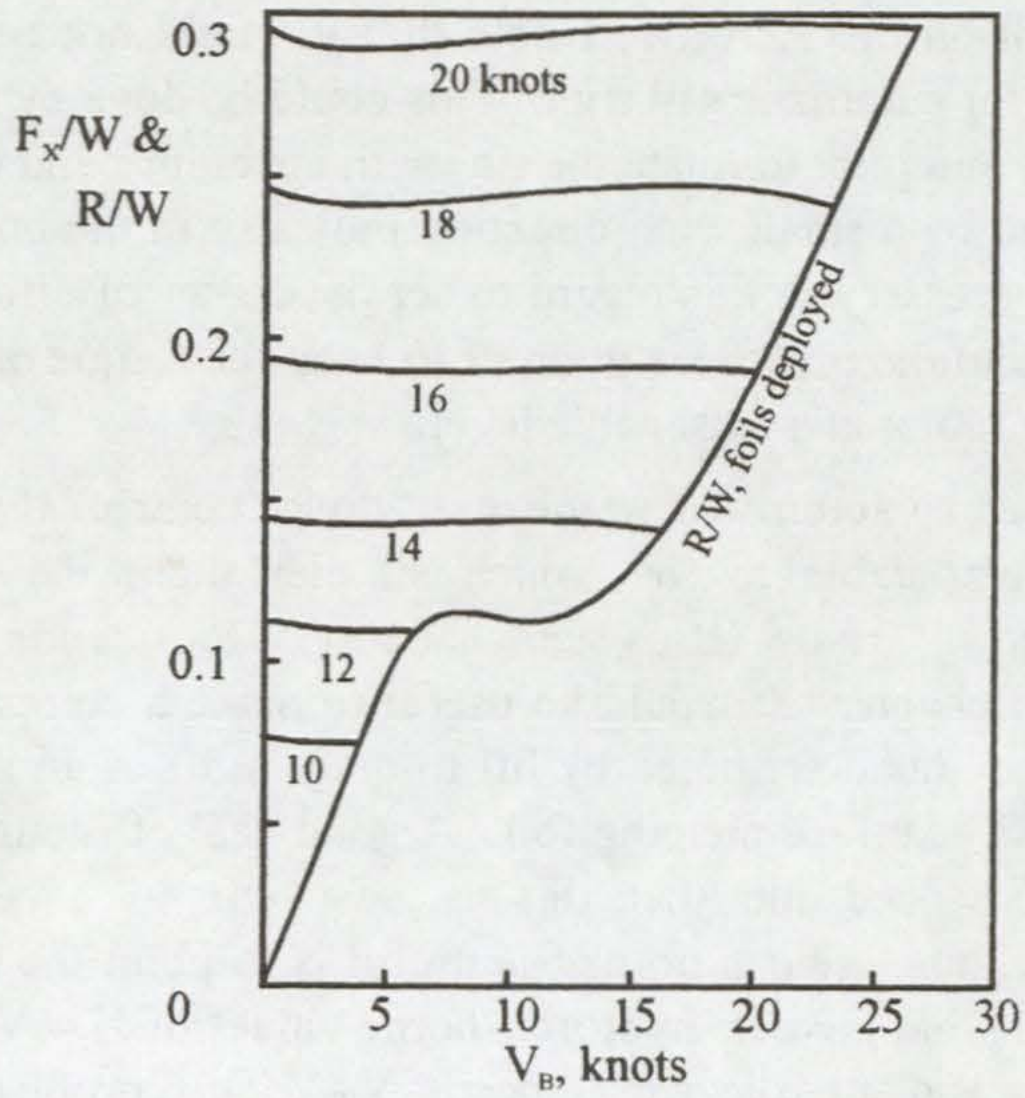

Fig. 11-6. Graphical solution of the speed of a foil-borne multihull for = 90°.

the hull-borne resistance-to-weight ratio for *Williwaw* ($\alpha V_B^2/L$, where α = 0.0286 and L = 26 ft) and the corresponding curve for R/W when the hydrofoils are deployed. From chapter 2, we can write F_x/W as

$$F_x/W = (\tfrac{1}{2}\rho A_S/W)\, V_T^2\, (X^2 + 2X\cos\gamma + 1)^{1/2}[C_L \sin\gamma - C_D(X + \cos\gamma)] \quad (11\text{-}6)$$

For simplicity, let us consider the case $\gamma = 90°$. With $\frac{1}{2}\rho = 1.19 \times 10^{-3}$ slugs /ft^3 and all speeds expressed in knots, Eq. (11-6) becomes

$$F_x/W = 4.96 \times 10^{-4}\, V_T^2 (X^2 + 1)^{1/2}\, (C_L - XC_D) \quad (11\text{-}7)$$

In Fig. 11-6, we show a replot of R/W for deployed foils together the curves of Fx/W using Eq. (11-7). We see that at the critical speed for liftoff (around 13 knots in this example), the boat speed jumps from 10-12 knots up to 20-22 knots. Indeed, this is what is observed. As soon as we have good data on R/W as a function of boat speed for a given set of hydrofoils, and know A_s, W, C_L and C_D for the boat, we can then calculate polar curves of $V_B(\ , V_T)$ with confidence. For the calculation, the curve of R/W can be simulated by a power series of the form

$$R/W \approx aV_B + bV_B^2 + cV_B^3 + ... + zV_B^n \quad (11\text{-}8)$$

Experience shows that five terms are required for an adequate simulation of a curve of this sort.

It is interesting to note that all of our analysis throughout this book has concluded the superiority of the canard configuration in rig, rudder, and hydrofoil arrangements. The canard is not currently in "fashion" and neither are surface- piercing foils, however I will stand by my conclusions and recommend that development work proceed in that direction.

In closing, I am reasonably certain that realization of the sort of boats that we have discussed is mostly a matter of having the courage to do it. Dave Keiper had that sort of courage when he built *Williwaw* 30 years ago. We have not gotten back to that point yet as far as ocean-going hydrofoil flyers are concerned. John Walker had the courage to pursue his dream of the automated wingsail yacht and has made it a reality. Practical use of Alexander Thom's data to make a high- performance rotor yacht will hopefully come soon. The AeroRig is already well developed and is sure to give yacht design a healthy push in the right direction.

1-1. Norwood, J., High Speed Sailing - Design Factors: Adlard Coles, Ltd., 1979.
2-1. Kelsall, D. and J. Shuttleworth, Multihull International, 111, 67 (1977).
2-2. Bruce, E. and H. Morss, Design for Fast Sailing, AYRS 82 (1973).
2-3. International Offshore Multihull Rule, IYRU, London.
2-4. Norwood, J. Performance Prediction for Multihull Sailing Yachts. AYRS.

3-1. Norwood, J., High Speed Sailing - Design Factors. St. Albans: Adlard Coles, Ltd., 1979.
3-2. Bruce, E. and H. Morss, Design for Fast Sailing. Hermitage: AYRS 82, 1976.

4-1. Hoyt, G. Ready About. Camden, ME: International Marine Publishing Co. 1986.
4-2. Abbott, I. H. and A. E. von Doenhoff. Theory of Wing Sections. New York: Dover Publications, Inc. 1959.
4-3. Norwood, J. High Speed Sailing - Design Factors. St. Albans: Adlard Coles Ltd. 1979.
4-4. Herreshoff, L. Francis. The Common Sense of Yacht Design. Jamaica, NY: Caravan-Maritime Books. 1974.
4-5. Griswold, L. M. Multihulls Magazine, Oct/Nov 1988. pp. 43-44.

5-1. Rainey, R. C. T., "The Wind Turbine Ship". Atkins Research and Development.
5-2. Blackford, B. L., Am. J. Phys., 46, 1004 (1978); Am. J. Phys., 49, 282
5-3. Frank, Reg, "Power from the Wind", AYRS No. 91, 1979.
5-4. Woodward, J. B., R. F. Beck, R. Scher, and C. M. Cary, "Feasibility of Sailing Ships for the American Merchant Marine". Maritime Admin., Contract 4-37110. Feb. 1975. Univ. of Michigan.
5-5. Bergeson, L., G. L. Clemmer, et al, "Wind Propulsion for Ships of the American Merchant Marine". Maritime Admin., Contract MA-80-SAC-01027. Jan. 1981. Windship Development Corp.

6-1. Norwood, J. High Speed Sailing - Design Factors. St. Albans: Adlard Coles, Ltd. 1979. pp 5-6.
6-2. Castles, W., AYRS 83B, March 1976. p 14.
3. Bruce, E. and H. Morss, Design for Fast Sailing. AYRS 82. .
6-4. Hannay, I. (ed), Rig Efficiency. AYRS 111, 1993; private communication.
6-5. Olsen, K. J. Rudder Design for Sailing Craft. AYRS 79.
6-6. Bolger, P. Different Boats. pp 185-191; 30 Odd Boats. pp191- 193. Camden, ME: International Marine Publishing Co.

7-1. Wylie, C. R. *Advanced Engineering mathematics*. New york: McGraw-hill Book Co 1951. *pp* 416-421.
7-2. Marchaj, C. A. – *Aero - Hydrodynamics of Sailing*. 2nd Ed. Camden ME. International Marine Publishing 1988 *pp*189 - 198
Charrier, B. *"Etude Theorique et Experimentale de l'Effet 'Magnus, Destine a laPropulsion Eolienne de Navires"*. Doctoral dissertation, University of Paris, Oct 1979.
7-4. Busemann, A. *"Messungen an Rotierenden Zylindern."* Ergebnisse der Aerodynamischen Versuchsanstalt zu Göttingen. IV. Lief., *p* 101 (Oldenburg, Munich. 1932).
7-5. Flettener, A. *The Sttory of the Rotor*. New York: F. O. Willhofft. 1926.
7-6. Woodward, J B, Beck R F, Scher R and Cary C M. "Feasibility of Sailing Ships for the American Merchant Marine." Maritime Administration Contract 4-37110. feb 1975. University of Michigan.
7-7. Bergeson L, Clemmer G L *et al* "Wind Propulsion for Ships of the American Merchant Marine." Maritime Administration Contract MA-80-SAC-01027. Jan 1981. Windships Development Corp.
7-8. Swanson W M. *"The Magnus Effect*: A summery of investigations to Date". J Basic Eng Transactions of ASME. Sept 1961 *pp* 461-470.
7-9. Thom A. *"Effects of Discs on the Air Forces on a Rotating Cylinder"*. ARC R&M 1623. 1934
7-10. Norwood J *Intermediate Classical Mechanics*, Englewood Cliffs, NJ: Prentice-Hall 1979. *p* 287.
7-11. Goldstein S. *Modern Developments in Fluid Dynamics*. Vol 1. New York: Dover Publications. 1965. *p* 7.

8-1. Wadlin, K.L., C. L. Shuford, and J. R. McGehee, A Theoretical and Experimental Investigation of the Lift and Drag Characteristics of Hydrofoils at Subcritical and Supercritical Speeds. NACA Report 1232/55.
8-2. Vladimirov, A. N., Approximate Hydrodynamic Design of a Finite Span Hydrofoil. CAHI 1937. Translated as NACA Tech. Memo. 1341/55.
8-3. duCane, P., High Speed Small Craft. Tuckahoe, NY: John deGraff, Inc. 1972. p. 38.
8-4. Hoerner, S. F., Fluid-Dynamic Drag. 1958.
8-5. Hook, C. and A. C. Kermode, Hydrofoils. London: Sir Isaac Pitman & Sons, Ltd. 1967.
8-6. Alexander, A., J. Grogono, and D. Nigg, Hydrofoil Sailing. London: Juanita Kalerghi. 1972.
8-7. Ketterman, G., Multihulls, M/J, 1990. pp63-65.
8-8. Keiper, D., Multihulls, J/F, 1994. pp44-50.
8-9. Norwood, J., High Speed Sailing - Design Factors. St. Albans: Adlard Coles, Ltd. 1979.
8-10. Chapman, G., Why Aren't Hydrofoils Faster? Multihull International, Mar 1985. pp68-70.
8-11. AYRS, Sailing Hydrofoils (AYRS 74). London: Amateur Yacht Research Society.
8-12. Bruce, E. and H. Morss, Design for Fast Sailing (AYRS 82). London: Amateur Yacht Research Society.
8-13. Barkla, H., Sailing on Hydrofoils. Association of Northern Universities Sailing Clubs. 1953.
8-14. Grogono, J., Icarus, the Boat That Flies. London: Adlard Coles, Ltd.
8-15. Pelly, D., Faster! Faster! New York: Hearst Maritime Books. 1984. 8-16. Morwood, J., Hydrofoil Options (AYRS 90). London: Amateur Yacht Research Society.

9-1. James, Rob, Multihulls Offshore. New York: Dodd, Mead & Co. 1983.
9-2. Norwood, J.,High Speed Sailing - Design Factors. St. Albans: Adlard Coles, Ltd. 1979.
Fig 9-5. A symmetric multihull flying hydrofoil ocean cruiser.
9-3. Bolger, P., Different Boats. Camden, ME: International Marine Publishing Co. pp 185-190.
9-4. Bolger, P., 30 Odd Boats. Camden, ME: International Marine Publishing Co. pp 191-195.
9-5. Keiper, D. "Hydrofoil Ocean Voyager Williwaw". Proc. of 3 AIAA Symposium on Aero-Hydronautics of Sailing. Nov. 1971.

9-6. Keiper, D. and J. Fifield, "Progress with Hydrofoil Sailing". Proc. of 6 AIAA Symposium on Aero-Hydronautics of Sailing. Jan. 1975.
9-7. Keiper, D., "Hydrofoil Cruising and Daysailing". Proc. of 18 Annual Conference on Sailing Technology. AIAA and SNAME. Oct. 1989.
9-8. Keiper, D., "The Joy of Foiling". Multihulls, J/F 1994. pp 4**

10-1. Follet, T., D. Newick, and J. Morris, Project Cheers. London: Adlard Coles, Ltd. 1969.
10-2. Haddon, A. C. and J. Hornell, Canoes of Oceania. Honolulu: Bishop Museum Publications 27, 28, and 29. 1936-1938.
10-3. O'Brien, M., "R Brown & his Proven Proas". WoodenBoat, J/A 1983.
10-4. Norwood, J., "The Challenge of Proa Design". Multihulls, M/A, 1994. pp 41-46.

11-1. Kelsall, D. and J. Shuttleworth, Multihull Inter., 111, 67 (1977).
11-2. Milgram, J. H., "Sail Force Coefficients for Systematic Rig Variations". SNAME T & R Report R-10. New York. 1971.
11-3. Payne, B., "Cousteau loses experimental rig in the Atlantic". Sail, Feb 1984. p 172.
11-4. Desoutter, D., "The Rig of the Future?", Practical Boat Owner, Oct 1993. p 30-32.
11-5. Boyd, J., "Swings and Roundabouts". Yachting World, Sept 1993.
11-6. Desoutter, D., "The Rig of the Future?", Practical Boat Owner, Dec 1994.

Design and layout for AYRS by Ian Hannay

Printed by ***Speed Print.*** *Gladiator Works, Forest Hill, London. SE23 1NA*

AYRS Publications inc. p & p. (surface rates)

1	Catamarans	1955	£1.50
2	Hydrofoils	1955	£5.50*
3	Sail Evolution	1955	£5.50*
4	Outriggers	1956	£1.50
5	Sailing Hull Design	1956	£5.50*
6	Outrigger Craft	1956	£1.50
7	Cat. Construction	1956	£5.50*
8	Dinghy Design	1956	£5.50*
9	Sails & Aerofoils	1956	£5.50*
10	American Catamarans	1956	£1.50
11	The Wishbone Rig	1957	£5.50*
12	Amateur Research	1957	£5.50*
13	Self Steering (book)	1957	O. of P.
14	Wingsails	1957	£5.50*
15	Catamaran Design	1957	£5.50*
16	Trimarans & Outriggers	1957	£5.50*
17	Commercial Sail	1958	£5.50*
18	Cat Developments	1958	£5.50*
19	Hydrofoil Craft	1958	£1.50
20	Modern Boatbuilding	1958	£5.50*
21	Ocean Cruising	1958	£5.50*
22	Catamarans 1958	1958	£5.50*
23	Outriggers 1958	1959	£5.50*
24	Yacht Wind Tunnels	1959	£5.50*
25	Fibreglass	1959	£5.50*
26	Sail Rigs	1959	£5.50*
27	Cruising Cats. (book)	1959	£6.00
28	Catamarans 1959	1959	£5.50*
29	Outriggers 1959	1960	£5.50*
30	Tunnel & Tank	1960	£5.50*
31	Sailing Theory	1960	£5.50*
32	Sailboat Testing	1960	£5.50*
33	Sails 1960	1960	£5.50*
34	Ocean Trimarans	1961	£1.50
35	Catamarans 1960	1961	£5.50*
36	Floats, Foils & Flows	1961	£5.50*
37	Aerodynamics I	1961	£5.50*
38	Catamarans 1961	1962	£1.50
39	Trimarans 1961	1962	£5.50*
40	Yacht Research I	1962	£5.50*
41	Yacht Research II	1962	£5.50*
42	Catamarans 1962	1963	£1.50
43	Trimarans 1962	1963	£5.50*
44	A.Y.R.S. Yachts	1963	£1.50
45	Basic Research	1963	£1.50
46	Catamarans 1963	1964	£5.50*
47	Outriggers 1963	1964	£1.50
48	Yacht Electronics	1964	£5.50*
49	Keel Yachts	1964	£1.50
50	Catamarans 1964	1965	£1.50
51	Foils & Floats	1965	£5.50*
52	Trimarans 1964	1965	£5.50*
53	Solo Cruising	1965	£1.50
54	Catamarans 1965	1965	£5.50*
55	Trimarans 1965	1966	£5.50*
56	Sailing Figures	1966	£1.50
57	Round Britain 1966	1966	£1.50
58	Practical Hydro foils	1966	£5.50*
59	Multihull Design/Cats.	1967	£5.50*
60	Multihull Seamanship	1967	£5.50*
61	Sailing Analysis	1967	£5.50*
62	Hydofoil Victory	1967	£5.50*
63	Multihull Capsizing	1966	£5.50*
64	Catamarans 1967	1968	£5.50*
65	Trimarans 1968	1968	£5.50*
66	Foils/Ice Yachts/Sails	1968	£5.50*
67	Catamarans 1969	1969	£1.50
68	Outriggers 1969	1969	£1.50
69	Multihull Safety Study	1969	£5.50*
70	Retirement Yachts/Polars	1969	£1.50
71	S/H Transatlantic Races	1970	£1.50
72	Catamarans 1970	1970	£5.50*
73	Trimarans 1970	1970	£1.50
74	Sailing Hydrofoils (book)	1970	O.of P.
75	Deepwater Seamanship(book)	1971	£5.50
76	Sail Trim, Test & Theory	1971	£1.50
77	Trimaran Selection	1971	£1.50
78	Cruising Cats. (book)	1971	O. of P.
	AIRS 1 - 11	1971-5	£1.50 each
79	Rudder Design (book)	1974	£7.00
80	Round Britain Race 1974	1974	£1.50
81	Sail Rigs 1976	1976	£5.50*
82	Design/Fast Sailing (book)	1976	£11.00
83.A	Journal 83A	1976	£5.50*
83.B	Journal 83 B	1976	£5.50*
84.	Hydrofoils'76	1976	£5.50*
84.B	Hull Research '76	1976	£5.50*
85.A	Kite sail rigs '76	1976	£1.50
85.B	Boatbuilding & Materials	1976	£1.50
86	Ostar '76 & Safety	1977	£1.50
87	Kites & Sails	1977	£3.50
88	Yacht Tenders & Boats	1977	£3.50
89	Facts & Figures	1977	£3.50
90	Hydrofoil Options	1978	£3.50
91	Power from the Wind	1979	£3.50
92	Deep sea Seamanship	1979	£3.50
93	Speed Sailing	1979	£3.50
94	Shallow Draft Craft	1980	£3.50
95	Racing Hydrofoils	1982	£3.50
96	Cruiser Development	1983	£3.50
97	Sails, Rigs & Hydrofoils	1983	£3.50
98	Windmills & Kites	1983	£3.50
99	Megalithic Boats	1984	£3.50
100	Efficient performance	1985	£3.50
101	Windmills and Hydrofoils	1985	£3.50
102	Sailboards & Speedweek	1986	£3.50
103	Optimum Yachts	1987	£3.50
104	Multihull Cruisers	1988	£3.50
105	High Speed Sailing	1989	£3.50
106	Seaworthiness/Stability	1989	£3.50
107	Low Drag Craft	1990	£3.50
108	Foils & Hapas	1991	£3.50
109	Propellers & Solar Boats	1991	£3.50
110	Developments in Yacht Design	1992	£3.50
111	Rig Efficiency	1993	£3.50
112	AYRS Projects	1993	£3.50
113	Rig Theory	1993	£5.50
114	Ultimate Sailing	1994	£5.50
115	Speed Sailing	1994	£5.50
116	Ultimate Sailing II	1994	£5.50
117	Natural Aerodynamics	1995	£5.50
118	Ultimate Sailing III	1995	£5.50
119	Instrumentation & Performance	1995	£5.50
120	21st Century Multihulls I & II	1996	£10.00

* Photocopies = Out of print. Prices subject to change

21st CENTURY MULTIHULLS

PART I

INTRODUCTION
the wind on a moving object and how a sailing boat utilizes it

PERFORMANCE CRITERIA
the general theory of multihull sailing craft performance

HULLS AND OUTRIGGERS
the criteria for minimum-resistance hulls and a method to design them

WINGSAILS
the pros and cons of rigid permanently deployed wingsails

WIND AND WATER TURBINES
sailing directly into the wind and downwind faster than the wind

BOARDS AND RUDDERS
leeway prevention and steering for advanced multihulls

PART II

ROTORS
a rotating circular cylinder with fences may provide
the maximum sailing performance at minimum cost

HYDROFOIL APPLICATIONS
hydrofoils applied to pitch and roll stability, also to
seakeeping and performance enhancement

SYMMETRIC MULTIHULLS
the foregoing bits and pieces are arranged into
laterally symmetric catamarans and trimarans

ASYMMETRIC MULTIHULLS
a critical look at proas, they may constitute
the ultimate multihull configuration